Journal of Chemistry

# Applications of Green Chemistry to Meet Sustainable Development Goals

Lead Guest Editor: Mahmoud Nasr
Guest Editors: Ravindran Balasubramani and Sanjay Kumar Gupta

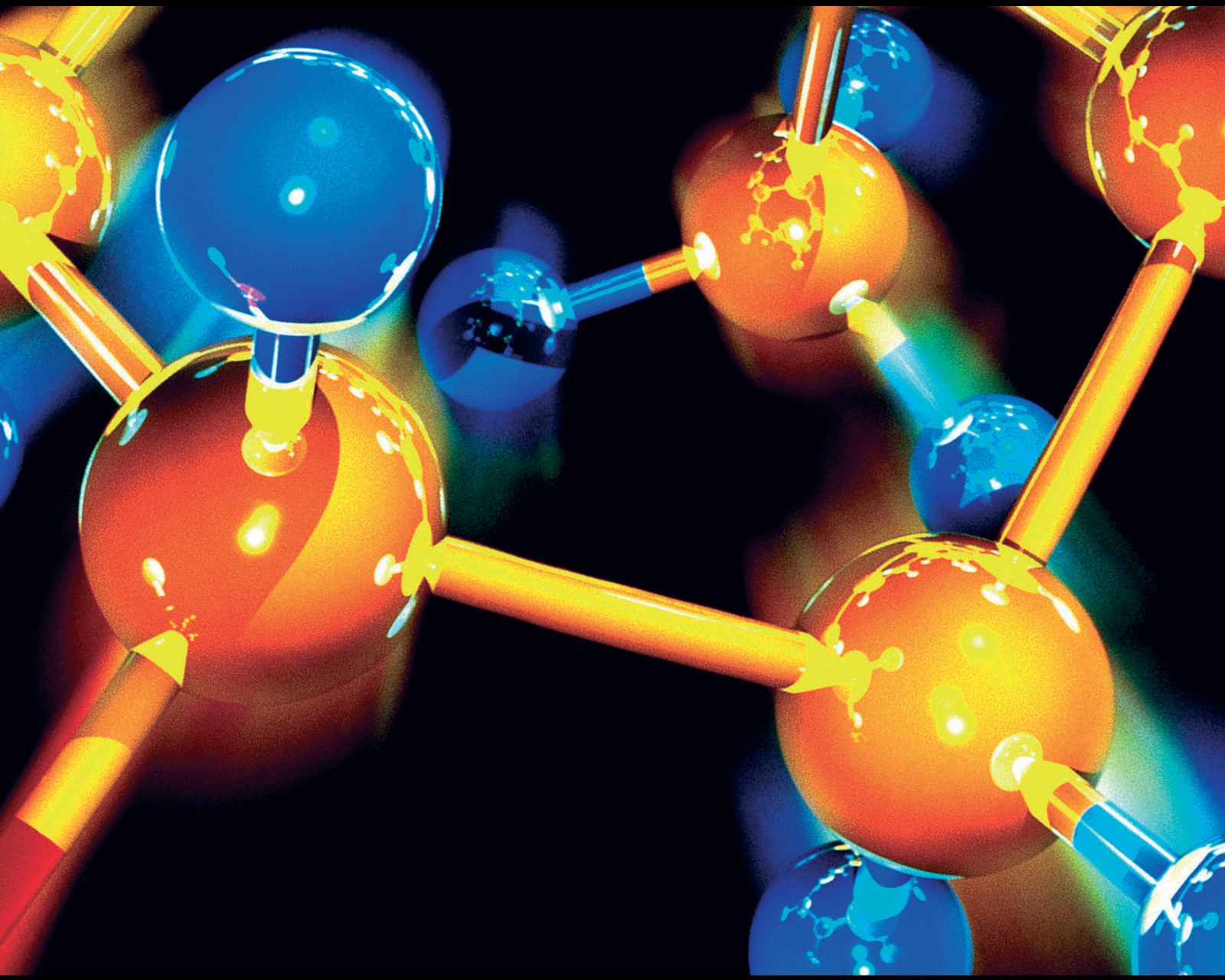

# Applications of Green Chemistry to Meet Sustainable Development Goals

Journal of Chemistry

# Applications of Green Chemistry to Meet Sustainable Development Goals

Lead Guest Editor: Mahmoud Nasr
Guest Editors: Ravindran Balasubramani and Sanjay Kumar Gupta

# Chief Editor

Kaustubha Mohanty, India

## Associate Editors

Mohammad Al-Ghouti, Qatar
Tingyue Gu, USA
Teodorico C. Ramalho, Brazil
Artur M. S. Silva, Portugal

## Academic Editors

Jinwei Duan , China
Luqman C. Abdullah, Malaysia
Dr Abhilash, India
Amitava Adhikary, USA
Amitava Adhikary, USA
Mozhgan Afshari, Iran
Daryoush Afzali, Iran
Mahmood Ahmed, Pakistan
Islam Al-Akraa, Egypt
Juan D. Alché, Spain
Gomaa A. M. Ali, Egypt
Mohd Sajid Ali, Saudi Arabia
Shafaqat Ali, Pakistan
Patricia E. Allegretti, Argentina
Marco Anni, Italy
Alessandro Arcovito, Italy
Hassan Arida, Saudi Arabia
Umair Ashraf, Pakistan
Narcis Avarvari, France
Davut Avci, Turkey
Chandra Azad, USA
Mohamed Azaroual, France
Rasha Azzam, Egypt
Hassan Azzazy, Egypt
Renal Backov, France
Suresh Kannan Balasingam, Republic of Korea
Sukanta Bar, USA
Florent Barbault, France
Maurizio Barbieri, Italy
James Barker, United Kingdom
Salvatore Barreca, Italy
Jorge Barros-Velázquez, Spain
THANGAGIRI Baskaran, India
Haci Baykara, Ecuador
Michele Benedetti, Italy
Laurent Billon, France
Marek Biziuk, Poland
Jean-Luc Blin, France
Tomislav Bolanca, Croatia
Ankur Bordoloi, India
Cato Brede, Norway
Leonid Breydo, USA
Wybren J. Buma, The Netherlands
J. O. Caceres, Spain
Patrizia Calaminici, Mexico
Claudio Cameselle, Spain
Joaquin Campos, Spain
Dapeng Cao, China
Domenica Capasso, Italy
Stefano Caporali, Italy
Zenilda Cardeal, Brazil
Angela Cardinali, Italy
Stefano Carli, Italy
Maria F. Carvalho, Portugal
Susana Casal, Portugal
David E. Chavez, USA
Riccardo Chelli, Italy
Zhongfang Chen, Puerto Rico
Vladislav Chrastny, Czech Republic
Roberto Comparelli, Italy
Filomena Conforti, Italy
Luca Conti, Italy
Christophe Coquelet, France
Filomena Corbo, Italy
Jose Corchado, Spain
Maria N. D.S. Cordeiro, Portugal
Claudia Crestini, Italy
Gerald Culioli, France
Nguyen Duc Cuong, Vietnam
Stefano D'Errico, Italy
Matthias D'hooghe, Belgium
Samuel B. Dampare, Ghana
Umashankar Das, Canada
Victor David, Romania
Annalisa De Girolamo, Italy
Antonio De Lucas-Consuegra, Spain
Marcone A. L. De Oliveira, Brazil
Paula G. De Pinho, Portugal
Damião De Sousa, Brazil
Francisco Javier Deive, Spain
Tianlong Deng, China

# Contents

Hindawi
Journal of Chemistry
Volume 2023, Article ID 7891518, 27 pages
https://doi.org/10.1155/2023/7891518

*Review Article*

# A Review on Cassava Residues as Adsorbents for Removal of Organic and Inorganic Contaminants in Water and Wastewater

**Vasu Gajendiran**,[1] **Prabu Deivasigamani**,[1] **Selvaraju Sivamani**,[2] **and Ponnurengam Malliappan Sivakumar**[3,4]

[1]*School of Bio and Chemical Engineering, Sathyabama Institute of Science and Technology, Chennai, India*
[2]*Engineering Department, University of Technology and Applied Sciences, Salalah, Oman*
[3]*Institute of Research and Development, Duy Tan University, Da Nang, Vietnam*
[4]*School of Medicine and Pharmacy, Duy Tan University, Da Nang, Vietnam*

Correspondence should be addressed to Prabu Deivasigamani; dprabhu78@gmail.com and Ponnurengam Malliappan Sivakumar; sivamedchem@gmail.com

Received 21 September 2022; Revised 4 November 2022; Accepted 24 November 2022; Published 26 April 2023

Academic Editor: Mahmoud Nasr



An increase in water demand for drinking, agriculture, and industries necessitates the treatment of water and wastewater. Among various conventional treatment techniques available, adsorption is found to be one of the most economical and feasible methods. Adsorbents from plant biomass are effective for the removal of organic and inorganic pollutants. Cassava has gained attention among researchers during the past decades due to its plentiful availability and resilient characteristics. Even though cassava contains cyanogenic glucosides as toxins, it is used in industries for development of various products. Cassava stem, rhizome, peel, and bagasse are industrial residues that are generated in abundance. The present review focusses on factors affecting adsorption using cassava residues, adsorbent preparation and activation methods, equilibrium, mass transfer, kinetics, and thermodynamic studies of adsorption.

## 1. Introduction

According to the Food and Agricultural Organization (FAO), cassava is considered to be one of the significant crops in the tropical region of the world [1]. The cassava plant consists of leaves and tubers as feed and food, respectively, and stem and rhizome being nonedible parts [2]. Cassava-producing industries generate peel and bagasse as residues and utilize the pulp to produce starch, flour, chips, and bioethanol [3]. The production statistics of cassava tubers reveal an average production of 268, 283.8, and 293.5 MMT during 2011–13, 2014–16, and 2018–20, respectively, with a sharp decline in 2017 at 277 million tons (Figure 1). As production increased during the mentioned periods, cassava-producing industries emerged as a promising sector for economic growth [4]. Hence, the waste generated from cassava-producing industries requires a suitable alternate option for waste to wealth conversion. Adsorbents could be the potential route for utilization of cassava peel, bagasse, stem, and rhizome.

Adsorption is an exothermic process in which liquid, dissolved solid, or gas atoms, ions, or molecules (adsorbate) accumulate inside the top surface of another solid substance (adsorbent) [5]. Adsorption is caused by an imbalance of forces forming hydrogen, Van der Waals, covalent, and ionic bonds among the two species, the adsorbent and the adsorbate [6]. Adsorption is used in chemical process industries for sugar refining, wastewater treatment, chromatography, gas purification, moisture removal, metallurgy, etc. [7]. The advantages of adsorption include operating in mild conditions and having simpler designs. Conventional methods are available to treat wastewater, but adsorption creates interest among researchers due to its economics [8, 9].

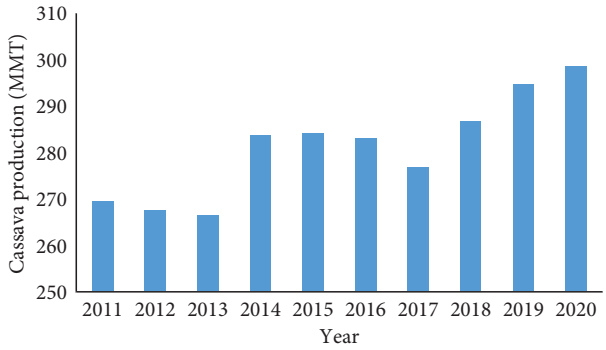


Figure 1: Cassava production in the world from 2011 to 2020 (FAOSTAT, 2021).

In the literature, various parts of cassava are reported to be adsorbents used in the removal of heavy metals, for example, zinc ([10–13]), copper ([11, 13–21]), lead ([20–28]), cobalt ([29, 30]), vanadium [30], chromium ([13, 17, 30, 31]), and cadmium ([12, 15, 32–34]), dyes such as rhodamine B [35], direct red [36], methylene blue ([36–40]), methyl orange [40], and reactive dyes [41], antibiotics ([22, 42–44]), phosphorous [45], biodiesel purification [46], organic pollutants from industrial effluents ([29, 47, 48]), and free fatty acid [49]. In addition, ZnO nanoparticles synthesized from cassava starch are used as adsorbents [50].

The present review highlights various activation methods, process parameters, isotherms, kinetics, thermodynamics, and binding mechanisms of adsorption using cassava-based adsorbents.

## 2. Factors Affecting Adsorption

Adsorption can be affected by various factors such as pH, initial concentration of adsorbates, contact time, adsorbent dosage, adsorbent size, and temperature, in addition to agitation speed (Figure 2). The process optimization of the aforementioned factors is required to maximize outcomes of adsorption, percentage removal, and adsorption capacity, the latter being the predominant.

*2.1. Effect of pH.* In the study of the adsorption process, the parameter pH is critical as the degree of electrostatic charges given by ionized adsorbates is controlled by it. As a result, the rate of adsorption varies with the medium pH, not in a particular pattern. At low pH, the adsorption capacity for anionic molecules generally increases, whereas it decreases for cationic molecules [51]. The electrostatic repulsion between the positively charged adsorbate and the adsorbent surface diminishes when the pH of the medium elevates, resulting in a rise in charge density of surfaces [52].

By adjusting the pH between 3 and 6, Belcaid et al. [7] examined the impact of pH on the process of chromium and cobalt removal from the solution by cassava peel carbon. They discovered that, in acidic environments, $H^+$ ions protonate the carbon surface of the cassava peel, favouring the electrostatic interaction between $HCr_2O_7^{-2}$ and the positively charged surface while creating competition

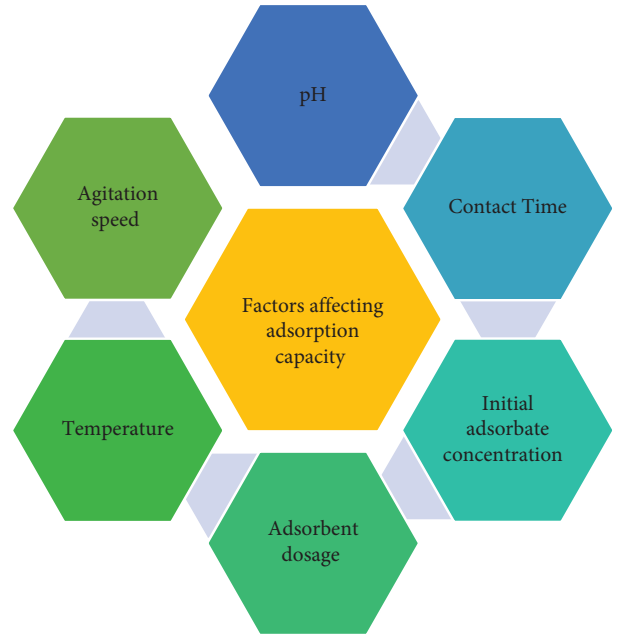


Figure 2: Factors affecting adsorption capacity.

between $H^+$ ions and $CO_2^+$ ions for the adsorption site. They discovered that a pH of 3 is ideal for removing chromium and a pH of 6 for removing cobalt.

Beakou et al. varied the pH from 3 to 9 to investigate the impact of pH on the cassava rind carbon's ability to remove malachite green, which is a pigment, from an aqueous solution [53]. They discovered that the adsorption of malachite green increases noticeably at pH levels that correspond to those of primary malachite green solutions. The quantity of malachite green absorption marginally rises in the ideal basic pH zone. It is possible that negative electrostatic forces will help the process of adsorption (surface charges change by means of cationic dye malachite green and cassava rind carbon). Because $H^+$ ions participate with cationic malachite green for the same adsorption sites at pH levels below 6.98, malachite green absorption is minimal.

Kurniawan et al. calculated the outcome of pH variation on Ni(II) ion uptake from an aqueous solution by fluctuating pH from 1 to 9 [5]. The findings demonstrate that the quantity of Ni(II) ion absorption rises gradually as pH rises from 1 to 5, peaking at pH 4.5. Compared to pH 4.5, less Ni(II) is adsorbed at higher pH levels. The occurrence of metal hydroxide [$Ni(OH)_2$], which occurs at alkali pH ranges ($pH > 7$), may be the origin of this phenomenon. Ni(II) ions are less concentrated in the solution due to the production of $Ni(OH)_2$, and as a result, less Ni(II) is removed by the cassava peel. Because of this, a pH of 4.5 is chosen for biosorption of metal investigations and helps as the ideal means for Ni(II) elimination.

*2.2. Effect of Contact Time.* According to equilibrium analysis, adsorption capacity increases as the contact time increases to a point, after which further increase in the contact time does not increase adsorbate uptake on

adsorbent due to saturation. The quantity of the adsorbate desorbing from the adsorbent present in the solution and the quantity of the adsorbate being adsorbed onto the adsorbent are in dynamic equilibrium. The time to establish this condition is known as the equilibrium time, and the quantity of the adsorbate adsorbed at that time represents the maximal adsorption capacity of the adsorbent under the operating conditions [54]. The contact time between adsorbents and adsorbates has a substantial impact on adsorption performance.

Abia et al. studied the outcome of time on adsorption of cadmium on thioglycolic acid-modified cassava fibre by changing the contact time from 5 to 30 minutes [55]. They found that the adsorption of cadmium was rapid at first 5 to 10 minutes and that adsorption capacity was achieved at 30 minutes. Also, they concluded that the faster rate of adsorption at the initial time of 5 to 10 minutes may be due to availability of uncovered active sites on the adsorbent surface.

Gunasekaran analysed the outcome of time for elimination of Metanil Yellow from an aqueous solution by using cassava peel and varying the time in the range of 0–1440 minutes [56]. He concluded that the percentage of Metanil Yellow dye removal increases rapidly with time but slows on attaining equilibrium. At the first 480 minutes of the contact time, the percentage dye slowly increased as availability of vacant sites on the adsorbent surface increased. At 480 minutes of the contact time, the Metanil Yellow dye reached an equilibrium state. At this stage, a dynamic equilibrium state between the amount of dye desorbing from the adsorbent and that being adsorbed on the adsorbent is established. After 960 minutes of the contact time, it started to decrease because of the saturation of active sites which do not allow further adsorption to take place.

Belcaid et al. [7] investigated the outcome of the contact time for elimination of chromium and cobalt from an aqueous solution by using cassava peel carbon and varying the time between 5 and 180 minutes. They discovered that there was rapid sorption uptake after 40 minutes of metal ion contact with activated carbon. Due to the nature of the accessible surface sites for the process of adsorption, the second stage is a sluggish phase of metal ion elimination that evolved from 50 min until 180 min. There are many sites available for sorption to take place when the interaction between the heavy metal ion and carbon from the cassava peel is established at the beginning of sorption, which accounts for the rapid metal ion uptake seen. The repulsive interactions between the already adsorbed metal ion and the entering sorbate and the constrained number of available sites for occupation cause the rate of subsequent adsorption to decrease as the uptake progresses, and the available sites are occupied.

*2.3. Effect of Initial Adsorbate Concentration.* The percentage removal increases and the adsorption capacity decreases with an increase in initial adsorbate concentrations. The effect of initial adsorbate concentrations is performed by preparing adsorbate solution at different concentrations using fixed pH, temperature, and contact time. The effect of initial adsorbate concentrations is used to study the interaction between adsorbates and adsorbents through isotherm models [57].

Hassan [58] studied the effect of initial dye concentrations on removal of malachite green dye from an aqueous solution by varying the concentration from 10 to 300 mg/L, and he found that maximum dye removal was achieved at a malachite green dye concentration of 100 mg/L.

By adjusting the quantity of 3 M $H_3PO_4$-activated cassava peel carbon from 10 to 50 mg/L, Thompson et al. [59] studied the impact of the initial lead ion concentration on the % removal and adsorption capabilities of lead ions from wastewater. They observed that as concentration increased, adsorption capacities increased, while % clearance decreased. This could be explained by the fact that there were initially few lead ions on the surface of adsorbents at lower concentrations, but as lead ion concentrations rose for a fixed number of sites and stayed constant, the number of substances that could be accommodated inside the diffusion layer enhanced, and the disposal of lead ions decreased. Cassava peels showed a maximum adsorption capacity of 27 mg/g at an initial concentration of 200 mg/g; however, with a preliminary concentration in the range of 50 mg/g, the adsorption capacity was 50.2 mg·g. With cassava peels, the highest clearance percentage of 89 was achieved at an initial concentration of 50 mg/g.

Ja'afar et al. [60] analysed the result of heavy metallic ion concentrations for adsorption elimination of copper ions from aqueous solvents by using amidoxime-modified polyacrylonitrile-grafted-cassava starch (AN-g-CS) and changing the preliminary concentration of cuprum ions at 25, 50, 75, 100, and 200 ppm, respectively. It validates that amidoxime-improved poly(AN-g-CS) increased and reached its saturation point at 100 ppm as the original volume per unit mass of cuprum ions (28 ppm) was raised up to 150 ppm.

Due to more widely accessible solutes as well as electrostatic interactions between solute and active sites, the adsorption capacity rose as the number of potential binding sites grew.

*2.4. Effect of the Adsorbent Dosage.* Adsorption capacity is calculated as the mass of the adsorbate removed per adsorbent mass. The rate of adsorption surges as the adsorbent dosage rises as a rise in the adsorbent dosage increases the number of sorption sites at the exterior of adsorbents. To study the consequence of the adsorbent dose on the process of adsorption, trials are executed by preparing different levels of mass of adsorbents at the fixed initial adsorbate concentration and equilibrium time [56].

Navya et al. [61] investigated the consequence of the adsorbent dosage for elimination of mixed responsive dye from simulated effluents using cassava trunk biochar adsorbents and by varying the adsorbent dosage from 0.6 g/l to 4.1 g/l. They discovered that the highest dye removal was 78 percent and that the adsorption capacity was 13.93 mg/g at an optimal concentration of 100 mg per 100 mL of dye solution.

Dos Santos et al. [62] studied the effect of the adsorbent dosage on removal of tartrazine yellow dye from the experimental solution by means of cassava waste biosorbents and by altering the dosage of adsorbents from 2.4 g/L to 12.4 g/L. They concluded that greater biosorbent concentrations encourage greater adsorption effectiveness. Adsorption was 35.8 percent at 0.1 at a dosage of 2.5 g/L, and efficiency improved to 83.3 percent at 0.1 at a concentration of 12.5 g/L. Therefore, there are a proportion of active sites that can be occupied by TAR molecules that have been adsorbed because the contact area increases with increasing biosorbent mass. A dose of 7.4 g/L was determined to be the most suitable for further studies since it is close enough to the border value and offers material savings.

Okorocha et al. [63] analysed the outcome of the adsorbent dosage for adsorptive elimination of crystal violet using raw cassava peels as adsorbents and by varying the adsorbent dosage. They noticed that, as the dosage of adsorbents rose, the removal effectiveness of the crystal violet dye also increased. This finding can be explained by the fact that, as the dosage of the adsorbent was raised, the quantity of active surface sites in pure cassava peel areas increased. Although the adsorption equilibrium capacity dropped with an increase in the adsorbent dosage, the percentage of crystal violet removal of dye rose. The accessibility of all active sites during the adsorption process may be limited because of duplication or agglomeration of the energetic or adsorption sites.

*2.5. Effect of Temperature.* Temperature affects the adsorption process based on the properties of bonds formed between adsorbate sites and adsorbents and the solubility of the adsorbate in the medium. At low temperature, adsorption due to strong and weak bonds increases, whereas it increases for strong bonds and decreases for weak forces [64].

Theng and Tan [65] investigated the outcome of temperature of the environment on the adsorption potential of one of the most reactive methylene blue dyes in addition to Congo red dye on powder of cassava leaf by changing the temperature within the range of 25°C to the extent of 75°C. They concluded that, as soon as the temperature improved from 25°C to 45°C, an increasing trend was seen for the removal rate of methylene blue dye (from 99.45% to 99.91%) because the frequency of collisions between the adsorbent and adsorbate (dye solution) increased at higher temperature, which promotes adsorption on the adsorbent surface. Only 98.95 percent removal was achieved at 75°C when the temperature was increased further to 50°C because the high temperature of the dye solution may have broken intermolecular hydrogen bonds between the dyes and the adsorbent, which are the key contributors to the adsorption process. The clearance rate of Congo red dye, on the other hand, showed a declining trend as the temperature was raised from 25 to 75 C (from 99.67 percent to 97.95 percent). This might be because a higher temperature results in more acidic pH. Congo red dye was more likely to dissolve in water under these very acidic conditions and was more challenging to remove from the solution.

By altering the temperature from 30°C to 50°C, Scheufele et al. [66] investigated the impact of temperature on the biological sorption of straight black dye on cassava root husks. They drew the conclusion that straight black dye sorption using the cassava root husk is by nature an exothermic process since larger yields of adsorption occurred at lower temperatures (30°C). However, only a very little change was seen for the elevated temperature (between 40 and 50°C).

Li et al. [67] investigated the consequence of temperature change for elimination of Congo red dye from an aqueous solution using cassava residue and by changing the temperature from 30°C to 50°C. They found that the adsorptive capacity did not vary markedly with an increase in temperature from 30°C to 50°C, indicating that energy gained or released through the process of adsorption was insignificant.

*2.6. Effect of Adsorbent Size.* Because of the greater surface area, the adsorption rate increases with decreasing particle diameter. The restriction to the adsorbate's penetration into the adsorbent resulting from internal diffusion as well as transfer of mass is lessened with smaller particle size. Due to this circumstance, equilibrium is reached more quickly, and the greatest amount of adsorption capacity is possible [7].

Tejada-Tovar et al. [68] investigated the outcome of particle size on hexavalent chromium adsorption from the experimental solution using cassava peels as an adsorbent with different sizes between 0.355 and 1 mm. They found that the highest amount of adsorbed metal ions on cassava peel biomass was achieved at the smallest particle size (0.355 mm). The particle size of adsorbent materials influences the adsorption process because the surface area is increased to carry out the transfer of different ions from a liquid phase to a solid phase. The number of heavy metal ions that can be adsorbed is directly proportional to volume, and it is well known that this volume is directly proportional to the surface area. In addition, there is a greater surface area for small particle size; hence, a greater number of pores per mass unit are available for uptake of heavy metal ions.

Using 0.3 M $HNO_3$-activated cassava peels as an adsorbent, Sulaiman et al. [69] investigated the impact of particle size on the adsorption of copper and zinc ions from an aqueous solution. They found that, compared to the size of mesh, 100 mesh (150 micron), and 80 mesh, 120 mesh size (125 micron) is generally more successful in absorbing copper ($Cu^{2+}$) and zinc ($Zn^{2+}$) metal ions (180 micron). This finding supports the notion that, due to a larger surface area of contact between the adsorbent and the adsorbate, the ability of the adsorbent increases with decreasing particle size.

Rubio et al. [70] investigated the consequence of size of the particle on deletion of methylene blue from the experimental solution by using raw cassava bark residue and acid- and alkali-modified cassava bark residue with different particle sizes from 20 to 400 mesh numbers. They discovered that the adsorption phenomena of methylene blue of 20 (88.0 percent), 30 (87.8 percent), and 40 were not significantly affected by particle size (88.4 percent). However, the

alkalinization of CBR led to a significant improvement, exhibiting 94.3 percent of methylene blue removal, while the acidification of CBR showed a minor drop in methylene blue separation (85.5 percent).

*2.7. Effect of Mixing Speed.* Horsfall and Abia [11] calculated the result of mixing speediness for adsorption of cadmium from an aqueous solution by using cassava waste biomass (tuber bark) and conducting the experiment with different speeds from 50 to 200 rpm. They concluded that the agitated samples showed a 35 percent increase in adsorption over the first 30 minutes of contact so that sorbate ions can effectively be transferred onto the sorbent surface by adequate interactions between metallic ions and biomass binding sites. The sorption efficiency was discovered to be marginally lower at 200 rotations per minute (rpm) than it was at 150 rpm. This finding might point to weak Van der Waals contacts between sorbents and chromium ions, which might be broken in the presence of intense turbulence. Therefore, an agitation speed is 150 rpm.

Ndlovu et al. [30] considered the consequence of agitation speeds on the deletion of cobalt, chromium, and vanadium from the experimental solution by using cassava-peel biomass (both raw/treated with thioglycolic acid). The agitation speed ranged from 50 to 200 rpm during the experiment. They discovered that, as the agitation speed rose from 50 to 150 rpm, there was an increase in sorption. This is such that the mass transfer rate of metal ions on the surface of the biomass is maximized as the agitation speed is increased. However, as the agitation speed increased from 150 to 200 rpm, sorption decreased. This happens when there is a break in the link between metal ions and adsorbents, which causes metal ions to desorb from the surface sites. The outcomes also suggest that physical adsorption, not chemical adsorption, is occurring.

Aulia et al. [71] examined the outcome of the mixing speed for the dye elimination from screen printing industry wastewater using cassava peels (20% $H_2SO_4$ acid activated) and by varying the speed of 50, 100, 150, 200, and 250 rpm. The researchers discovered that 100 rpm was the ideal stirring speed for removing colours, removing 96.78 percent. The adsorbate and the adsorbent were dispersed equally at the maximum speed and throughout the maximum contact duration, increasing the adsorption process.

Table 1 summarizes the effect of parameters on adsorption using cassava residues as adsorbents.

## 3. Preparation of Adsorbents and Activation Methods

The materials used for preparation of adsorbents are rich in carbon [74]. Among the plant biomass, lignocellulosic materials are more appropriate for adsorbent preparation. Lignocellulosic materials basically contain lignin, cellulose, and hemicellulose. Lignin is an organic polymer composed of coumaryl alcohol, sinapyl alcohol, and coniferyl alcohol. Cellulose is a homopolysaccharide that is composed of many units of glucose connected through $\beta$-1,6-glycosidic linkage. Hemicellulose is a heteropolysaccharide mainly comprises pentoses. Lignocellulosic materials rich in hemicellulose yield a less quantity of adsorbents, whereas materials rich in cellulose and lignin yield a high quantity of adsorbents. Lignocellulosic materials are either angiosperms (hardwood) or gymnosperms (softwood). Gymnosperms are rich in hemicellulose, and angiosperms are rich in cellulose.

The steps followed in adsorbent preparation are breaking of plant biomass to coarse particles and then to fine ones. Then, the fine particles are washed to remove debris and light particles, dried at around 100°C, and activated to produce effective adsorbents (Figure 3). The economics of adsorbent preparation are minimum so that the wastewater treatment by adsorption can be feasible. Pyrolysis at high temperatures for a short time is one of the feasible methods for adsorbent preparation as it avoids multiple steps ([75–81]). However, energy consumption is higher in pyrolysis. To overcome this problem, multistep drying followed by activation is recommended. Drying of materials reduces moisture, and activation increases porosity and surface areas.

Activation may be performed by using chemicals or other agents. It is performed by mixing the adsorbate and activating agents at a specific loading ratio and concentration of agents. The mixture is agitated at the explicit speed for definite time and temperature. Finally, the mixture is washed to remove excess activating agents and then dried to constant weight.

Cassava peel and bagasse are rich in starch, whereas cassava stem and rhizome are rich in cellulose based on the level of growth. Thioglycolic acid, sulphuric acid, reactive dye, potassium hydroxide, phosphoric acid, nitric acid, mercaptoacetic acid, sodium bicarbonate, sodium hydroxide, oxalic acid, citric acid, zinc chloride, hydrochloric acid, titanium dioxide, hydroxylamine hydrochloride, ammonium persulphate, hydrogen peroxide, ferric chloride, ferrous sulphate, silver nitrate, epichlorohydrin, pyridine, ethylenediaminetetraacetic acid, magnetite, zinc oxide, chloromethyl hydroxyquinoline are reported to be utilized as activating agents for cassava-based materials. Magnetite and titanium dioxide were used to improve the magnetic and photocatalytic properties of cassava substances.

Tejada-Tovar et al. [68] examined the removal of hexavalent chromium using raw cassava peel powder and by activating with citric acid. The percentage removal has been increased from 54.3% for raw powder to 56.2% for activated materials. Being a tricarboxylic acid, citric acid does not exhibit significant removal upon activation.

Rubio et al. [70] examined the consequence of acid and alkali activation on cassava bark residue particles of varied sizes. Mesh numbers 20, 30, and 40 were cast off to examine the outcome of particle sizes of cassava bark residue for the removal of methylene blue dye. Mesh number 20 produced significant dye removal of 88.5% against 87.7 and 88.8%, respectively, for mesh numbers 30 and 40. 0.1 M sulphuric acid and sodium hydroxide were used as activation agents to remove dye at 85.6 and 94.2%, respectively. 0.1 M sodium hydroxide was found to be an effective activating agent for cassava bark residue to remove methylene blue dye.

Table 1: Effect of parameters on adsorption using cassava residues as adsorbents.

| Adsorbate | Adsorbent | pH | Time (min) | Dosage (g/L) | Initial concentration (ppm) | Temperature (K) | Agitation speed (rpm) | Particle size | Reference |
|---|---|---|---|---|---|---|---|---|---|
| *Metal ions* | | | | | | | | | |
| Chromium | Cassava peel carbon (CPC) | 3–6 (3) | 5–180 | 0.02 | 10–60 (10) | 288.15–328.15 (328.15) | 300 | 40–63 $\mu$m | [7] |
| Cobalt | Cassava peel carbon (CPC) | 3–6 (6) | 5–180 | 0.02 | 10–60 (10) | 288.15–328.15 (318.15) | 300 | 40–63 $\mu$m | [7] |
| Chromium | Cassava peel carbon | 2–12 (6) | 5–180 (40) | 0.02 | 10–40 (35) | 298 | 300 | 40–63 mm | [7] |
| Nickel | Cassava peel | 1–9 (4.5) | 30–60 | 0.1–10 (0.5) | 200 | 333 | 200 | 125–750 mm | [5] |
| Lead | Cassava root husk | 4 | 2 | 0.1 | 0.5 | 298 | 240 | 50 $\mu$m | [6] |
| Copper | Cassava root husk | 4 | 25 | 1 | 0.5 | 298 | 240 | 50 $\mu$m | [6] |
| Chromium | Cassava peel modified by citric acid | 2–6 (2) | 120 | 0.5 | 100 | 298 | 150 | 0.355 nm | [68] |
| Mercury | Mod. cassava peel | 6 | 10–330 | 0.5 | 25–100 (100) | 298 | 150 | 0.355–0.5 mm | [72] |
| *Dyes* | | | | | | | | | |
| Malachite green | Cassava rind carbon (CRC) | 3–9 (7) | 180 | 5 | 150 | 298 | 300 | 40–63 $\mu$m | [73] |
| Metanil yellow | Cassava peel | 3–10 (8) | 30–1440 (480) | 0.5–7 (3) | 30–400 (125) | 298 | 150 | 0.125–0.710 (0.125 mm) | [56] |
| *Other pollutants* | | | | | | | | | |
| Norfloxacin | Cassava dreg biochar BC 350, pyrolysis at 350 K | 3–9 (6) | 480 | 0.5 | 10 | 298 | 200 | 0.45 $\mu$m | [54] |
| Norfloxacin | Cassava dreg biochar BC 450, pyrolysis at 450 K | 3–9 (6) | 480 | 0.5 | 10 | 298 | 200 | 0.45 $\mu$m | [54] |
| Norfloxacin | Cassava dreg biochar BC 550, pyrolysis at 550 K | 3–9 (6) | 480 | 0.5 | 10 | 298 | 200 | 0.45 $\mu$m | [54] |
| Norfloxacin | Cassava dreg biochar BC 650, pyrolysis at 650 K | 3–9 (6) | 480 | 0.5 | 10 | 298 | 200 | 0.45 $\mu$m | [54] |
| Norfloxacin | Cassava dreg biochar BC 750, pyrolysis at 750 K | 3–9 (6) | 480 | 0.5 | 10 | 298 | 200 | 0.45 $\mu$m | [54] |
| Nitrate | Modified cassava straw | 2–12 (7) | 30 | 0.01–1.0 (0.2) | 25–75 mg/dm$^3$ | 293 | 120 | 150–200 $\mu$m | [64] |

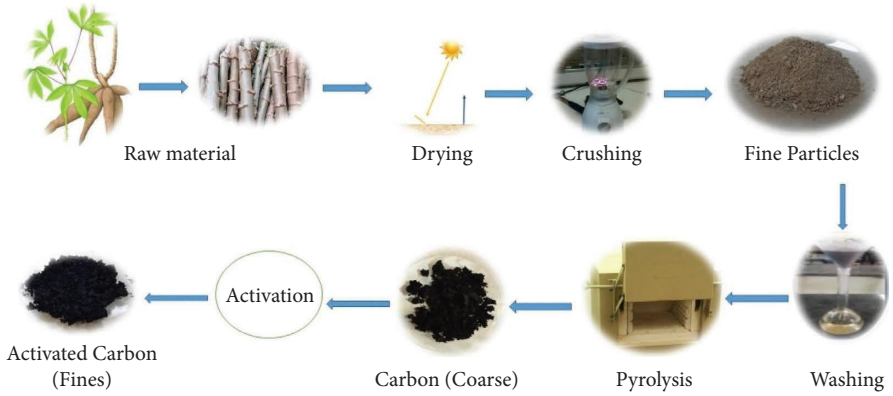


Figure 3: Preparation of adsorbents and activation methods.

Tri Widayati et al. [82] studied the removal of the total suspended solid present in batik liquid waste by using inactivated cassava peel carbon and activating carbon by 0.1 M hydrochloric acid and 1.0 M sodium hydroxide. They observed a decrease in the total suspended solid for the activating agent (hydrochloric acid) with an adsorption percentage of 47.83%, whereas with the activating agent (sodium hydroxide), the percentage of adsorption was 34.84%, and then, without the activating agent, the percentage of adsorption was found to be 28.57%.

Ndongo et al. [83] examined the synthesis and characterization of ferric chloride-activated cassava peel.

Table 2 summarizes several activation methods reported for adsorbent preparation from cassava residues.

## 4. Adsorption Isotherms

The adsorption isotherm is cast off to explain the interactions between adsorbates and adsorbents at the point of equilibrium [108] (Figure 4).

### 4.1. One-Parameter Isotherm Model

*4.1.1. Henry's Isotherm Model.* Henry's adsorption isotherm model is the most straightforward one since the partial pressure of the gas, which is being adsorbed, is proportional to the quantity of the surface adsorbate [109]. Henry's model offers an excellent fit for the sorption of the adsorbate at lower concentrations in most cases, while entire adsorbate substances are separated from one another. As a result, the following linear formula is used in Equation (1) to represent the concentrations of the used adsorbate in equilibrium conditions in the liquid phase (Ce) in addition to the adsorbed phases.

$$q_e = K_{HE} C_e, \tag{1}$$

where $k_{\mathrm{HE}}$ is Henry's constant.

### 4.2. Two-Parameter Isotherm Models

*4.2.1. Langmuir Isotherm Model.* The original purpose of this isotherm model for adsorption was to explain the sorption of gases onto solid-phase adsorbates, such as activated carbon. The process of molecules adhering to a solid surface, according to Langmuir, is centered on a kinetic concept in which there is continual bombarding of particles onto the surface and matching desorption or evaporating of particles from the interface with the zero rate of the accumulation at the substratum [110]. In other words, the rates of adsorption and desorption ought to be equal. The adsorption capabilities of various adsorbents have typically been evaluated and compared using the Langmuir isotherm model.

An empirical model called the Langmuir isotherm assumes that adsorbed coating is almost equal to one molecule level thick (monolayer adsorption) and that the process of adsorption takes place at equivalent, identical, and clearly localized spots. Even on adjacent sites, there should not be any sideway interaction or steric hindrance among the experimented adsorbed layer of molecules. This isotherm model presupposes that the phenomenon of adsorption is homogeneous and that separated molecules have sorption activation energy and constant enthalpies [111]. There should be no adsorbate migration in the superficial plane and equal adsorbate affinities at all sites. According to Langmuir theory, there is a connection between increasing distance and a sharp decline in attractive forces between molecules. The equation derived from the Langmuir isotherm can be improved for adsorption of an aqueous phase as given in the equation.

$$q_e = q_m \frac{K_L C_e}{1 + K_L C_e}, \tag{2}$$

where $q_m$ and $K_L$ are the maximum adsorption capacity and Langmuir constant, respectively.

The isotherm equation becomes Henry's law isotherm at small concentrations and low pressure. Pressure causes the amount of adsorbed material to increase linearly, and when the pressure is strong enough to cover a monolayer, the capacity of saturation of the quantity of adsorbed material is attained. Due to their strong attraction for one another, a greater affinity constant (b) results in extra surface exposure with the adsorbate particle [112]. The affinity constant decreases as the temperature ($T$) rises because the adsorption process is exothermal. For the adsorption

Table 2: Activation methods reported in the literature for adsorbent preparation from cassava residues.

| Adsorbate | Adsorbent | Activation | Outcomes | Reference |
|---|---|---|---|---|
| *Metal ions* | | | | |
| Cadmium | Thioglycolic acid-modified cassava fibre (MCF) | Chemical: 0.5 M and 1.0 M and thioglycolic acid modified | 0.5 M MCF = 53.66% & 1.0 M MCF = 58.66% | [55] |
| Lead | Cellulose nanocrystal from cassava peel | Acid hydrolysis with 64% sulphuric acid | 6.4 mg/g | [84] |
| Copper and zinc | Undyed cassava mesocarp (UDCM) and dyed cassava mesocarp (DCMI: 0.40 mm and DCMII: 0.63 mm) | Reactive dye | Copper: UDCP = 63 DCMI = 375.5 DCMII = 224/Zinc: UDCP = 12 DCMI = 34 DCMII = 21 | [85] |
| Nickel | Activated carbon from cassava peel tubers | Alkali activation (87.9% KOH)/ACPH | 51.81 mg/g | [51] |
| Nickel | Activated charcoal from cassava peel tubers | Acid activation (phosphoric acid 85%)/ACPA | 51.86 mg/g | [51] |
| Nickel | Activated carbon from cassava peel tubers | Nonimpregnated carbon (NIC) | 48.86 mg/g | [51] |
| Copper | Modified cassava fibre | Acid activation (0.3 M nitric acid) + 0.5 M mercaptoacetic acid-0.5 MCF | 20.33% | [86] |
| Copper | Modified cassava fibre | Acid activation (0.3 M nitric acid) + 1.0 M mercaptoacetic acid-1.0 MCF | 21.00% | [86] |
| Cadmium | Cassava starch-based super adsorbent polymer | Copolymerization | 374.7 mg/g | [87] |
| Chromium | Cassava peel carbon (CPC) | Acid (phosphoric acid)/alkali ($NaHCO_3$) | 166.33 mg/g | [7] |
| Cobalt | Cassava peel carbon (CPC) | Acid(phosphoric acid)/alkali ($NaHCO_3$) | 301.63 mg/g | [7] |
| Chromium | Cassava peel carbon | Phosphoric acid (1 : 1) before carbonisation + 1% $NaHCO_3$ after carbonisation | 166.35 mg/g | [7] |
| Cobalt | Cassava peel carbon | Phosphoric acid (1 : 1) before carbonisation + 1% $NaHCO_3$ after carbonisation | 301.63 mg/g | [7] |
| Chromium | Cassava peel | 1.5 M $HNO_3$ | 61.72% | [88] |
| Tartrazine | Cassava sievate | 85% $H_3PO_4$ (1 : 1) | 20.83 mg/g | [89] |
| Zinc | Cassava peel | HCl/0.5/1.0/1.5 M | 7.8%/2.1%/1.1% | [90] |
| Copper | Cassava peel | HCl/0.5/1.0/1.5 M | 298%/17.2%/18.4% | [90] |
| Iron | Cassava peel | HCl/0.5/1.0/1.5 M | 55.4%/43.4%/61.4% | [90] |
| Lead | Cassava peel | HCl/0.5/1.0/1.5 M | 80%/20%/100% | [90] |
| Zinc | Cassava peel | $ZnCl_2$/0.5/1.0/1.5 M | 2.3%/2.6%/2.3% | [90] |
| Copper | Cassava peel | $ZnCl_2$/0.5/1.0/1.5 M | 50.6%/60.5%/35.6% | [90] |
| Iron | Cassava peel | $ZnCl_2$/0.5/1.0/1.5 M | 88%/89.1%/67.5% | [90] |
| Lead | Cassava peel | $ZnCl_2$/0.5/1.0/1.5 M | 100%/100%/20% | [90] |
| Chromium | Cassava sludge-activated carbon | $ZnCl_2$ (sludge: $ZnCl_2$ ratio = 1 : 5) | 98.22% | [91] |
| Lead | Cassava biomass modified with $TiO_2$ nanoparticles | $TiO_2$ | 99.84% | [92] |
| Nickel | Cassava biomass modified with $TiO_2$ nanoparticles | $TiO_2$ | 81.51% | [92] |
| Cadmium | Untreated cassava peel biomass/ acid-treated cassava peel biomass | 0.5 M and 1.0 M thioglycolic acid treated | 86.68 mg/g/647.48 mg/g | [11] |
| Zinc | Untreated cassava peel biomass/ acid-treated cassava peel biomass | 0.5 M and 1.0 M thioglycolic acid treated | 55.52 mg/g/559.74 mg/g | [11] |
| Cadmium | Unmodified cassava tuber bark/ acid-modified cassava tuber bark | 0.5 M and 1.0 M thioglycolic acid treated | 2.69 mg/g/11.48 mg/g/5.98 mg/g | [93] |

Table 2: Continued.

| Adsorbate | Adsorbent | Activation | Outcomes | Reference |
|---|---|---|---|---|
| Copper | Unmodified cassava tuber bark/ acid-modified cassava tuber bark | 0.5 M and 1.0 M thioglycolic acid treated | 11.48 mg/g/14.88 mg/g/28.49 mg/g | [93] |
| Zinc | Unmodified cassava tuber bark/ acid-modified cassava tuber bark | 0.5 M and 1.0 M thioglycolic acid treated | 11.48 mg/g/14.86 mg/g/37.88 mg/g | [93] |
| Copper from single-ion solution/wastewater | Unmodified cassava tuber bark/ acid-modified cassava tuber bark | 1.0 M thioglycolic acid (ratio: 25 g : 250 ml) | Untreated: 71.3 mg/g acid treated: 85.2 mg/ g | [52] |
| Zinc from single-ion solution/wastewater | Unmodified cassava tuber bark/ acid-modified cassava tuber bark | 1.0 M thioglycolic acid (ratio: 25 g : 250 ml) | Untreated: 43.4 mg/g acid treated: 58.1 mg/ g | [52] |
| Zinc | Cassava peel carbon | Impregnated with $ZnCl_2$ | 28% | [12] |
| Nickel | Cassava peel carbon | Impregnated with $ZnCl_2$ | 66.60% | [12] |
| Cadmium | Cassava peel carbon | Impregnated with $ZnCl_2$ | 50% | [12] |
| Copper | Modified cassava starch | Hydroxylamine hydrochloride | 75.76 mg/g | [60] |
| Lead | Modified cassava stalk | EDTAD + $Fe_3O_4$ | 163.93 mg/g | [94] |
| Zinc | Modified cassava stalk | EDTAD + $Fe_3O_4$ | 84.74 mg/g | [94] |
| Pb/refinery wastewater | Unfermented cassava peel carbon | 11.0 M $ZnCl_2$ | 95% | [95] |
| Cu/refinery wastewater | Unfermented cassava peel carbon | 1.0 M $ZnCl_2$ | 80% | [95] |
| Fe/refinery wastewater | Unfermented cassava peel carbon | 1.0 M $ZnCl_2$ | 70% | [95] |
| Pb/refinery wastewater | Fermented cassava peel carbon | 1.0 M $ZnCl_2$ | 100% | [95] |
| Cu/refinery wastewater | Fermented cassava peel carbon | 1.0 M $ZnCl_2$ | 94% | [95] |
| Fe/refinery wastewater | Fermented cassava peel carbon | 1.0 M $ZnCl_2$ | 74% | [95] |
| Pb/refinery wastewater | Commercially activated carbon | 1.0 M $ZnCl_2$ | 57% | [95] |
| Cu/refinery wastewater | Commercially activated carbon | 1.0 M $ZnCl_2$ | 76% | [95] |
| Fe/refinery wastewater | Commercially activated carbon | 1.0 M $ZnCl_2$ | 56% | [95] |
| Cadmium | Cassava peel biochar | 300°C/activated by 1.63 M KOH | 84% | [96] |
| Chromium | Cassava peel modified by citric acid | 0.6 M citric acid | 54% (raw) and 56% (citric acid modified) | [68] |
| Cadmium | Modified cassava peel | By 0.1 mol/L of NaOH (99%) | 19.54 mg/g | [97] |
| Chromium | Modified cassava peel | By 0.1 mol/L of NaOH (99%) | 42.46 mg/g | [97] |
| Chromium | Modified cassava peel | By 0.1 mol/L of $H_2O_2$ (36%) | 43.97 mg/g | [97] |
| Copper | Grafted cassava starch | Grafting cassava starch with 5-chloromethyl-8-hydroxyquinoline | 28.75 mg/g | [98] |
| Lead | Grafted cassava starch | Grafting cassava starch with 5-chloromethyl-8-hydroxyquinoline | 46.512 mg/g | [98] |
| Copper | Cassava peel act. by 0.3 m $HNO_3$ | Cassava peel act. by 0.3 m $HNO_3$ | 55.19% | [69] |
| Zinc | Cassava peel act. by 0.3 m $HNO_3$ | Cassava peel act. by 0.3 m $HNO_3$ | 41.70% | [69] |
| Mercury | Mod. cassava peel | By 0.6 M citric acid | 72.98% | [72] |
| Chromium | Cassava peel | Unmodified | 54.33% | [68] |
| Chromium | Cassava peel | By 0.6 M citric acid | 56.20% | [68] |
| Arsenic | Root husks of cassava nanoparticles loaded by using ZnO | ZnO | 39.52 mg/g | [99] |
| Cadmium | Root husks of cassava nanoparticles loaded by using ZnO | ZnO | 4205 mg/g | [99] |
| Lead | Root husks of cassava nanoparticles loaded by using ZnO | ZnO | 44.27 mg/g | [99] |
| Chromium | Root husks of cassava nanoparticles loaded by using ZnO | ZnO | 28.37 mg/g | [99] |
| Lead | Cassava peel carbon | 2 M $H_3PO_4$ | 96.83% | [59] |

Table 2: Continued.

| Adsorbate | Adsorbent | Activation | Outcomes | Reference |
|---|---|---|---|---|
| *Dyes* | | | | |
| Methylene blue | Modified cassava peel | Acid activation (phosphoric acid 85%) | 99.98%/79.975 mg/g | [100] |
| Methylene blue | Cassava peel biochar | Acid activation (phosphoric acid 14%) | 4.75 mg/g | [101] |
| Rhodamine B | Activated charcoal from cassava peel | Thermal (700°C)/chemical (phosphoric acid 1 : 1 ratio | 100%/100% | [102] |
| Direct brown | Activated charcoal from cassava peel | Thermal (700°C)/chemical (phosphoric acid 1 : 1 ratio | 10.35%/100% | [102] |
| Procion orange | Activated charcoal from cassava peel | Thermal (700°C)/chemical (phosphoric acid 1 : 1 ratio | 5.3%/100% | [102] |
| Acid violet | Activated charcoal from cassava peel | Thermal (700°C)/chemical (phosphoric acid 1 : 1 ratio | 83.0%/86.32% | [102] |
| Malachite green | Activated charcoal from cassava peel | Thermal (700°C)/chemical (phosphoric acid 1 : 1 ratio | 100%/100% | [102] |
| Methylene blue | Activated charcoal from cassava peel | Thermal (700°C)/chemical (phosphoric acid 1 : 1 ratio | 100%/100% | [102] |
| Naphthol blue black | Activated charcoal from cassava peel | Acid activation (60% phosphoric acid) | 99.70% | [103] |
| Dye from printing industry wastewater | Activated charcoal from cassava peel | Acid activation (20% sulphuric acid) | 96.78% | [71] |
| Malachite green | Cassava rind carbon (CRC) | Acid (phosphoric acid 1 : 1 ratio)/alkali (NaOH 1 M) | 932.975 mg/g | [73] |
| Methylene blue | Cassava rind carbon (CRC) | Acid (phosphoric acid 1 : 1 ratio)/alkali (NaOH 1 M) | 565 mg/g | [53] |
| Reactive red + Drimarene turquoise | Cassava stem biochar (CSB) | Acid/oxalic acid (1%) | 88.40% | [61] |
| Sunset yellow | Cassava sievate | 85% $H_3PO_4$ (1 : 1) | 0.091 mg/g | [89] |
| Malachite green | Cassava peel carbon | Act. by (0.5 N $AgNO_3$) | 93% | [8] |
| Malachite green | Cassava peel carbon | Act. by ($H_2SO_4$) | 82.70% | [8] |
| Reactive dye | AC from cassava peel impregnates with $AgNO_3$/ | AC from cassava peel impregnates with $AgNO_3$ (1%)/ 4 N $H_2SO_4$/4 N NaOH | 90% ($AgNO_3$ impregnated) | [41] |
| Methylene blue | Cassava bark residue (raw/mod. $H_2SO_4$/ NaOH (20, 30, and 40 mesh size) | 0.1 M $H_2SO_4$ and NaOH | 88% (20 mesh no) 87.7% (30 mesh no) 88.5 (40 mesh no) 94.2% (alkali-activated 20 mesh no) | [70] |
| Methylene blue | Cassava leaf powder | By 95% ethanol | 99.90% | [104] |
| *Other pollutants* | | | | |
| Tartrazine | Cassava sievate | 85% $H_3PO_4$ (1 : 1) | 20.83 mg/g | [89] |
| Nitrate | Modified cassava straw | Epichlorohydrin and pyridine | 2.14 mM/$dm^3$ | [64] |
| Glucose | Carbon from cassava stems | KOH 1 : 2 w/w | 3.33 mg/g | [105] |
| Cholesterol | Carbon from cassava stems | KOH 1 : 2 w/w | 6.84 mg/g | [105] |
| COD/refinery wastewater | Unfermented cassava peel carbon | 1.0 M $ZnCl_2$ | 64% | [95] |
| BOD/refinery wastewater | Unfermented cassava peel carbon | 1.0 M $ZnCl_2$ | 83% | [95] |
| Phenol/refinery wastewater | Unfermented cassava peel carbon | 1.0 M $ZnCl_2$ | 93% | [95] |
| COD/refinery wastewater | Fermented cassava peel carbon | 1.0 M $ZnCl_2$ | 73% | [95] |
| BOD/refinery wastewater | Fermented cassava peel carbon | 1.0 M $ZnCl_2$ | 86% | [95] |
| Phenol/refinery wastewater | Fermented cassava peel carbon | 1.0 M $ZnCl_2$ | 96% | [95] |
| COD/refinery wastewater | Commercially activated carbon | 1.0 M $ZnCl_2$ | 55% | [95] |
| BOD/refinery wastewater | Commercially activated carbon | 1.0 M $ZnCl_2$ | 72% | [95] |
| Phenol/refinery wastewater | Commercially activated carbon | 1.0 M $ZnCl_2$ | 83% | [95] |
| Nitrate | Cassava peel carbon | $ZnCl_2$ (1 : 1, 1 : 3 and 2 : 3) | 81.6%(1 : 1 $ZnCl_2$) | [106] |
| Phenol | Cassava peel carbon act. by $ZnCl_2$ | 0.75 : 1 ($ZnCl_2$: cassava peel ratio) | 16.67 mg/g | [107] |
| TSS of Bakaran batik | Cassava peel carbon | Raw | 28.57% | [82] |
| TSS of Bakaran batik | Cassava peel carbon | 0.1 M HCl | 47.83% | [82] |

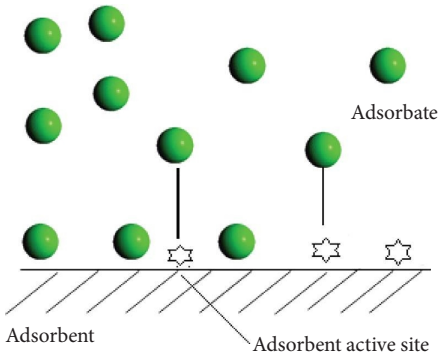


Figure 4: Adsorption isotherm explaining interactions between adsorbates and adsorbents.

procedure to take place, free energy ($\Delta G$) reduces, and the reduction in the degrees of freedom is found to be negative conversion for the entropy ($\Delta S$); thus, equation (3) is

$$\Delta H = \Delta G + T\Delta S < 0. \quad (3)$$

Enthalpy ($H$) negativity shows that heat was released throughout the adsorption process. Analogous to this, raising the heat of adsorption causes a rise in the quantity of surfactant adsorption, which means that the energy barrier for molecules to recover to the gas phase is larger. Because the molecules adsorbed require more energy to evaporate at higher temperatures, the amount of adsorbed material at a specific pressure falls as temperature increases.

Since sediments are in the form of heterogeneous adsorbents with dissimilar adsorption energies at every location, as well as the Langmuir model presumes a surface of homogeneous adsorbents with similar adsorption energies for each site, there are some shortcomings in the Langmuir isotherm model's explanation of how toxicant sediments facilitate adsorption. However, Henry's adsorption isotherm approach is thought to be the most straightforward one since the partial pressure of the adsorbing gas is proportional to the number of surface adsorbates, as per [109]. When all adsorbate molecules are kept apart from one another, Henry's model typically offers an excellent fit for the adsorption of adsorbates at small doses. Furthermore, the separation factor ($R_L$) is defined as a dimensionless constant which is represented in the equation.

$$R_L = \frac{1}{1 + K_L C_O}, \quad (4)$$

where $C_o$ is the initial concentration of the adsorbate expressed in mg/L and $K_L$ is the adsorption capacity expressed in mg/g. Variations in the appropriate area and the adsorbent's porosity can be associated with the $K_L$ constant, suggesting that larger surface areas and pore volumes can lead to increased adsorption capacities. The separation factor reveals the kind of adsorption, which might be linear ($R_L = 1$), irreversible ($R_L = 0$), unfavourable ($R_L > 1$), or advantageous ($0 < R_L < 1$).

The Langmuir isotherm model fitted well for adsorption of malachite green by cassava rind carbon [53], cadmium, copper and zinc on cassava tuber bark [93], lead and zinc on modified cassava stalk [94], cadmium, zinc, and chromium on modified cassava peel, lead on grafted cassava starch [113], mixed dye of reactive red and Drimarene turquoise on cassava stem biochar [61], chromium, cobalt on cassava peel carbon [7], and ciprofloxacin on cassava dreg biochar at various pyrolysis temperatures ranging from 350–750 K [114].

*4.2.2. Freundlich Isotherm Model.* The Freundlich adsorption isotherm model describes the reversible cycle and the nonideal adsorption process. The Freundlich model, in contrast to the Langmuir isotherm model, is relevant to multilayer adsorption and is not restricted to monolayer creation. In this isotherm model, the heat of adsorption and affinities do not necessarily need to be distributed equally across the heterogeneous surface. The Freundlich isotherm model formulation defines surface heterogeneity and thus the exponential distribution of the active sites and active site energy [115]. For the adsorption of animal charcoal, the Freundlich isotherm adsorption concept was developed in the past. It demonstrated that, at different solution concentrations, the amount of solute that could be adsorbed on a given mass of a specific adsorbent was not constant.

The adsorbed amount in this instance is calculated by adding the amount of adsorption at each site. Stronger binding sites will first be occupied, and once the adsorption process is complete, the adsorption energy will begin to fall exponentially. The Freundlich isotherm model is now extensively cast off in heterogeneous irregular systems, for example, the adsorption of extremely interacting organic chemicals or species on molecular sieves or activated carbon. For systems with heterogeneous surfaces in the gas phase, this adsorption isotherm model is suitable. Due to this isotherm's inappropriate behaviour towards Henry's law at low pressure, it offers a constrained range of pressure. It does not have a finite limit when the pressure is high enough. This adsorption isotherm model therefore only applies to the limited amount of adsorption data. The nonlinearized form of the Freundlich model is given in the equation.

$$q_e = K_F C_e \frac{1}{n}. \quad (5)$$

The data of $n$, where $K_F$ and $n$ parameters are influenced by temperature, serve as an identifier of the type of isotherm. The strength of the adsorption process or heterogeneity of the surface, $1/n$, indicates the relative distribution of energy and the heterogeneity of the location of adsorbates. The adsorption process is favourable when $1/n$ is greater than zero ($0 < 1/n < 1$), unfavourable when $1/n$ is greater than 1, and irreversible when $1/n = 1$. The fact that pressure or concentration must drastically reduce to a low value prior to desorption of adsorbate molecules from the surface explains why the isotherm is irreversible [116].

The Freundlich isotherm model fitted well for adsorption of norfloxacin at various pyrolysis temperatures ranging from 350–750 K [54], nickel on cassava peel [5], and rhodamine on cassava slag carbon [57].

*4.2.3. Dubinin–Radushkevich (D–R) Isotherm Model.* For explaining the mechanism of adsorption with the distribution of Gaussian energy onto heterogeneous surfaces, the D–R adsorption isotherm model is typically utilized. The description of the adsorption of gases and vapours on microporous sorbents like activated carbon and zeolites typically uses this model. Due to the unrealistic asymptotic behaviour that is displayed, this model was successful in fitting the high solute activity and the intermediate adsorbate concentration range [117]. When pressure is low, the D–R isotherm model does not, however, predict Henry's law.

The D–R model is a semiempirical equation in contrast to Langmuir and Freundlich isotherm models, where the adsorption of this model follows the mechanism of pore filling. This model's underlying presumption is that it may be applied to physical adsorption processes and has a multilayer character that involves Van der Waals forces. This isotherm model is typically used to differentiate between the chemical and physical adsorption of metal ions. Temperature affects the D–R isotherm model. It is regarded as a defining and distinctive characteristic; as a result, when the potential energy square is plotted against the logarithm of the adsorbed amount, the appropriate data will form the characteristic curve, on which it is located. The D–R isotherm model has nonlinear form as given in the equation.

$$q_e = q_s e^{-K\varepsilon^2}. \tag{6}$$

In addition, where $P_s$ is the saturation vapour pressure (atm) and $P$ is the adsorbate equilibrium pressure (atm), the following equation can be used to calculate: (atm). A fundamental need for using the D–R isotherm model is accurately estimating the adsorption potential ($\varepsilon$). Following the adsorption of a unit of molar mass of the used adsorbate, it reflects the Gibbs free energy change of adsorbents. This isotherm model has been expanded to include the adsorption in the aqueous phase.

The Dubinin–Radushkevich isotherm model fitted well for adsorption of crystal violet on raw cassava peel [63] and mixed dye of reactive red and Drimarene turquoise on cassava stem biochar [61].

*4.2.4. Temkin Isotherm Model.* The Temkin empirical isotherm model was initially used to describe the chemisorption system known as hydrogen adsorption over platinum electrodes in an acidic solution. This isotherm model ignores extremely high and extremely low concentration values while considering the interaction between the adsorbent and the adsorbate. This model implies that, as surface coverage increases, the adsorption heat ($H_{\text{ads}}$) of all molecules in the layer drops linearly rather than logarithmically as a function of temperature [118]. Only an intermediate concentration range can be used with this adsorption isotherm model. Like the isotherm models presented above, the Temkin model has a nonlinear form as given in the equation.

$$q_e = \frac{RT}{b_T} \ln A_T C_e. \tag{7}$$

Both the $A_{\text{T}}$ and $b_T$ constants can be determined by displaying $q_e$ vs. ln ($C_e$). This model is quite good at forecasting the equilibrium of the gas phase, assuming that it is not necessary for it to be arranged in a tightly packed structure with the same orientation. Its equation implies that binding energies are equally distributed. On the other hand, the presentation of complicated adsorption systems, such as aqueous phase adsorption isotherms, does not suit this isotherm model.

*4.2.5. Flory–Huggins Isotherm Model.* The solution theory of the Flory–Huggins equation provides a straightforward yet effective mathematical model for the thermodynamics of polymer mixtures. Entropy and enthalpy are combined to create the dissolution process, which may then be explained using the Flory–Huggins equation. According to this theory, solvent molecules occupy single sites, whereas polymer segments occupy lattice sites [119]. This premise allows for the calculation of the entropy of long-chain mixed compounds.

The kind and extent of the adsorbate's surface coverage on the adsorbent are considered by this isotherm adsorption model. Regarding the viability and spontaneity of the process, the Flory–Huggins isotherm model characterizes the nature of the adsorption process. The equation displays the nonlinear equations for this adsorption isotherm model. The parameters $\theta$ and $C_o$ can be determined by using a nonlinear form as

$$\frac{\theta}{C_O} = F_{FH}(1-\theta)^{n_{FH}}. \tag{8}$$

In this context, $n_{\text{FH}}$ stands for the number of metal ions that occupy the adsorption sites on two membranes and ($\theta$) represents the degree of surface coverage. The adsorption equilibrium constant is $K_{\text{FH}}$ as well. The spontaneous free Gibbs energy is typically calculated using it as it is related to the following expression:

$$\Delta G^o = -RT \ln K_{FH}. \tag{9}$$

*4.2.6. Hill Isotherm Model.* The requisite of various types of substrates which are homogeneous in nature is explained by the adsorption isotherm model. The adsorbate's capacity to attach at the single site on the surface of adsorbents may be impacting other binding sites on the same adsorbent, according to the isotherm model, which assumes that adsorption is a cooperative occurrence [120]. The nonlinear representation as well as the form of this isotherm model is stated as

$$q_e = \left[\frac{q_{SH} \cdot C_e^{nH}}{K_D + C_e^{nH}}\right]. \tag{10}$$

*4.2.7. Halsey Isotherm Model.* The multilayer adsorption system is evaluated by this adsorption isotherm, which also describes how it condenses at a significant distance from the

surface. Similar to the Freundlich isotherm model, the Halsey model is appropriate for multilayer adsorption and heterogeneous surfaces with nonuniformly distributed adsorption heat [121]. The nonlinearized form is

$$q_e = e^{\left(\ln K_H - \ln C_e\right)/n_H}, \tag{11}$$

where $k_H$ and $n_H$ are the Halsey constant and exponent, respectively.

*4.2.8. Jovanovic Isotherm Model.* The Langmuir isotherm model has all the underlying hypotheses for this model, plus the potential addition of mechanical contact between the molecules that are adsorbing and desorbing. The Jovanovic model's adsorption surface is taken into account, although its equation is frequently discared in physical analysis of adsorption for both mobile and single layer adsorption with no lateral interactions [122]. When the concentration is high, this model's equation can spread the saturation limit; once the concentration is small, Henry's law replaces it. The nonlinearization form is

$$q_e = q_{\max}\left(1 - e^{K_J C_e}\right), \tag{12}$$

where $K_J$ is the Jovanovic constant (L/g).

*4.2.9. BET (Brunauer–Emmett–Teller) Isotherm and Changed BET Isotherms.* The equilibrium of gas-solid systems is where the Brunauer–Emmett–Teller hypothetical isotherm equation is utmost useful. The invention of the BET isotherm led to the creation of multiple layer adsorption schemes through comparative pressures between 0.06 and 0.34, which resemble a single-layer treatment between 0.5 and 1.50 [123]. This approach is frequently used to calculate the binding energy of the present state. The simplified form is given in Equation (13) as both $C_{BET}$ and $C_{BET}(C_e/C_s)$ are greater than 1.

$$q_e = \frac{q_s}{1 - C_e/C_s}. \tag{13}$$

This model is prolonged towards the interface of liquid-solid, and it is designated as

$$q_e = \frac{q_{mBET} C_{BET} C_e}{\left(C_e - C_s\right)\left[1 + \left(C_{BET} - 1\right)C_e/C_s\right]}. \tag{14}$$

The BET model is regarded as a particular variety of the Langmuir model. With the addition of additional simplified assumptions, it incorporates the same fundamental assumptions as the Langmuir model; specifically, the second, third, and higher layers all contain the same adsorption energy. This energy is equivalent to the heat from fusion that is not predisposed by the connections among the localized adsorbent in addition to the adsorbate. The energy for the first layer, however, is distinct from that for the remaining layers. The number of layers goes to infinity when the concentration hits the saturation concentration.

*4.3. Three-Parameter Isotherm Models*

*4.3.1. Redlich–Peterson Isotherm Model.* This is a three-parameter amalgam isotherm model that combines the Freundlich and Langmuir isotherm models. This is not the phenomenon of single-layer adsorption because this model combines both concepts. The adaptable Redlich–Peterson isotherm model can be used in both heterogeneous and homogeneous systems. Both the denominator and the numerator of this isotherm model have an exponential function. The equilibrium of the adsorption onto a large range of concentrations is represented by its linear dependency on concentrations [124]. Since the numerator comes from the Langmuir isotherm model, it can get close to the Henry area at infinite dilution.

The nonlinear equation of this isotherm model is represented as

$$q_e = \frac{K_R C_e}{1 + a_R C_e^g}. \tag{15}$$

The expression of the reduced Freundlich model used in higher concentrations is given as

$$q_e = \frac{K_R}{a_R} C_e^{1-\beta}, \tag{16}$$

where $(1-\beta) = 1/n$ of the Freundlich isotherm model and $K_R/a_R = K_F$ are used. However, when $\beta = 1$, $a_R = b$, and $K_R = \text{bQ}\square$ it reduces to the Langmuir equation, and when $\beta = 0$ and Henry's constant is represented by $1/(1+b)$, it reduces to the Henry equation.

To solve the equations, this isotherm model uses a minimized approach. It increases the coefficient of correlation between the theoretical model's predictions and the data points from the experiment. Regarding the limitations, this model is consistent with the high concentration limit of the Freundlich isotherm model, where the exponent tends to be zero, and it approaches the ideal Langmuir condition at the low concentration limit when values are close to one.

The Redlich–Peterson isotherm model fitted well for adsorption of chromium and cobalt on cassava peel carbon [7] and methylene blue on cassava rind carbon [53].

*4.3.2. Toth Isotherm Model.* The objective of this type of isotherm model, an empirically changed version of the most familiar model derived from the Langmuir equation, is to lessen the predicted error between the data of the investigational result and the data predicted by the model. This isotherm model is mostly used to define the system of heterogeneous adsorption that fulfils equally small and large concentrations of adsorbates [125]. The nonlinear form of this isotherm model can be expressed as

$$q_e = \frac{K_T C_e}{\left(a_T + C_e\right)^{(1/t)}}. \tag{17}$$

When $t = 1$, the equation becomes the Langmuir isotherm equation. As a result, $(t)$ is a parameter that represents the adsorption system's heterogeneity; the adsorption system is

regarded as heterogeneous when ($t$) is not equal to unity. Due to the independent relationship between temperature and the parameter $t$, the increasing temperature also causes a quick increase in $a_T$.

At low concentrations, the Toth equation simplifies to Henry's law, whereas at high concentrations, the Langmuir isotherm model approaches a finite capacity more slowly. This isotherm model is frequently used to describe the adsorption of different gases and vapours of organic substances. Additionally, the Toth isotherm model equation is seen as superior to the Sips equation in that it can describe the behaviour of the data at both high and low concentrations.

This isotherm model's slope has a constant limit at zero loading, but it begins to decline at given loading at a pace that is far faster than that of the Langmuir equation. This is explained by the heterogeneity's impact, which is reflected by the parameter $t$. Physically, molecules prefer to bind to high-energy sites, and as the adsorption process advances, molecules bind to locations with lower energies. This results in a slower increase in the adsorbed amount vs. pressure compared to that predicted by the Langmuir equation.

*4.3.3. Sips Isotherm Model.* The Sips isotherm model, which is derived to forecast the heterogeneity of adsorption systems and get over the restrictions connected with the rising concentrations of the adsorbate of the Freundlich model, was created by combining the Langmuir and Freundlich isotherm models. As a result, at high concentrations, an expression with a finite limit is created [126]. Without adsorbate-adsorbate interactions, the Sips model is valid for localizing adsorption. The Sips equation is given by the following nonlinear expression:

$$q_e = \frac{K_S C_e^{\beta} S}{1 + a_S C_e^{\beta} S}. \tag{18}$$

Due to the reduction to the Freundlich model at low adsorbate concentrations, the Sips isotherm model does not follow Henry's law. On the other hand, it predicts the monolayer adsorption characteristic of the Langmuir model at high adsorbate concentrations. The parameters in the equation are controlled by operating conditions like changes in temperature, pH, and concentration. Both the Freundlich and Sips models have the same drawbacks, in which they fail to provide the correct Henry's law limit when the pressure is low.

*4.3.4. Khan Isotherm Model.* This isotherm model, which represents both the Langmuir and Freundlich models, is a generalized model proposed for the adsorbate adsorption from pure solutions. This isotherm model was created for both single-component and multicomponent adsorption systems [127]. The equation of this model is expressed as

$$q_e = \frac{q_S b_K C_e S}{\left(1 + b_K C_e\right)^{a_K}}. \tag{19}$$

*4.4. Four-Parameter Isotherm Models*

*4.4.1. Fritz–Schlunder Isotherm.* Due to numerous coefficients in the isotherm, the Fritz–Schlunder isotherm is an empirical equation of the Langmuir–Freundlich type that can accommodate a variety of experimental results [128]. The equation of this isotherm model can be expressed as

$$q_e = \frac{q_{mFSS} K_{FS} C_e}{1 + q_m C_e^{MFS}}, \tag{20}$$

where MFS (the equilibrium model of Fritz–Schlunder) decreases to the Freundlich model for large adsorbate concentrations but becomes the Langmuir model if it is = 1. The isotherm parameters can be found via nonlinear regression analysis.

*4.4.2. Baudu Isotherm Model.* The Langmuir isotherm was compacted to the isotherm of Baudu as a result of the observation that determines the coefficients of the equation derived by Langmuir (b and $q_m$); using tangent measuring at different concentrations of the equilibrium reveals that these coefficients, which are derived from the equation, are not at all constants within the broader concentration range [129]. The selected range is between $(1 + x + y) < 1$ and $(1 + x) < 1$; this model is appropriate. When surface coverage is minimal, the Baudu-referred isotherm model is transformed into the isotherm model of Freundlich. To identify the parameters of this isotherm, the nonlinear regression investigation can be utilized in the equation as

$$q_e = \frac{q_m b_0 C_e^{1+x+y}}{1 + b_0 C_e^{1+x}}. \tag{21}$$

*4.4.3. Weber–Van Vliet Isotherm Model.* Weber and van Vliet projected an observed connection through four types of parameters to explain the equilibrium, which results in a variety of adsorption systems shown in the equation:

$$C_e = P_1 q_e^{\left(P_2 q_e^{P_3} + P_4\right)}, \tag{22}$$

where the isotherm parameters $P_1$, $P_2$, $P_3$, and $P_4$ are constants. The multiple nonlinear curve fitting method can predict the isotherm parameters by minimizing the summation of squares of residuals [130].

*4.4.4. Marczewski–Jaroniec Isotherm Model.* The four-parameter general Langmuir equation is another name for this isotherm model. The equation provides an expression for the isotherm equation as follows:

$$q_e = q_{MMJ} \left( \frac{\left(K_{MJ} C_e\right)^{nMJ}}{1 + C_e^{1+x+y}} \right)^{\left(M_{MJ}/n_{MJ}\right)}, \tag{23}$$

where $n_{\mathrm{MJ}}$ and $M_{\mathrm{MJ}}$ are variables describing the heterogeneity of the adsorbent surface. This isotherm model reduces to the Langmuir isotherm if $n_{\mathrm{MJ}}$ and $M_{\mathrm{MJ}}$ are both equal to 1

but to the Langmuir–Freundlich isotherm model if $n_{MJ}$ and $M_{MJ}$ are not equal. Based on the assumption of the local Langmuir isotherm model and the distribution of adsorption energy in the active sites on the adsorbent, this isotherm model is advised [131].

### 4.5. Five-Parameter Isotherm Models

*4.5.1. Fritz–Schlunder Isotherm Model.* A five-parameter observed model for the isotherm has been created that is considered to simulate model variations more accurately for use with a variety of equilibrium sets [128]. This isotherm model is expressed as

$$q_e = \frac{1_m FS_S K_1 C_e^{\alpha_{FS}}}{1 + K_2 C_e^{\beta_{FS}}}. \tag{24}$$

This model approaches the Langmuir isotherm model when $\alpha_{FS}$ and $\beta_{FS} = 1$, but it decreases to the Freundlich isotherm model for larger adsorbate concentrations.

The isotherm models for organic and inorganic pollutant adsorption in water and wastewater are listed in Table 3.

## 5. Adsorption Kinetics

Adsorption kinetics relate the adsorption rate to its capacity. The rate constant is directly related to the change in adsorption capacity with time.

*5.1. Pseudofirst-Order (PFO) Model.* The model of PFO was initially planned by the author of [132]. Equation (25) describes the PFO model's differential form [132]:

$$\frac{dq_t}{dt} = k_1 (q_e - q_t). \tag{25}$$

Integration in Equation (25), for the settings of $q_0 = 0$, produces Equation (26) as follows:

$$q_t = q_e\left(1 - e^{-k_1 t}\right). \tag{26}$$

The nonlinear technique, which can give precise model parameter estimates, is described in the section that follows. The equilibrium adsorption amount planned by the PFO model is the PFO parameter $q_e$. How quickly the adsorption equilibrium is reached is typically expressed using the PFO parameter $k_1$. On the other hand, Equation (1) demonstrates that the adsorption rate $d_{qt}/dt$ is connected to both $k_1$ and $(q_e - q_t)$. When adsorption is sluggish, it is possible to achieve large values of $(q_e - q_t)$ and small values of $k_1$. To describe the adsorption rate with greater accuracy, the PFO rate presented in Equation (27) should be calculated rather than the values of $k_1$.

$$\text{PFOrate} = k_1 (q_e - q_t). \tag{27}$$

*5.2. Pseudosecond-Order (PSO) Model.* The adsorption process of lead upon peat was first modelled using the PSO model (Ho and McKay [133]). The PSO model was then widely used to explain the adsorption processes. In most published publications, the adsorption experimental values were predicted using the PSO model, and the rate constants of adsorption were calculated using the equation as follows:

$$\frac{dq_t}{dt} = k_2 (q_e - q_t)^2. \tag{28}$$

The integrated PSO model is described as

$$q_t = \frac{q_e^2 k_2 t}{1 + q_e k_2 t}. \tag{29}$$

The following part offers the nonlinear approach to resolving the PSO model. The PSO rate constant $k_2$ is being used to characterize the rate of adsorption equilibrium in a manner like that of the PFO rate constant $k_1$. However, both $k_2$ and $(q_e - q_t)^2$ are related to the adsorption rate, $dq_t/dt$. As a result, using the equation to compute the PSO rate is more accurate.

$$\text{PSOrate} = k_2 (q_e - q_t)^2. \tag{30}$$

*5.3. Mixed-Order (MO) Model.* The mixed-order (MO) model is considered in the form as

$$\frac{dq_t}{dt} = k_1' (q_e - q_t) + k_{21}' (q_e - q_t)^2. \tag{31}$$

The PFO and PSO rates for the MO model are calculated as

$$\text{PSOrate}' = k_1' (q_e - q_t), \tag{32}$$

$$\text{PSOrate}' = k_{21}' (q_e - q_t)^2. \tag{33}$$

The steps of diffusion and adsorption on active sites are typically described by the PFO rate and PSO rates, respectively. The MO model also depicts the entire adsorption process. The following requirements are necessary for the MO model's assumption to be met: (1) arbitrary adsorption stage, (2) either diffusion or adsorption serves as the rate-regulating phase, and (3) arbitrary initial concentration of the adsorbate in solution [91].

*5.4. Elovich Model.* The Elovich model's fundamental presumptions were as follows: (1) the activation energy increased with adsorption time and (2) the adsorbent surface was heterogeneous. An empirical model without clear physical implications is the Elovich model. The chemisorption of gas onto material is frequently modelled using this technique. The Elovich model has been described as follows [134]:

$$\frac{dq_t}{dt} = ae^{-bq_t}. \tag{34}$$

Integrating Equation (34), for the condition of $q_0 = 0$, yields Equation (35) as follows:

Table 3: Isotherm models reported in the literature for adsorption of organic and inorganic contaminants.

| Adsorbate | Adsorbent | Adsorption isotherm | Reference |
|---|---|---|---|
| *Metal ions* | | | |
| Chromium | Cassava peel carbon (CPC) | Redlich–Peterson | [7] |
| Cobalt | Cassava peel carbon (CPC) | Redlich–Peterson | [7] |
| Chromium | Cassava peel carbon | Langmuir, Redlich–Peterson | [7] |
| Cobalt | Cassava peel carbon | Langmuir, Redlich–Peterson | [7] |
| Cadmium | Unmodified cassava tuber bark/acid-modified tuber bark of the specimen cassava | Langmuir | [93] |
| Copper | Unmodified cassava tuber bark/acid-modified tuber bark of the specimen cassava | Langmuir | [93] |
| Zinc | Unmodified cassava tuber bark/acid-modified tuber bark of the specimen cassava | Langmuir | [93] |
| Lead | Modified cassava stalk | Langmuir | [94] |
| Zinc | Modified cassava stalk | Langmuir | [94] |
| Nickel | Cassava peel | Freundlich | [5] |
| Cadmium | Modified cassava peel activated by 0.1 mol/L of 36% $H_2O_2$/98% $H_2SO_4$/99% NaOH | Langmuir | [97] |
| Lead | Modified cassava peel activated by 0.1 mol/L of 36% $H_2O_2$/98% $H_2SO_4$/99% NaOH | Langmuir | [97] |
| Chromium | Modified cassava peel activated by 0.1 mol/L of 36% $H_2O_2$/98% $H_2SO_4$/99% NaOH | Langmuir | [97] |
| Lead | Grafted cassava starch | Langmuir | [113] |
| Lead | Cassava peel carbon | | [59] |
| *Dyes* | | | |
| Malachite green | Cassava rind Carbon (CRC) | Langmuir | [73] |
| Methylene blue | Cassava rind Carbon (CRC) | Redlich–Peterson | [53] |
| Reactive red + Drimarene turquoise | Cassava stem biochar (CSB) | Langmuir, Dubinin–Radushkevich | [61] |
| Crystal violet | Raw cassava peel powder | Dubinin–Radushkevich | [63] |
| Rhodamine B | Cassava slag biochar | Freundlich | [57] |
| *Other pollutants* | | | |
| Norfloxacin | Cassava dreg biochar BC 350, pyrolysis at 350 K | Freundlich | [54] |
| Norfloxacin | Cassava dreg biochar BC 450, pyrolysis at 450 K | Freundlich | [54] |
| Norfloxacin | Cassava dreg biochar BC 550, pyrolysis at 550 K | Freundlich | [54] |
| Norfloxacin | Cassava dreg biochar BC 650, pyrolysis at 650 K | Freundlich | [54] |
| Norfloxacin | Cassava dreg biochar BC 750, pyrolysis at 750 K | Freundlich | [54] |
| Ciprofloxacin | Cassava dreg biochar (BC350, 550, 750) | Freundlich, Langmuir | [114] |

$$q_t = \frac{1}{b}\ln(1 + abt). \quad (35)$$

The nonlinear least squares regression method can be used to solve the nonlinear equation (35) in this example. The nonlinear approach is more difficult than the linear method.

*5.5. Ritchie's Equation.* The adsorption kinetic data of gases on solids were initially modelled using Ritchie's equation (135). Ritchie's equation's physical significance is that adsorption in active sites dominates all other types of adsorption. Active sites can be occupied by a single adsorbate ion or molecule. In this model, the desorption process is not considered. Ritchie's equation is presented as follows:

$$\frac{d\theta}{dt} = a(1 - \theta)^n. \quad (36)$$

*5.6. Pseudo-nth-Order (PNO) Mode.* Pb(II) adsorption kinetic data on wheat bran treated with sulphuric acid were modelled by Ozer [136] using pseudo-nth-order (PNO) theory.

$$\mathbf{\frac{dq_t}{dt} = k_n(q_e - q_t)^n}. \quad (37)$$

Table 4 summarizes the kinetic models reported in the literature for adsorption of organic and inorganic contaminants in water and wastewater.

## 6. Mass Transfer in Adsorption

*6.1. External Diffusion Models.* The slowest step, according to external diffusion models, is the diffusion of adsorbed species in an enclosing liquid film. To model the intraparticle diffusion process, various equations have been proposed.

*6.1.1. Boyd's External Diffusion Equation.* Boyd et al. [137] presumed a kinetic expression to designate the diffusion of the adsorbate over a bounding liquid film, as given in equation.

$$\mathbf{\frac{dq_t}{dt} = 4\pi r_o^2 D^1\left(\frac{\partial C_f}{\partial r}\right)_{r=r_o}}. \quad (38)$$

*6.1.2. Furusawa–Smith (F–S) Model.* Furusawa et al. [138] established an adsorption rate model.

$$\mathbf{\frac{C_t}{C_o} = \frac{1}{1 + m_s K} + \frac{m_s K}{1 + m_s K} e^{-(1+m_s K/m_s K)k_{F\&S}St}}. \quad (39)$$

The value of $k_{F\&S}$ St is used to characterize the exterior diffusional process. The F–S model presupposes that the isotherm is linear, intraparticle diffusion is insignificant, and external diffusion is the slowest step [138]. It should be noted that the adsorption requirement that the isotherm is not linear cannot be modelled by equation (39).

*6.1.3. Mathews–Weber (M–W) Model.* The Mathews–Weber (M–W) model is offered as follows [139]:

$$\mathbf{k_{M\&W} = \frac{r_O \rho(1 - \varepsilon)}{3m_s} \frac{\ln(C_o/C_t)}{t}}. \quad (40)$$

*6.1.4. Phenomenological External Mass Transfer (EMT) Model.* According to the EMT model (Equation (41)), equilibrium is reached on the interface of the adsorbent, and film diffusion is assumed to be the slowest process [140]. The gradient in adsorbent concentrations within the liquid film is what drives external diffusion.

$$\mathbf{\frac{dq_t}{dt} = \frac{k_s}{\rho}(C_t - C_{et}) + K_{ext}(C_t - C_{et})}. \quad (41)$$

Then, the adsorption isotherm model describes the equilibrium phenomenon. The isotherm model is presented as $q_{et} = f(C_{et})$. Then, $C_{et} = f^{-1}(q_{et})$.

*6.2. Internal Diffusion Models.* The slowest step, according to internal diffusion theories, is the diffusion of the adsorbate within the adsorbent. Instantaneous adsorption onto the active sites and adsorbate diffusion in the aqueous film occurs from place to place in the adsorbent. The three most common internal diffusion models, the intraparticle Boyd's diffusion model, Weber and Morris (W–M) model, and phenomenological interior mass transfer (IMT) model, were evaluated in this study.

*6.2.1. Boyd's Intraparticle Diffusion Model.* Using an intraparticle diffusion model [137], the equation is as follows:

$$\mathbf{F = 1 - \frac{6}{\pi^2}\sum_{n=1}^{\infty}\frac{1}{n^2}e^{-n^2Bt}}. \quad (42)$$

The adsorption equilibrium model yields $q$ (mg·g$^1$) when $F = q_t/q_\infty$, $q_\infty$ (mg·g$^{-1}$), and ($q_\infty = f(C_e)$).

*6.2.2. Weber–Morris (W–M) Model.* A model was developed by Weber and Morris in 1963 to explain the intraparticle diffusion process [141]. The equation presents the W–M model as follows:

$$\mathbf{q_t = k_{W\&M} t^{(1/2)}}. \quad (43)$$

If the intercept is zero, then the governing mechanism is intraparticle diffusion. Otherwise, several processes regulate adsorption.

*6.2.3. Phenomenological Internal Mass Transfer (IMT) Model.* The simplified form of the IMT model is given as

$$\mathbf{\frac{dq_t}{dt} = k_{int}(q_{et} - q_t)}. \quad (44)$$

Table 4: Kinetic models reported in the literature for adsorption of organic and inorganic contaminants in water and wastewater.

| Adsorbate | Adsorbent | Adsorption kinetics | Reference |
|---|---|---|---|
| *Metal ions* | | | |
| Chromium | Cassava peel carbon (CPC) | $2^{nd}$ order (pseudo) | [7] |
| Cobalt | Cassava peel carbon (CPC) | $2^{nd}$ order (pseudo) | [7] |
| Chromium | Cassava peel carbon | $2^{nd}$ order (pseudo) | [7] |
| Cobalt | Cassava peel carbon | $2^{nd}$ order (pseudo) | [7] |
| Lead | Modified cassava stalk | $2^{nd}$ order (pseudo) | [94] |
| Zinc | Modified cassava stalk | $2^{nd}$ order (pseudo) | [94] |
| Nickel | Cassava peel | $2^{nd}$ order (pseudo) | [5] |
| Cadmium | Modified cassava peel activated by 0.1 mol/L of 36% $H_2O_2$/98% $H_2SO_4$/99% NaOH | $2^{nd}$ order (pseudo) | [97] |
| Lead | Modified cassava peel activated by 0.1 mol/L of 36% $H_2O_2$/98% $H_2SO_4$/99% NaOH | $2^{nd}$ order (pseudo) | [97] |
| Chromium | Modified cassava peel activated by 0.1 mol/L of 36% $H_2O_2$/98% $H_2SO_4$/99% NaOH | $2^{nd}$ order (pseudo) | [97] |
| Lead | Cassava peel carbon | $2^{nd}$ order (pseudo) | [59] |
| *Dyes* | | | |
| Rhodamine B | Cassava slag biochar | $2^{nd}$ order (pseudo) | [57] |
| Malachite green | Cassava rind Carbon (CRC) | $2^{nd}$ order (pseudo) | [73] |
| Methylene blue | Cassava rind Carbon (CRC) | $2^{nd}$ order (pseudo) | [53] |
| Reactive red + Drimarene turquoise | Cassava stem biochar (CSB) | Pseudofirst-order and Elovich second-order | [61] |
| *Other pollutants* | | | |
| Norfloxacin | Cassava dreg biochar BC 350, pyrolysis at 350 K | $2^{nd}$ order (pseudo) | [54] |
| Norfloxacin | Cassava dreg biochar BC 450, pyrolysis at 450 K | $2^{nd}$ order (pseudo) | [54] |
| Norfloxacin | Cassava dreg biochar BC 550, pyrolysis at 550 K | $2^{nd}$ order (pseudo) | [54] |
| Norfloxacin | Cassava dreg biochar BC 650, pyrolysis at 650 K | $2^{nd}$ order (pseudo) | [54] |
| Norfloxacin | Cassava dreg biochar BC 750, pyrolysis at 750 K | $2^{nd}$ order (pseudo) | [54] |
| Ciprofloxacin | Cassava dreg biochar (BC350, 550, 750) | $2^{nd}$ order (pseudo) | [114] |

Table 5: Mass transfer models reported in the literature for adsorption of organic and inorganic contaminants in water and wastewater.

| Adsorbate | Adsorbent | Mass transfer/mechanism | Reference |
|---|---|---|---|
| *Metal ions* | | | |
| Nickel | Activated carbon from cassava peel tubers | Solid diffusion | [51] |
| Nickel | Activated carbon from cassava peel tubers | Solid diffusion | [51] |
| Nickel | Activated carbon from cassava peel tubers | Solid diffusion | [51] |
| Nickel | Raw material (RM) | Solid diffusion | [51] |
| Copper | Modified cassava fibre | Intraparticle diffusion | [86] |
| Copper | Modified cassava fibre | Intraparticle diffusion | [86] |
| Chromium | Cassava peel carbon | Solid-liquid diffusion | [7] |
| Cobalt | Cassava peel carbon | Solid-liquid diffusion | [7] |
| Cadmium | Untreated cassava peel biomass/acid-treated cassava peel biomass | Diffusion is film diffusion controlled/sorption is particle diffusion controlled | [11] |
| Zinc | Untreated cassava peel biomass/acid-treated cassava peel biomass | Diffusion is film diffusion controlled/sorption is particle diffusion controlled | [11] |
| *Dyes* | | | |
| Congo red | Cassava residue | Correlation coefficient <0.95) controlling step distributed between intraparticle and film diffusion | [67] |
| *Other pollutants* | | | |
| Nitrate | Modified cassava straw | Both surface adsorption and intraparticle diffusion | [64] |

Table 6: Evaluation of thermodynamic parameters for adsorption of organic and inorganic contaminants using cassava residues as adsorbents.

| Adsorbate | Adsorbent | ΔH (kJ/mol) | ΔS (kJ/mol·K) | ΔG (kJ/mol) | Reference |
|---|---|---|---|---|---|
| *Metal ions* | | | | | |
| Chromium | Cassava peel carbon (CPC) | +18.28 | +0.063 | −5.58 (288.14 K), −6.29 (298.14 K), and −7.24 (308.14 K) | [7] |
| Cobalt | Cassava peel carbon (CPC) | +39.64 | +0.16 | −7.28 (288.14), −8.73 (298.14 K), and −10.45 (308.14 K) | [7] |
| Lead | Modified cassava stalk | +19.33 | +0.148 | −24.79 (298.1 K), −26.22 (308.1 K), and −27.75 (318.1 K) | [94] |
| Zinc | Modified cassava stalk | +34.62 | +0.187 | −21.24 (298.1 K), −22.72 (308.1 K) and −24.98 (318.1 K) | [94] |
| Nickel | Cassava peel | +46.584 | +0.162 | −2.738 (303.15 K), −5.077 (318.15 K), and −7.623 (333.15 K) | [5] |
| Cadmium | Modified cassava peel activated by 0.1 mol/L of 36% $H_2O_2$/98% $H_2SO_4$/99% NaOH | +15.5/5.6/−29.7 | 43.6/6.5/−0.0852 | +3.0, +3.8 | [97] |
| Lead | Modified cassava peel activated by 0.1 mol/L of 36% $H_2O_2$/98% $H_2SO_4$/99% NaOH | −59.5/−59.6/−0.26 | −0.1942/−0.2039/−0.0755 | +3.8 | [97] |
| Chromium | Modified cassava peel activated by 0.1 mol/L of 36% $H_2O_2$/98% $H_2SO_4$/99% NaOH | −5.7/−9.9/+18.1 | −0.0151/−0.034/+0.074 | — | [97] |
| Lead | Grafted cassava starch | −7.6971511 | −0.0079078 | −5.327971 (298 K), −5.2810872 (308 K), and −5.1681819 (318 K) | [113] |
| Lead | Cassava peel carbon | +12.762 | +0.0672 | −7.67492 (303 K), −8.16296 (313 K), −8.80059 (323 K), and −9.71912 (333 K) | [59] |
| *Dyes* | | | | | |
| Methylene blue | Cassava rind carbon (CRC) | +17.4 | +0.074 | −4.86 (298.15 K), −5.02 (303.14 K), −5.47 (308.14 K), −6.00 (313.14 K), and −6.24 (318.14 K) | [53] |
| Malachite green | Cassava rind carbon (CRC) | +20–80 | +0.23 | −8.791 (293.14 K), −12.775 (308.14 K), and −14.947 (323.14 K) | [73] |
| Reactive red + Drimarene turquoise | Cassava stem biochar (CSB) | −15.92 | −66.13 | — | [61] |
| Crystal violet | Raw cassava peel powder | −20.536 | −46.484 | −6.65(303.1 K), −6.01 (313.1 K), −5.18 (325.1 K), −4.93 (333.01 K), and − 4.76 (343.1 K) | [63] |
| Rhodamine B | Cassava slag biochar | +0.2225 | +0.001192 | −8.116 (308 K), −8.478 (318 K), and −9.196 (328 K) | [57] |

Table 6: Continued.

| Adsorbate | Adsorbent | ΔH (kJ/mol) | ΔS (kJ/mol·K) | ΔG (kJ/mol) | Reference |
|---|---|---|---|---|---|
| *Other pollutants* | | | | | |
| Norfloxacin | Cassava dreg biochar BC 350, pyrolysis at 350 K | −34.14 | −0.10 | −6.29 (288.1 K), −5.54 (298.1 K), and −4.36 (308.1 K) | [54] |
| Norfloxacin | Cassava dreg biochar BC 450, pyrolysis at 450 K | +1.45 | +0.05 | −13.24 (288.1 K), −13.98 (298.1 K), and −14.27 (308.1 K) | [54] |
| Norfloxacin | Cassava dreg biochar BC 550, pyrolysis at 550 K | +47.45 | +0.21 | −11.85 (288 K), −14.37 (298 K), and −15.98 (308 K) | [54] |
| Norfloxacin | Cassava dreg biochar BC 650, pyrolysis at 650 K | +331.41 | +1.31 | −47.59 (288 K), −58.34 (298 K), and −73.85(308 K) | [54] |
| Norfloxacin | Cassava dreg biochar BC 750, pyrolysis at 750 K | +326.40 | +1.32 | −52.28 (288 K), −66.12 (298 K), and −78.60 (308 K) | [54] |
| Ciprofloxacin | Cassava dreg biochar (BC350/550/750) | −48.93 (350 K), −15.23 (550 K), and −83.62 (750 K) | −0.13 (350 K), −1.19 (550 K), and −0.25 (750 K) | −11.63 (350 K), −14.29 (550 K), and −13.03 (750 K) | [114] |

*6.3. Pore Volume and the Surface Diffusion (PVSD) Model.* The PVSD model's fundamental presumptions are as follows: the adsorbent particle is globular, the solution is homogeneous, the convective mass transfer in pores is low, and the adsorption of substances on active sites is simultaneous. The equation describes the PVSD model [142].

$$\mathbf{V}\frac{\mathbf{dC_t}}{\mathbf{dt}} = -\mathbf{mS_p k_F}\left(\mathbf{C_t} - \mathbf{C_{tr@r=r_0}}\right). \tag{45}$$

Table 5 summarizes the mass transfer models reported in the literature for adsorption of organic and inorganic contaminants in water and wastewater.

## 7. Adsorption Thermodynamics

The Van't Hoff equation is used to explain the thermodynamics in adsorption systems [143]. The equation is as follows:

$$\ln \mathbf{K_e} = -\frac{\Delta \mathbf{H^o}}{\mathbf{RT}} + \frac{\Delta \mathbf{S^o}}{\mathbf{R}}. \tag{46}$$

Table 6 shows the thermodynamic values for standard enthalpy, entropy, and Gibbs free energy of adsorption for various cassava-based adsorbents.

## 8. Challenges and Future Prospectives

Cassava has drawbacks of quick deterioration, lack of active sites, and lesser surface areas when it is used in raw powder. Also, presence of toxins in cassava limits its applications for food and feed. Hence, cassava requires carbonisation and activation to utilize it as an adsorbent with improved thermal stability, abundance of active sites, and enhanced surface areas.

## 9. Conclusion

The present review focussed on parameters affecting adsorption, preparation, and activation methods of cassava-based adsorbents, adsorption isotherms, kinetics, thermodynamics, and binding mechanisms through mass transfer studies. As cassava contains active functional groups, has better electron transfer, and has smaller particle size, cassava stem, rhizome, peel, and bagasse could be potential materials for adsorbents for removal of organic and inorganic pollutants from water and wastewater.

## Data Availability

The authors confirm that the data supporting the findings of this study are available within the article.

## Conflicts of Interest

The authors declare that they have no conflicts of interest.

## Acknowledgments

The authors would like to express their deep gratitude to the management of the Sathyabama Institute of Science and Technology, India, and the University of Technology and Applied Sciences, Oman, for their support to carry out the present work.

## References

[1] O. A. Otekunrin and B. Sawicka, "Cassava, a 21st century staple crop: how can Nigeria harness its enormous trade potentials," *Acta Scientific Agriculture*, vol. 3, no. 8, pp. 194–202, 2019.

[2] A. A Fathima, M Sanitha, L. Tripathi, S. Muiruri, L. Tripathi, and S. Muiruri, "Cassava (Manihot esculenta) dual use for food and bioenergy: Cassava (*Manihot esculenta*) dual use for food and bioenergy," *Food and Energy Security*, vol. 12, p. 380, 2022.

[3] F. S. Dinata and I. S. Kartawiria, "Bioethanol potential from whole parts of cassava plant in Indonesia," *Jurnal Teknologi Industri Pertanian*, vol. 31, no. 1, pp. 20–33, 2021.

[4] Fao, "Food agricultural organization statistics," 2019, https://knoema.com/atlas/sources/FAO.

[5] A. Kurniawan, A. N. Kosasih, J Febrianto et al., "Evaluation of cassava peel waste as lowcost biosorbent for Ni-sorption: Evaluation of cassava peel waste as lowcost biosorbent for Ni-sorption: Equilibrium, kinetics, thermodynamics and mechanismquilibrium, kinetics, thermodynamics and mechanism," *Chemical Engineering Journal*, vol. 172, no. 1, pp. 158–166, 2011.

[6] K. Philip, R. Jacob, and J. Gopalakrishnan, "Characterization of Characterization of Cassava Root Husk Powder: Equilibrium, Kinetic and Modeling Studies as Bioadsorbent for Copper(II) and Lead(II)assava root husk powder: equilibrium, kinetic and modeling studies as bioadsorbent for copper (II) and lead (II)," *Journal of Encapsulation and Adsorption Sciences*, vol. 11, no. 02, pp. 69–86, 2021.

[7] A. Belcaid, B. H Beakou, K. El Hassani, A. Anouar, S. Bouhsina, and A. Anouar, "Efficient removal of Cr (VI) and Co (II) from aqueous solution by activated carbon from Manihot esculenta Crantz agricultural bio-waste," *Water Science and Technology*, vol. 83, no. 3, pp. 556–566, 2021.

[8] C. Parvathi, T. Maruthavanan, S. Sivamani, and C. Prakash, "Biosorption studies for the removal of malachite green from its aqueous solution by activated carbon prepared from cassava peel," *E-Journal of Chemistry*, vol. 8, no. 1, pp. S61–S66, 2011.

[9] I. S. Bădescu, D Bulgariu, I. Ahmad, L. Bulgariu, I. Ahmad, and L. Bulgariu, "Valorisation possibilities of exhausted biosorbents loaded with metal ions – Valorisation possibilities of exhausted biosorbents loaded with metal ions – A review review," *Journal of Environmental Management*, vol. 224, pp. 288–297, 2018.

[10] J. Fonseca, A. Albis, A. Montenegro, and R. R. Montenegro, "Evaluation of zinc adsorption using cassava peels (Manihot esculenta) modified with citric acid," *Contemporary Engineering Sciences*, vol. 11, no. 72, pp. 3575–3585, 2018.

[11] M. Horsfall and A. A. Abia, "Sorption of cadmium (II) and zinc (II) ions from aqueous solutions by cassava waste biomass (Manihot sculenta Cranz)," *Water Research*, vol. 37, no. 20, pp. 4913–4923, 2003.

[12] O. Ijaola, O. Omotosho, and A. Sangodoyin, "Comparison of heavy metal adsorption form carbons activated with zinc chloride salt (A case study of cassava and bamboo biomass)," 2012, https://www.researchgate.net/profile/Ijaola-Opololaoluwa/publication/348280634_PosterPresentations_for_ICWRE_2014_by_Ijaola_and_Omotosho/links/5ff620084585155

3a0262671/PosterPresentations-for-ICWRE-2014-by-Ijaola-and-Omotosho.pdf.

[13] S. Daniel, C. G Affonso, C. Juliana, P. Ad iacute lson, G. P. Ivone, and F. C. Gustavo, "Removal of Cr (III) from contaminated water using industrial waste of the cassava as natural adsorbents," *African Journal of Agricultural Research*, vol. 10, no. 46, pp. 4241–4251, 2015.

[14] K. N. Awokoya, O. J. Owoade, B. A. Moronkola et al., "Morphological characteristics of cassava peel and its effect on the adsorption of heavy metal ions from aqueous media," *Journal of Multidisciplinary Engineering Science and Technology*, vol. 3, no. 8, pp. 5342–5348, 2016.

[15] M. J. Horsfall, A. I. Spiff, and A. A. Abia, "Studies on the influence of mercaptoacetic acid (MAA) modification of cassava (Manihot sculenta Cranz) waste biomass on the adsorption of Cu 2+ and Cd 2+ from aqueous solution," *Bulletin of the Korean Chemical Society*, vol. 25, no. 7, pp. 969–976, 2004.

[16] S. Ismadji, . *Utilization of Agricultural Waste Biomass for Treatment of Wastewater Containing Heavy Metal*, Academia.Edu, San Francisco, CA, USA, 2009.

[17] Y. Ja'afar and A. O. Lawal, "Studies on interference of adsorption of heavy metal ions on chelating sorbents from cassava and Amidoxime-modified Polyacrylonitrile-grafted-Cassava Starch," *Nigerian Journal of Chemical Research*, vol. 22, no. 2, pp. 54–60, 2017.

[18] A. Jorgetto, R Silva, M. Saeki et al., "Cassava root husks powder as green adsorbent for the removal of Cu (II) from natural river water," *Applied Surface Science*, vol. 288, pp. 356–362, 2014.

[19] E. C. Junior, D. Schwantes, A. C. Gonçalves, and A. G. Rosenberger, "Modified cassava barks as an adsorbent of copper ions," in *Book of Proceedings 5th International Conference on Sustainable Development*p. 23, European Center of Sustainable Development Cesare Anselmi, Rome Italy, 2017.

[20] H. Owamah, "Sorption kinetic models of Pb (II) and Cu (II) from a typical hospital wastewater using modified cassava peels (MCP) biomass," *Journal of International Environmental Application & Science*, vol. 7, no. 4, pp. 721–733, 2012.

[21] H. I. Owamah and I. Owamah, "Biosorptive removal of Pb(II) and Cu(II) from wastewater using activated carbon from cassava peels," *Journal of Material Cycles and Waste Management*, vol. 16, no. 2, pp. 347–358, 2014.

[22] J. Luo, C. Ge, H. Yu, D. Fenk, P. Huang, and F. Li, "Cassava waste derived biochar as soil amendments: effects on Kinetics, equilibrium and thermodynamic of atrazine adsorption," *Fresenius Environmental Bulletin*, vol. 25, pp. 4607–4617, 2016.

[23] T. Mutiara, F. I. Muhandi, A. Alhumaini, A. Chafidz, and H. Pratikno, "Removal of lead ($Pb^{2+}$) from aqueous solution using bio-adsorbent prepared from cassava stem pith," in *Materials Science Forum*, vol. 981, pp. 331–335, Trans Tech Publications Ltd, Wollerau, Switzerland, 2020.

[24] J. Shi, H. Luo, D. Xiao et al., "Bio-sorbents from cassava waste biomass and its performance in removal of $Pb^{2+}$ from aqueous solution," *Journal of Applied Polymer Science*, vol. 131, no. 2, 2014.

[25] N. Supamathanon, N. Butwong, K. Jansungnean, and P. Voanok, "Modification of cassava residue for the adsorption of Pb (II) ion from aqueous solution," *Burapha Science Journal*, vol. 22, no. 2, pp. 274–287, 2017.

[26] A. Suprabawati, N. W. Holiyah, J. Jasmansyah, U. Jenderal Achmad Yani, and J. Terusan Jenderal Sudirman, "Activated Kulit Singkong (Manihot esculenta Crantz) sebagai Karbon Aktif Dengan berbagai langkah pembuatan untuk Adsorpsi Logam Timbal (Pb2+) dalam airarbon from cassava peel as adsorbent of lead metal (Pb2+) in the water," *Jurnal Kartika Kimia*, vol. 1, 2018.

[27] C. Tejada-Tovar, A. Villabona-Ortíz, and A. D. González-Delgado, *Agricultural Residues of cocoa, Lemon, Yam, Cassava and Oil palm for lead-loaded Wastewater Treatment*, Universidad Santiago de cali, Valle del Cauca, Colombia, 2000.

[28] A. Villabona-Ortíz, C. Tejada-Tovar, and A. Gonzalez-Delgado, "Application of cement-based solidification/stabilization technique for immobilizing lead and nickel ions after sorption-desorption cycles using cassava peels biomass," *Indian Journal of Science and Technology*, vol. 11, no. 45, pp. 1–4, 2017.

[29] E. A. Pondja Jr, K M Persson, N. P. Matsinhe, K. M. Persson, and N. P. Matsinhe, "The potential use of cassava peel for treatment of mine water in Mozambique," *Journal of Environmental Protection*, vol. 08, no. 3, pp. 277–289, 2017.

[30] S. Ndlovu, G. S. Simate, L. Seepe, A. Shemi, V. Sibanda, and L. D. Van Dyk, "The removal of $Co^{2+}$, $V^{3+}$ and $Cr^{3+}$ from waste effluents using cassava waste," *South African Journal of Chemical Engineering*, vol. 18, no. 1, pp. 51–69, 2013.

[31] M. Vasudevan, P. Ajithkumar, R Singh, N. Natarajan, R. P. Singh, and N. Natarajan, "Mass transfer kinetics using two-site interface model for removal of Cr (VI) from aqueous solution with cassava peel and rubber tree bark as adsorbents," *Environmental Engineering Research*, vol. 21, no. 2, pp. 152–163, 2016.

[32] A. D. O. Jorgetto, A. C. P. D. Silva, B. Cavecci, R. C. Barbosa, M. A. U. Martines, and G. R. D. Castro, "Cassava root husks as a sorbent material for the uptake and pre-concentration of cadmium (II) from aqueous media," *Orbital - The Electronic Journal of Chemistry*, vol. 5, pp. 206–212, 2013.

[33] Z. Luo, S. Luo, C. Niu, S. Hu, L. Chen, and C. Fan, "Removal of $Pb^{2+}$ and $Cd^{2+}$ from aqueous solutions by chemically modified cellulose of cassava waste," *Fresenius Environmental Bulletin*, vol. 25, p. 5326, 2016.

[34] E. Ofudje, E. Sodiya, F. Ibadin, A. Ogundiran, O. Osideko, and A. Uzosike, "Sorption of $Cd^{2+}$ from aqueous solutions using cassava (manihot esculenta) waste: equilibrium and kinetic studies," *Journal of Chemical Society of Nigeria*, vol. 45, no. 3, 2020.

[35] K. Kadirvelu, C. Karthika, N. Vennilamani, and S. Pattabhi, "Activated carbon from industrial solid waste as an adsorbent for the removal of Rhodamine-B from aqueous solution: Activated carbon from industrial solid waste as an adsorbent for the removal of Rhodamine-B from aqueous solution: Kinetic and equilibrium studiesinetic and equilibrium studies," *Chemosphere*, vol. 60, no. 8, pp. 1009–1017, 2005.

[36] P. Ndagijimana, X. Liu, Q. Xu et al., "Cassava flour extracts solution to induce gelatin cross-linked activated carbon-graphene oxide composites: Cassava flour extracts solution to induce gelatin cross-linked activated carbon-graphene oxide composites: The adsorption performance of dyes from aqueous mediahe adsorption performance of dyes from aqueous media," *Environmental Advances*, vol. 5, Article ID 100079, 2021.

[37] K. Junlapong, P. Maijan, C. Chaibundit, and S. Chantarak, "Effective adsorption of methylene blue by biodegradable superabsorbent cassava starch-based hydrogel," *International Journal of Biological Macromolecules*, vol. 158, pp. 258–264, 2020.

[38] Y. Lisafitri, "Preliminary studies of cassava leaves' ability to remove dyes from water," *Journal of Mathematical & Fundamental Sciences*, vol. 52, no. 1, 2020.

[39] L. Meili, R. P. S Godoy, J I Soletti et al., "Cassava (Manihot esculenta Crantz) stump biochar: Cassava (*Manihot esculenta* Crantz) stump biochar: Physical/chemical characteristics and dye affinityhysical/chemical characteristics and dye affinity," *Chemical Engineering Communications*, vol. 206, no. 7, pp. 829–841, 2019.

[40] D. Soto, O. León, A. Muñoz-Bonilla, and M. Fernandez-García, "Succinylated starches for dye removal," *Starch - Stärke*, vol. 73, no. 2, Article ID 2000043, 2021.

[41] C. Parvathi, U. S. Shoba, C. Prakash, and S. Sivamani, "Manihot esculenta peel powder: effective adsorbent for removal of various textile dyes from aqueous solutions," *Journal of Testing and Evaluation*, vol. 46, no. 6, Article ID 20170160, 2018.

[42] P. Huang, C. Ge, D. Feng et al., "Effects of metal ions and pH on ofloxacin sorption to cassava residue-derived biochar," *Science of the Total Environment*, vol. 617, pp. 1384–1391, 2018.

[43] J. Luo, X. Li, C. Ge et al., "Preparation of ammonium-modified cassava waste-derived biochar and its evaluation for synergistic adsorption of ternary antibiotics from aqueous solution," *Journal of Environmental Management*, vol. 298, Article ID 113530, 2021.

[44] R. Rinawati, S. Supriyanto, and Y. O. Kasih, "Preparation of magnetic activated carbon from cassava peel for removal of tetracycline antibiotic in aquatic environment," 2020, http://repository.lppm.unila.ac.id/25713/1/Abstract%20icasmi%202020.pdf.

[45] C. Netoa, W. Costab, Y. Diasc, and M. Santosa, *Phosphorus Adsorption in Aqueous Medium Using Biocarbon from Cassava Agricultural Residue (Manihot Esculenta)*, Universidade Federal do Ceará, Fortaleza, Brazil, 2021.

[46] M. G. Gomes, D Q Santos, L. C. d. Morais et al., "Purification of biodiesel by dry washing and the use of starch and cellulose as natural adsorbents: Part II–study of purification times," *Biofuels*, vol. 12, no. 5, pp. 579–587, 2021.

[47] I. Ilaboya, R. Ilaboya, E. O. Oti, G. O. Ekoh, and L. O. Umukoro, "Performance of Activated Carbon from Cassava Peels for the Treatment of Effluent Wastewater," *Iranica Journal of Energy and Environment*, vol. 4, no. 4, 2013.

[48] O. A. Omotosho, A Y Sangodoyin, A. Omotosho, and A. Y. Sangodoyin, "Production and utilization of cassava peel activated carbon in treatment of effluent from cassava processing industry," *Water Practice and Technology*, vol. 8, no. 2, pp. 215–224, 2013.

[49] D. F Simatupang, JF. Tarigan, Simatupang, and J. Tarigan, "The effect of active carbon adsorbents from some wastes in reducing free fatty acids and acid number to improve vco quality," *IOP Conference Series: Materials Science and Engineering*, vol. 885, no. 1, Article ID 12011, 2020.

[50] J. d. O. Primo, C. Bittencourt, S. Acosta et al., "Synthesis of Synthesis of Zinc Oxide Nanoparticles by Ecofriendly Routes: Adsorbent for Copper Removal From Wastewaterinc oxide nanoparticles by ecofriendly routes: adsorbent for copper removal from wastewater," *Frontiers in Chemistry*, vol. 8, Article ID 571790, 2020.

[51] B. A. A. Alongamo, L D Ajifack, J. N. Ghogomu et al., "Activated Activated Carbon from the Peelings of Cassava Tubers (Manihot esculenta) for the Removal of Nickel(II) Ions from Aqueous Solutionarbon from the peelings of cassava tubers (manihot esculenta) for the removal of nickel (II) ions from aqueous solution," *Journal of Chemistry*, vol. 2021, Article ID 5545110, 14 pages, 2021.

[52] M. A Abia, S. Ai, A. A. Arbia, and A. I. Spiff, "Removal of Cu (II) and Zn (II) ions from wastewater by cassava (Manihot esculenta Cranz) waste biomass," *African Journal of Biotechnology*, vol. 2, no. 10, pp. 360–364, 2003.

[53] B. H. Beakou, K. El Hassani, M. A. Houssaini et al., "Novel activated carbon from Novel activated carbon from Manihot esculenta Crantz for removal of Methylene Blueanihot esculenta crantz for removal of methylene blue," *Sustainable Environment Research*, vol. 27, no. 5, pp. 215–222, 2017.

[54] D. Feng, H. Yu, H. Deng, F. Li, and C. Ge, "Adsorption characteristics of norfloxacin by biochar prepared by cassava dreg: kinetics, isotherms, and thermodynamic analysis," *Bioresources*, vol. 10, no. 4, pp. 6751–6768, 2015.

[55] E. A. Abia, O. B. Didi, and E. D. Asuquo, "Modeling of Cd" Modeling of Cd2+ Sorption Kinetics from Aqueous Solutions onto Some Thiolated Agricultural Waste Adsorbent-sorption kinetics from aqueous solutions onto some thiolated agricultural VVaste adsorbents," *Journal of Applied Sciences*, vol. 6, no. 12, pp. 2549–2556, 2006.

[56] M. Gunasegaran, "Removal of metanil yellow dye from aqueous solution using cassava peel," Doctoral dissertation, Universiti Malaysia Kelantan, Kota Bharu, Malaysia, 2019.

[57] J. Wu, J. Yang, G. Huang, C. Xu, and B. Lin, "Hydrothermal carbonization synthesis of cassava slag biochar with excellent adsorption performance for Rhodamine B," *Journal of Cleaner Production*, vol. 251, Article ID 119717, 2020.

[58] N. S. Hassan, "Cassava peel as adsorbent for removal of malachite green dye," Doctoral dissertation, Universiti Malaysia Kelantan, Kota Bharu, Malaysia, 2018.

[59] C. O. Thompson, A O Ndukwe, C. O. Asadu, A. O. Ndukwe, and C. O. Asadu, "Application of activated biomass waste as an adsorbent for the removal of lead (II) ion from wastewater," *Emerging Contaminants*, vol. 6, pp. 259–267, 2020.

[60] Y. Ja'afar, S. A. M. Jamil, A. O. Lawal, B. Y. Jamoh, and A. Muhammad, "Removal of Cu (II) by amidoxime-modified polyacrylonitrile-grafted-cassava starch," *Nigerian Journal of Chemical Research*, vol. 21, pp. 33–50, 2016.

[61] A. Navya, S. Nandhini, S. Sivamani et al., "Preparation and characterization of cassava stem biochar for mixed reactive dyes removal from simulated effluent," *Desalination and Water Treatment*, vol. 189, pp. 440–451, 2020.

[62] L. N. Dos Santos, C E Porto, M. K. Bulla et al., "Peach palm and cassava wastes as biosorbents of tartrazine yellow dye and their application in industrial effluent," *Scientia Plena*, vol. 17, no. 5, 2021.

[63] N. J. Okorocha, C. K. Enenebeaku, M. O. Chijioke-Okere, C. E. Ohaegbulam, and C. E. Ogukwe, "Adsorptive removal of crystal violet using agricultural waste: equilibrium, kinetic and thermodynamic studies," *American Journal of Engineering Research*, vol. 8, 2019.

[64] W. Li, W. Mo, M. Zhang, M. Meng, and M. Chen, "Adsorption of nitrate from aqueous solution onto modified cassava (Manihot esculenta) straw/Adsorpcja azotanow z roztworu wodnego na zmodyfikowanej slomie manioku Manihot esculenta," *Ecological Chemistry and Engineering S*, vol. 19, no. 4, pp. 629–638, 2012.

[65] M. L. Theng and L. S. Tan, "Optimization on methylene blue and Congo red dye adsorption onto cassava leaf using response surface methodology," *Malaysian Journal of Catalysis*, vol. 4, no. 2, 2020.

[66] F. B Scheufele, J Staudt, M. H. Ueda et al., "Biosorption of direct black dye by cassava root husks: Biosorption of direct black dye by cassava root husks: Kinetics, equilibrium, thermodynamics and mechanism assessmentinetics, equilibrium, thermodynamics and mechanism assessment," *Journal of Environmental Chemical Engineering*, vol. 8, no. 2, Article ID 103533, 2020.

[67] H. X Li, R J Zhang, L. Tang et al., "Use of cassava residue for the removal of Congo red from aqueous solution by a novel process incorporating adsorption and in vivo decolorization," *BioResources*, vol. 9, no. 4, pp. 6682–6698, 2014.

[68] C. Tejada-Tovar, A. Villabona-Ortz, A. Herrera-Barros et al., "Adsorption kinetics of Cr (VI) using modified residual biomass in batch and continuous system," *Indian Journal of Science and Technology*, vol. 11, no. 14, pp. 1–8, 2018.

[69] F. Sulaiman, M. Septiani, S. Aliyasih, and N. Huda, "Effectiveness of a cassava peel adsorbent on the absorption of copper (Cu2+) and zinc (Zn2+) metal ions," *International Journal on Advanced Science, Engineering and Information Technology*, vol. 9, no. 4, pp. 1296–1301, 2019.

[70] A. J. Rubio, I. Z. Da Silva, F. Gasparotto et al., "Removal of methylene blue using cassava bark residue," *Chemical Engineering Transactions*, vol. 65, pp. 751–756, 2018.

[71] S. D. Aulia, A Wijayanti, R. Hadisoebroto, A. Wijayanti, and R. Hadisoebroto, "The effect of mixing speed and contact time on dye removal using Cassava Peel adsorbents," *IOP Conference Series: Earth and Environmental Science*, vol. 737, no. 1, Article ID 12013, April, 2021.

[72] C. Tejada Tovar, A. Villabona Ortiz, and L. E. Garcés Jaraba, "Kinetics of adsorption in mercury removal using cassava (Manhiot esculenta) and lemon (Citrus limonum) wastes modified with citric acid," *Ingeniería Y Universidad*, vol. 19, no. 2, pp. 283–298, 2015.

[73] B. H. Beakou, K. El Hassani, M. A. Houssaini, M. Belbahloul, E. Oukani, and A. Anouar, "A novel biochar from Manihot esculenta Crantz waste: application for the removal of Malachite Green from wastewater and optimization of the adsorption process," *Water Science and Technology*, vol. 76, no. 6, pp. 1447–1456, 2017.

[74] A. R. Lucaci, D Bulgariu, I. Ahmad et al., "Potential use of biochar from various waste biomass as biosorbent in Co (II) removal processes," *Water*, vol. 11, no. 8, p. 1565, 2019.

[75] S. Y. Foong, N S Abdul Latiff, R. K. Liew et al., "Production of biochar for potential catalytic and energy applications via microwave vacuum pyrolysis conversion of cassava stem," *Materials Science for Energy Technologies*, vol. 3, pp. 728–733, 2020.

[76] A. H. Omar, K Ramesh, A. M. A. Gomaa, B. M. Y. Rosli, A. M. A. Gomaa, and M. Y. Rosli, "Experimental design technique on removal of hydrogen sulfide using CaO-eggshells dispersed onto palm kernel shell activated carbon: Experimental design technique on removal of hydrogen sulfide using CaO-eggshells dispersed onto palm kernel shell activated carbon: Experiment, optimization, equilibrium and kinetic studiesxperiment, optimization, equilibrium and kinetic studies," *J. Wuhan Univ. Technol. Mater. Sci. Ed.*vol. 32, no. 2, pp. 305–320, 2017.

[77] O. A. Habeeb, K Ramesh, G. A. Ali, R. B. M. Yunus, G. A. Ali, and B. Rosli, "Low-cost and eco-friendly activated carbon from modified palm kernel shell for hydrogen sulfide removal from wastewater: Low-cost and eco-friendly activated carbon from modified palm kernel shell for hydrogen sulfide removal from wastewater: adsorption and kinetic studiesdsorption and kinetic studies," *Desalination and Water Treatment*, vol. 84, pp. 205–214, 2017.

[78] G. A. M. Ali, O A Habeeb, H. Algarni et al., "CaO impregnated highly porous honeycomb activated carbon from agriculture waste: symmetrical supercapacitor study," *Journal of Journal of Materials Scienceaterials Science*, vol. 54, no. 1, pp. 683–692, 2019.

[79] G. A. Ali, S A. Manaf, K. F Chong et al., "Superior supercapacitive performance in porous nanocarbons," *Journal of Journal of Energy Chemistrynergy Chemistry*, vol. 25, no. 4, pp. 734–739, 2016.

[80] G. A. Ali, M. M. Yusoff, and K. F. Chong, "Graphene: electrochemical production and its energy storage properties," *ARPN J Eng Appl Sci*, vol. 11, no. 16, pp. 9712–9717, 2016.

[81] G. Hegde, S. A. Abdul Manaf, A Kumar et al., "Biowaste sago bark based catalyst free carbon nanospheres: waste to wealth approach," *ACS Sustainable Chemistry & Engineering*, vol. 3, no. 9, pp. 2247–2253, 2015.

[82] N. Tri Widayati, T. Darsono, S. Negeri, J. Kiai Cebolang, and M. Pati, "Effectiveness of activated carbon from cassava peel waste to reduce TSS (total solid suspended) levels in batik liquid waste," in *Proceedings of the 5th International Conference on Science, Education and Technology, ISET 2019*, Central Java, Indonesia, June 2020.

[83] G. K Ndongo, N J Nsami, K. J. Mbadcam, N. J. Nsami, and K. J. Mbadcam, "Ferromagnetic activated carbon from cassava (Manihot dulcis) peels activated by Iron (III) chloride: Ferromagnetic activated carbon from cassava (Manihot dulcis) peels activated by iron(III) chloride: Synthesis and characterizationynthesis and characterization," *BioResources*, vol. 15, no. 2, pp. 2133–2146, 2020.

[84] C. V. Abiaziem, A. B. Williams, A. Ibijoke Inegbenebor, C. T. Onwordi, C. Osereme Ehi-Eromosele, and L. F. Petrik, "Adsorption of lead ion from aqueous solution unto cellulose nanocrystal from cassava peel," *Iopscience.Iop.Org.*vol. 12122, 2019.

[85] G. O. Agiri and O. Akaranta, "Adsorption of metal ions by dye treated cassava mesocarp," *Scientific Research and Essay*, vol. 4, no. 5, pp. 526–530, 2009.

[86] A. A. Augustine, B. D. Orike, and A. D. Edidiong, "Adsorption kinetics and modeling of Cu (II) ion sorption from aqueous solution by mercaptoacetic acid modified cassava (manihot sculenta cranz) wastes," *EJEAFChe*, vol. 6, no. 4, pp. 2221–2234, 2007.

[87] W. Bai, L. Fan, Y. Zhou et al., "Removal of $Cd^{2+}$ ions from aqueous solution using cassava starch–based superabsorbent polymers," *Journal of Applied Polymer Science*, vol. 134, no. 17, 2017.

[88] I. Candrawati, F. Martak, and Y. I. Cahyo, "Absorption activity of cassava peel (manihot utilissima) as chromium (VI) metal biosorbent in electroplating waste," *The Journal of Pure and Applied Chemistry Research*, vol. 6, no. 2, p. 117, 2017.

[89] H. O. Chukwuemeka-Okorie, F. K. Ekuma, K. G. Akpomie, J. C. Nnaji, and A. G. Okereafor, "Adsorption of tartrazine and sunset yellow anionic dyes onto activated carbon derived from cassava sievate biomass," *Applied Water Science*, vol. 11, 2021.

[90] W. A. Gin, A. Jimoh, A. S. Abdulkareem, and A. Giwa, "Kinetics and isotherm studies of heavy metal removals from electroplating wastewater using cassava peel activated carbon," *Adsorption*, vol. 1000, p. 1, 2014.

[91] X. Guo, C. Chen, and J. Wang, "Sorption of sulfamethoxazole onto six types of microplastics," *Chemosphere*, vol. 228, pp. 300–308, 2019.

[92] A. Herrera-Barros, C. Tejada-Tovar, A. Villabona-Ortiz, A. Gonzalez-Delgado, and L. Fornaris-Lozada, "Effect of pH and particle size for lead and nickel uptake from aqueous solution using cassava (Manihot esculenta) and yam (Dioscorea alata) residual," *Indian Journal of Science and Technology*, vol. 11, 2018.

[93] M. Horsfall, A. A. Abia, and A. I. Spiff, "Kinetic studies on the adsorption of $Cd^{2+}$, $Cu^{2+}$ and $Zn^{2+}$ ions from aqueous solutions by cassava (Manihot sculenta Cranz) tuber bark waste," *Bioresource Technology*, vol. 97, no. 2, pp. 283–291, 2006.

[94] C. Kang, Q. Li, H. Yi et al., "EDTAD-modified cassava stalks loaded with $Fe_3O_4$: highly efficient removal of $Pb^{2+}$ and $Zn^{2+}$ from aqueous solution," *Environ. Sci. Pollut. Res.*vol. 28, pp. 6733–6745, 2021.

[95] K. M. Oghenejoboh, S. O. Otuagoma, and E. O. Ohimor, "Application of cassava peels activated carbon in the treatment of oil refinery wastewater–a comparative analysis," *Journal of Ecological Engineering*, vol. 17, no. 2, 2016.

[96] S. Prapagdee, S. Piyatiratitivorakul, and A. Petsom, "Activation of cassava stem biochar by physico-chemical method for stimulating cadmium removal efficiency from aqueous solution," *EnvironmentAsia*, vol. 7, no. 2, 2014.

[97] D. Schwantes, A. C. Gonçalves, G. F. Coelho et al., "Chemical modifications of cassava peel as adsorbent material for metals ions from wastewater," *Journal of Chemistry*, vol. 2016, Article ID 3694174, 15 pages, 2016.

[98] P. U. Shah, N. P. Raval, and N. K. Shah, "Adsorption of copper from an aqueous solution by chemically modified cassava starch," *J Mater Environ Sci*, vol. 6, no. 9, pp. 2573–2582, 2015.

[99] P. T. Tho, H. T. Van, L. H. Nguyen et al., "Enhanced simultaneous adsorption of as (iii), Cd (ii), Pb (ii) and Cr (vi) ions from aqueous solution using cassava root husk-derived biochar loaded with ZnO nanoparticles," *RSC Advances*, vol. 11, no. 31, Article ID 18881, 2021.

[100] A. A. Albis, A. J. López and M. C. Romero, Removal of methylene blue from aqueous solutions using cassava peel (Manihot esculenta) modified with phosphoric acid," *Prospectiva*, vol. 15, no. 2, pp. 60–73, 2017.

[101] A. K. Anas, A. Izzah, S. Y. Pratama, and F. I. Fajarwati, "Removal of methylene blue using biochar from cassava peel (Manihot utilissima) modified by sodium dodecyl sulphate (SDS) surfactant," *AIP Conference Proceedings*, vol. 2229, 2020.

[102] S. Sivakumar, P. Senthilkumar, and V. Subburam, "Carbon from cassava peel, an agricultural waste, as an adsorbent in the removal of dyes and metal ions from aqueous solution," *Bioresource Technology*, vol. 80, no. 3, pp. 233–235, 2001.

[103] W. Astuti, M. Hidayah, L. Fitriana, M. A. Mahardhika, and E. F. Irchamsyah, "Preparation of activated carbon from cassava peel by microwave-induced H3PO4 activation for naphtho$_l$ b$_l$ue-black removal," *AIP Conference Proceedings*, vol. 2243, Article ID 20003, 2020.

[104] M. L. Theng, L. S. Tan, and W. C. Siaw, "Adsorption of methylene blue and Congo red dye from water onto cassava leaf powder," *Progress in Energy and Environment*, vol. 12, pp. 11–21, 2020.

[105] S. Mutiaradini, L. Efiyanti, G. Pari, and B. M. Soebrata, "The utilization of activated carbon from cassava stems on the glucose and cholesterol adsorption," *IOP Conference Series: Materials Science and Engineering*, vol. 980, no. 1, Article ID 12028, 2020.

[106] O. Omotosho, "Mitigation of nitrate pollution in wastewater: a case study of the treatment of cassava processing effluent using cassava peel carbon material," *International Journal of Environmental, Chemical, Ecological, Geological and Geophysical Engineering*, vol. 9, pp. 399–404, 2016.

[107] N. Salahudeen, S. Nakakana, N. Salahudeen, C. S. Ajinomoh, and S. Nakakana, "Adsorption isotherm study for activated carbon produced from cassava peel," *Researchgate.Net.*vol. 4, pp. 8–12, 2014.

[108] N. Ayawei, A. N. Ebelegi, D Wankasi, N. Ebelegi, and D. Wankasi, "Modelling and interpretation of adsorption isotherms," *Journal of Chemistry*, vol. 2017, Article ID 3039817, 11 pages, 2017.

[109] M. A. Al-Ghouti and D. A. Da'ana, "Guidelines for the use and interpretation of adsorption isotherm models: a review," *Journal of Hazardous Materials*, vol. 393, Article ID 122383, 2020.

[110] I. Langmuir, "The constitution and fundamental properties of solids and liquids. Part I. Solids," *Journal of the American Chemical Society*, vol. 38, no. 11, pp. 2221–2295, 1916.

[111] I. Langmuir, "The constitution and fundamental properties of solids and liquids. II. Liquids," *Journal of the American Chemical Society*, vol. 39, no. 9, pp. 1848–1906, 1917.

[112] I. Langmuir, "The adsorption of gases on plane surfaces of glass, mica and platinum," *Journal of the American Chemical Society*, vol. 40, no. 9, pp. 1361–1403, 1918.

[113] P. U. Shah, N P Raval, M. Vekariya et al., "Adsorption of lead (II) ions onto novel cassava starch 5-choloromethyl-8-hydroxyquinoline polymer from an aqueous medium," *Water Science and Technology*, vol. 74, no. 4, pp. 943–956, 2016.

[114] F Li, D Feng, H Deng et al., "Effects of biochars prepared from cassava dregs on sorption behavior of ciprofloxacin," *Procedia Environmental Sciences*, vol. 31, pp. 795–803, 2016.

[115] H. Freundlich, "Über die Adsorption in Lösungen," *Zeitschrift für Physikalische Chemie*, vol. 57, no. 1, pp. 385–470, 1907.

[116] H. Freundlich, "Kapillarchemie: eine darstellung der chemie der kolloide und verwandter gebiete," *Nature*, vol. 85, no. 2156, pp. 534-535, 1911.

[117] M M. Dubinin and M. Dubinin, "The potential theory of adsorption of gases and vapors for adsorbents with energetically nonuniform surfaces," *Chem. Rev.*vol. 60, no. 2, pp. 235–241, 1960.

[118] M. I. Temkin, "Kinetics of ammonia synthesis on promoted iron catalysts," *Acta Physiochim. URSS*, vol. 12, pp. 327–356, 1940.

[119] P. J. Flory, *Principles of Polymer Chemistry*, Cornell University Press, Ithaca, NY, USA, 1953.

[120] M. Hill and N. London, "Proceedings of the physiological society," *Measurement*, vol. 16, p. 17, 1953.

[121] G. Halsey, H. S. Taylor, and S. Taylor, "The adsorption of hydrogen on tungsten powders," *The Journal of Chemical Physics*, vol. 15, no. 9, pp. 624–630, 1947.

[122] D. S. Jovanović, "Physical adsorption of gases - II: practical application of derived isotherms for monolayer and multilayer adsorption," *Kolloid-Zeitschrift Zeitschrift Für Polym*, vol. 235, pp. 1214–1225, 1969.

[123] S. Brunauer, P. H Emmett, E H. Teller, Emmett, and E. Teller, "Adsorption of Adsorption of Gases in Multimolecular Layersases in multimolecular layers," *J. Am. Chem. Soc.*vol. 60, no. 2, pp. 309–319, 1938.

[124] O. Redlich, D. L Peterson, and L. Peterson, "A useful adsorption isotherm," *J. Phys. Chem.*vol. 63, no. 6, p. 1024, 1959.

[125] J. Toth, "State equation of the solid-gas interface layers," *Acta Chim. Hung.*vol. 69, pp. 311–328, 1971.

[126] R. Sips, "On the structure of a catalyst surface," *The Journal of Chemical Physics*, vol. 16, no. 5, pp. 490–495, 1948.

[127] A. Khan, R. Ataullah, A. Al-Haddad, R. Ataullah, and A. Al-Haddad, "Equilibrium adsorption studies of some aromatic pollutants from dilute aqueous solutions on activated carbon at different temperatures," *Journal of Journal of Colloid and Interface Scienceolloid and Interface Science*, vol. 194, no. 1, pp. 154–165, 1997.

[128] W. Fritz, E Schluender, U. Fritz, and E. U. Schluender, "Simultaneous adsorption equilibria of organic solutes in dilute aqueous solutions on activated carbon," *Chemical Engineering Science*, vol. 29, no. 5, pp. 1279–1282, 1974.

[129] M. Baudu, G. Guibaud, D. Raveau, and P. Lafrance, "Prévision de l'adsorption de molécules organiques en solution aqueuse en fonctions de quelques caractéristiques physico-chimiques de charbons actifs," *Water Quality Research Journal*, vol. 36, no. 4, pp. 631–657, 2001.

[130] W. J Weber, B van Vliet, M J. Weber, and B. M. van Vliet, "Synthetic adsorbents and activated carbons for water treatment: statistical analyses and interpretations," *Journal - American Water Works Association*, vol. 73, no. 8, pp. 426–431, 1981.

[131] A. W. Marczewski, "Basics of liquid adsorption," pp. 11–24, 2002, https://www.adsorption.org.

[132] S. K. Lagergren, "About the theory of so-called adsorption of soluble substances," *Sven. Vetenskapsakad. Handingarl*, vol. 24, pp. 1–39, 1898.

[133] Y. Ho, G McKay, S. Ho, and G. McKay, "The sorption of lead (II) ions on peat," *Water Water Researchesearch*, vol. 33, no. 2, pp. 578–584, 1999.

[134] S. Y. Elovich and O. G. Larinov, "Theory of adsorption from solutions of non-electrolytes on solid (I) equation adsorption from solutions and the analysis of its simplest form, (II) verification of the equation of adsorption isotherm from solutions," *Izv. Akad. Nauk. SSSR, Otd. Khim. Nauk*, vol. 2, no. 2, pp. 209–216, 1962.

[135] A. G. Ritchie and G. Ritchie, "Alternative to the Elovich equation for the kinetics of adsorption of gases on solids," *Journal of the Chemical Society, Faraday Transactions 1: Physical Chemistry in Condensed Phases*, vol. 73, pp. 1650–1653, 1977.

[136] A. Özer, "Removal of Pb (II) ions from aqueous solutions by sulphuric acid-treated wheat bran," *Journal of Hazardous Materials*, vol. 141, no. 3, pp. 753–761, 2007.

[137] G. E. Boyd, A W. Adamson, L. S. Myers, A. W. Adamson, and L. S. Myers, "The The Exchange Adsorption of Ions from Aqueous Solutions by Organic Zeolites. II. Kinetics[1]xchange adsorption of ions from aqueous solutions by organic zeolites. II. Kinetics," *Journal of the American Chemical Society*, vol. 69, no. 11, pp. 2836–2848, 1947.

[138] T. Furusawa, J. M. Smith, and M. Smith, "Fluid—Fluid-Particle and Intraparticle Mass Transport Rates in Slurriesarticle and intraparticle mass transport rates in slurries," *Industrial & Engineering Chemistry Fundamentals*, vol. 12, no. 2, pp. 197–203, 1973.

[139] A. P. Mathews and W. Weber, "Effects of external mass transfer and intraparticle diffusion on adsorption rates in slurry reactors AIChE Symposium Series," vol. 73, no. 166, 1977.

[140] A. L. Hines and R. N. Maddox, *Mass Transfer: Fundamentals and Applications*, Vol. 434, Prentice-Hall, , Englewood Cliffs, NJ, USA, 1985.

[141] W. J Weber, J Morris, C J. Weber, and J. C. Morris, "Kinetics of Kinetics of Adsorption on Carbon from Solutiondsorption on carbon from solution," *Journal of the Sanitary Engineering Division*, vol. 89, no. 2, pp. 31–59, 1963.

[142] R. Leyva-Ramos, C. Geankoplis, and J. Geankoplis, "Model simulation and analysis of surface diffusion of liquids in porous solids," *Chemical Chemical Engineering Sciencengineering Science*, vol. 40, no. 5, pp. 799–807, 1985.

[143] J. Halévy, "La Juive. Opéra en cinq actes de Scribe," *Musique de F. Halévy. Divertissement de M. Taglioni*, 1885.

Hindawi
Journal of Chemistry
Volume 2023, Article ID 2113151, 14 pages
https://doi.org/10.1155/2023/2113151

*Research Article*

# Aloe Vera Extract-Mediated CuO NPs as Catalysts for the Synthesis of 4-Hydroxy-3-Methoxybenzaldehyde-Connected Piperidine Derivatives and Their Antibacterial Activity

**Ponnusamy Packialakshmi,[1] Perumal Gobinath,[1] Anis Ahamed,[2] Hissah Abdulrahman Alodaini,[2] Ashraf Atef Hatamleh,[2] Mohamed Taha Yassin,[2] Akbar Idhayadhulla,[1] and Radhakrishnan Surendrakumar[1]**

[1]*Department of Chemistry, Nehru Memorial College (Affiliated Bharathidasan University), Puthanamapatti, Tamil Nadu, India*
[2]*Department of Botany & Microbiology, College of Sciences, King Saud University (KSU), P.O. Box 2455, Riyadh 11451, Saudi Arabia*

Correspondence should be addressed to Radhakrishnan Surendrakumar; surendrakumar@nmc.ac.in

Received 20 September 2022; Revised 6 December 2022; Accepted 20 March 2023; Published 19 April 2023

Academic Editor: Mahmoud Nasr



We have designed an easy, affordable, and eco-friendly technique for Schiff base preparation of vanillin-coupled piperidine analogues using CuO NPs as a catalyst. Using a green chemistry strategy using copper oxide nanoparticles (CuO NPs) as a catalyst, a unique one-pot synthesis of Schiff base vanillin-linked piperidine derivatives (2, 2a-2j) may be generated, with a potential yield in a short reaction time. The CuO NPs were synthesized with the aloe vera extract. The newly synthesized piperidin-4-ylidene analogues were investigated using FT-IR, NMR ($^1$H, $^{13}$C), mass spectra, and elemental analysis. The morphology of piperidine derivatives was studied using XRD and TEM. The compound 2a-2j was evaluated for antibacterial activity against gram +ve and gram −ve bacteria. Compound 2d is exceptionally active against (5.0 $\mu$g/mL, *E. coli*), and 2c is very effective against (4.0 $\mu$g/mL, *L. plantarum*) when compared to reference drug and other Schiff base of vanillin-associated piperidine derivatives. Finally, we concluded the compounds 2c and 2d have strong antibacterial activity and can be used as antibacterial drugs in the future.

## 1. Introduction

Antimicrobial drugs now on the market have a number of drawbacks, including drug resistance in microbes, toxicity, and a narrow range of activity. As a result, one of the most difficult aims in antifungal and antibacterial research today is finding innovative molecules to solve the aforementioned difficulties [1]. Currently available antibiotics include penicillins, tetracyclines, cephalosporins, nitrobenzene derivatives, polypeptide antibiotics (polymixin-B, Bacitracin, etc.), macrolide antibiotics (erythromycin, roxithromycine, etc.), and derivatives of nicotinic acid from diverse sources [2]. Furthermore, the majority of dangerous microorganisms have developed resistance to these medications. Antimicrobial drug development is a vital responsibility in combating this major medical problem [3]. The aromatic ring of vanillin contains aldehyde, hydroxyl, and ether functional groups. Furthermore, vanillin is a food additive that the Food and Drug Administration (FDA) has permitted and classify as "Generally Recognized as Safe" (GRAS) [4]. Vanillin is an antibacterial phenolic compound that has been used to remove infections in fruits and vegetables. On the other hand, its bactericidal and moderating properties have yet to be determined [5]. In the presence of a variety of chemical and physical agents of vanillin, a nutritional flavouring ingredient, has been demonstrated to have antimutagenic and antioxidant abilities, as well as being anticarcinogenic [6, 7]. Vanillin is widely considered to be one of the most extensively used flavouring substances. Due to its flavour qualities and antimicrobial properties, it has

been exploiting as a natural food additive [8]. Many natural substances, especially plant-derived phenolic compounds, have potent antibacterial properties and so could be employed as novel food preservatives [9]. According to study, vanillin affects the cytoplasmic membrane of the food-borne bacterial strains *Listeria innocua*, and *Escherichia coli*. The antibacterial activity of vanillin and their compounds were revealed to be depending on exposure period, target organism, and concentration. Nonlactic Vanillin resistance is higher in Gram-positive bacteria than in Gram −ve bacteria [10]. Vanillin has also been demonstrated to have antibacterial action in test bed medium, fruit juices, fruit purees, and fruit-based agar systems against a various mould and yeast species [11]. These derivatives are commonly used as flavours in the cosmetics and food sectors. The phenolic group in vanillin attributed to antibacterial activity. Because bacteria are so readily irritated, researchers are constantly working to improve their antimicrobial activity. Vanillin and cinnamon together have been shown to have a synergistic antibacterial and antifungal activity [12]. Vanillin was also oxidised to produce carboxylic acid, significantly enhanced its antibacterial action [13]. Piperidin-4-one oxime ester generated from vanillin has greater bactericidal activity than the positive control [14]. Acetyl vanillin compounds have also been shown to have bactericidal action [2]. When OH group are present, antibacterial action against *Pseudomonas* strains is boosted [15]. Piperidine has been associated to antibacterial, antifungal, anticancer, anticonvulsant, and antihyperlipidemic activities [16–23]. Piperidin-4-ones exhibit antiviral, antibacterial, and fungicidal effects, as well as analgesic, hypotensive, and central nervous system depressant qualities [24]. An *in vitro* study shows that piperidone compounds can inhibit human placental aromatase [25]. The compounds based on piperidinones, in particular those containing aryl substituents at the piperidinone ring's C-2 and C-6, were effective antibacterial and antioxidant agents [26]. Furthermore, thiosemicarbazones, oximes, sulphur, and nitrogen-containing hetero-cycles derived by investigating the reactivity of the keto moiety have been demonstrated to have higher microbial activities than ketone [27]. Schiff bases exhibit bacteriostatic and antibacterial effects, according to a literature study [28]. They have antibacterial, antifungal, antitumor, and anticancer properties, and they can kill *E. coli, C. albicans, S. aureus, P. viticola, B. polymyxa,* and other bacteria and fungi [29–31]. By combining active methylene compounds with aromatic aldehydes in ethanol in the presence of ammonium acetate, various 3-piperidein-2-ones, 2-aryl-4-piperidones, oxazolopiperidones, 3-amino-2-arylpiperidin-4-ones, 3-amino piperidin-2-ones, and hydroxy lactams were generated [32]. Recently, copper nitrate and leaf extract were used to make CuO nanospheres, and the antibacterial effectiveness against Gram-positive and Gram-negative human pathogenic bacteria was also assessed [33]. $CuAl_2O_4$ nanocomposite was made via microwave synthesis and multicomponent reactions, and CuO NPs were successfully active as a heterogeneous catalyst for the preparation of polyhydroquinoline derivatives [34, 35]. The catalysts in these reactions were reported on the literature [36–47]. Piperidones have antibacterial, antitubercular, antioxidant, antitumor [48], cytotoxic [49], analgesic, anticancer [50], anti-HIV, antiviral [51], and other activities. Some of the more modern techniques for synthesising Schiff bases include microwave irradiation and water as a medium and ultrasound irradiation of silica [52]. The antibacterial active compounds of vanillin and piperidine derivatives are present in Figure 1.

Nanotechnology is now widely recognized as the impending industrial revolution, as it is predicted to be the foundation of numerous biological advancements in the twenty-first century. Nanomaterials have been termed a "mystery of modern medicine" and have sparked a lot of curiosity in recent decades [53]. Nano ZnO as a heterogeneous catalyst has gotten a lot of interest because it is a cheap, nontoxic catalyst with environmental benefits like quick execution, catalyst recycling, low corrosion, easy transport, waste reduction, and disposal [54]. As a result, it is one of the most suitable catalysts for the production of piperidine derivatives. Figure 2 depicts pharmacologically active piperidinone molecules, while Figure 3 depicts clinically available piperidine medicines.

## 2. Materials and Methods

*2.1. General Methods.* Merck provided the ingredients vanillin, ammonium acetate, substituted aldehyde, and thiosemicarbazide. In open capillary tubes that were not adjusted, melting points were measured. The IR spectra (KBr) on a Shimadzu 8201pc ($4000–400\,cm^{-1}$) were recorded in KBr. In order to capture the $^1H$ and $^{13}C$ NMR spectra, a Bruker DRX-300 MHz was employed. Mass spectra were captured using the Clarus SQ8 model of Perkin Elmer GCMS (EI). All the supporting information of synthesized compounds (2, 2a-2j) is given in supplementary file. An elemental analyser model (Varian EL III) was used to do the elemental analysis (C, H, and N). The purity of the substances was determined using silica gel plates and thin layer chromatography (TLC).

*2.2. Preparation of Aloe Barbadensis Miller Leaf Extract.* Scrubbing, wiping, and scorching 30 g of Aloe barbadensis Miller leaves in 100 mL of deionized water until it became dark yellow was used to make the plant extract solution. The plant product was cooled to ambient temperature, filtered through Whatman filter paper, and kept at 10°C for further investigation.

*2.2.1. Preparation of CuO NPs Using ALE.* CuO NPs were made by dissolving a sample of $Cu(CH_3COO)_2$. $H_2O$ (0.2 g) in 70 mL of deionized (DI) water. After that, 10 mL of Aloe Vera Leaf Extract (ALE) was added, and the mixture was agitated with a magnetic stirrer for 30 mins (600 rpm). The solution's pH was then adjusted by adding 1 mL of 10% NaOH solution drop by drop while stirring. After the reaction was completed, the brown precipitates were filtered, washed several times with hot water, and dried at ambient temperature. Afterward, the powder was calcined for 3 hrs at

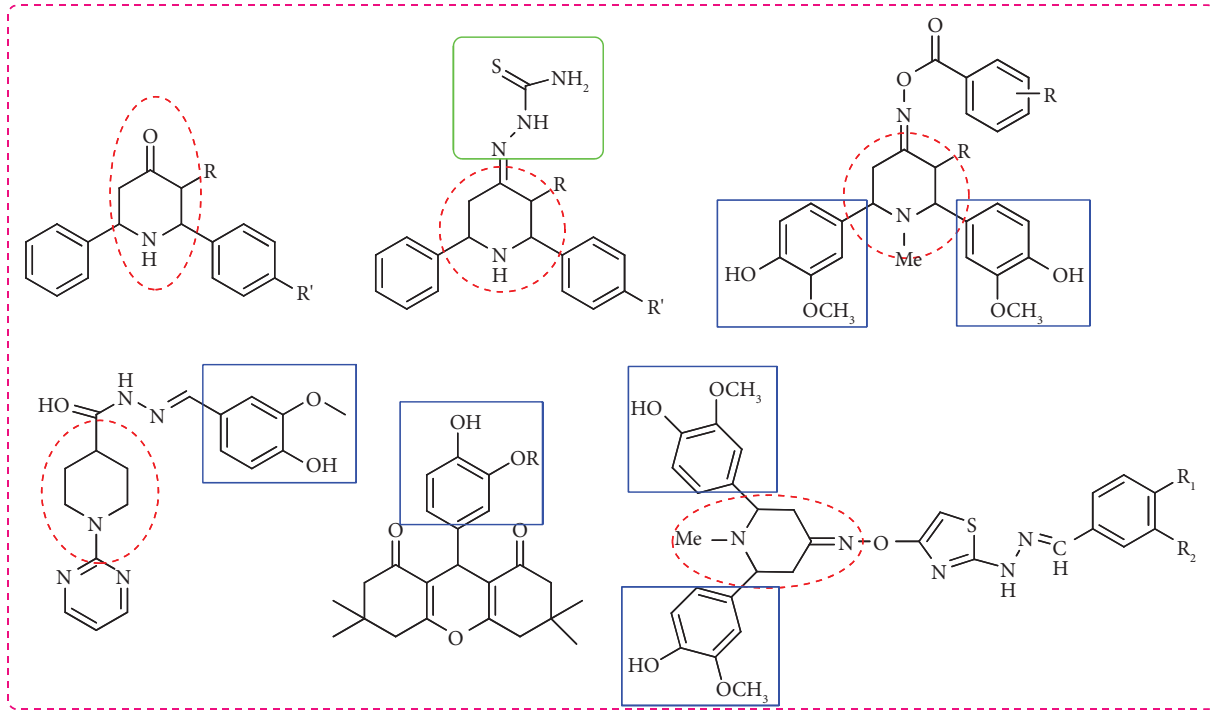

Figure 1: Antibacterial active compounds of Vanillin and piperidine derivatives.

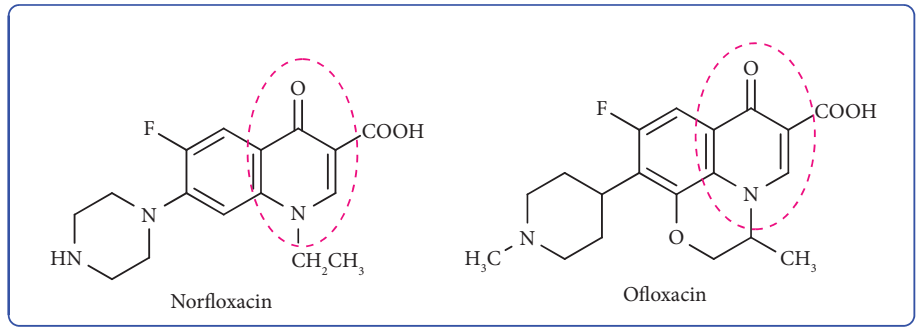


Figure 2: Structure of piperidinone pharmacologically active drug.

600°C before being crushed into fine powder with a pestle mortar. Figure 4 shows the steps for making CuO NPs with aloe vera extract. The above-given procedure was followed by previously reported method [55].

*2.3. Synthesis Procedure of 2-(2,6-Bis (4-Hydroxy-3-Methoxyphenyl) Piperidin-4-Ylidene) Hydrazinecarbothioamide (2).* CuO NPs are used as a catalyst to produce a brownish yellow colour precipitate of compound 2 from compound 1 of piperidine-4-one derivative (0.01 mol, 3.43 g), thiosemicarbazide (0.01 mol, 0.91 g) dissolved in ethanol solution 2 hours refluxed, and compound 1 of piperidine-4-one derivative (0.01 mol, 3.43 g) dissolved in ethanol solution under reflux for 2 hours. The yield was filtered and dried after being washed with ice-cold water to form the crude substance. TLC was used to validate the reaction's development. Ethanol was used to recrystallize the precipitate.

*2.4. General Procedure for the N-Benzylidene-2-(2,6-Bis (4-Hydroxy-3-Methoxyphenyl) Piperidin-4-ylidene) Hydrazinecarbothioamide (2a).* Compound 2 is a light brown color precipitate of piperidine-4-ylidene hydrazinecarbothioamide derivative (0.01 mol, 4.16 g), benzaldehyde (0.01 mol, 1.01 mL), combined with ethanol solution and CuO NPs as a catalyst. The crude product was formed, the yield was first cleanse with ice-cold water and then filtered and dried. The catalyst was separated from the crude precipitate by centrifuging it, and then it was washed multiple times with ethanol before being dried and used in all subsequent reactions. Thin layer chromatography was used to verify the product. Ethanol was used to recrystallize the precipitate. The same method was used to synthesis compounds 2b-j.

Preparation of 2-(2,6-bis (4-hydroxy-3-methoxyphenyl) piperidin-4-ylidene) hydrazinecarbothioamide (2) Brown solid (85%); Mp 168°C; IR ($cm^{-1}$) (KBr); 3503 (OH), 3343 (NH), 3173 ($NH_2$), 3045 (CH-str Ar), 1635 (C=N), 1429

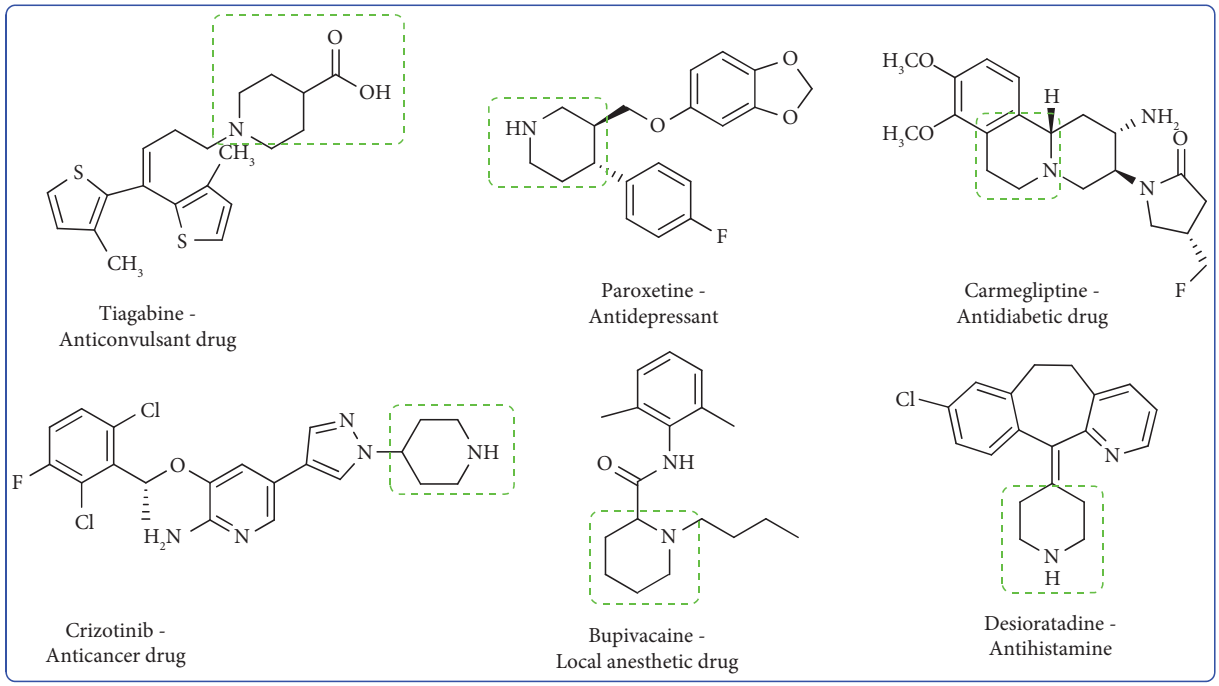


Figure 3: Clinically available piperidine drugs.

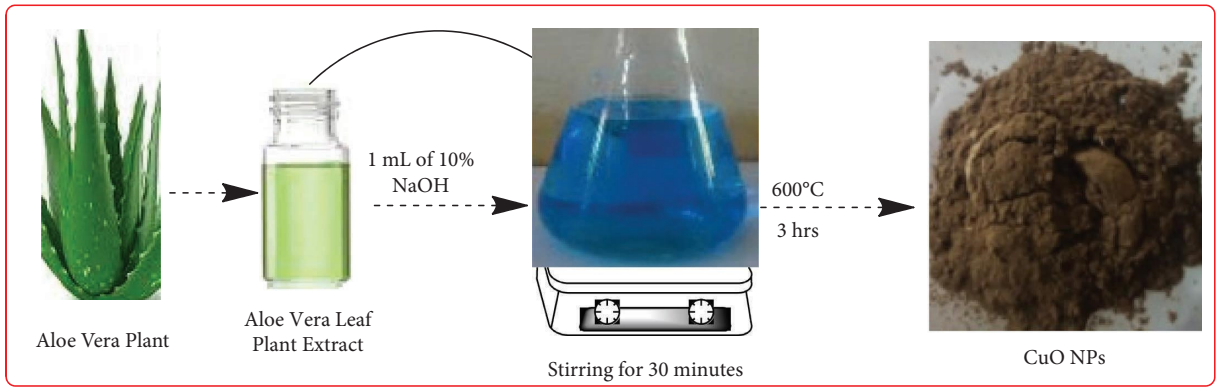


Figure 4: Synthesis of CuONPs using aloe vera leaf extract.

(C=S), 735 (C-N-C, str). $^1$H NMR ($CDCl_3$), $\delta$ (ppm) $J$ (Hz): 11.35 (1H, s, NH), 6.91, 6.72 (6H, m, Ar-H), 6.75 (s, 2H, $NH_2$), 5.32 (2H, s, OH), 4.12 (2H, m, CH in piperidin ring), 3.83 (s, 6H, $OCH_3$), 2.98–2.75 (m, 4H, $CH_2$ in piperidin), 2.14 (1H, s, NH, in piperidin ring). $^{13}$C NMR ($CDCl_3$) $\delta$ (ppm): 179.60 (1C, C=S), 147.61 (2C, Ar-C), 146.90 (2C, C-OH), 144.51, 143.52 (2C, Ar), 142.50 (1C, C=N), 127.71 (2C, Ar), 126.70 (2C, Ar), 119.72, 118.80 (2C, Ar), 61.40 (2C, CH of piperidin), 56.21 (2C, $OCH_3$), 51.72, 50.90 (2C, $CH_2$ of piperidin). EI-MS $m/z$ 417.16 ($M^+$, 22%). Elemental analysis: anal. $C_{20}H_{24}N_4O_4S$: C, 57.68; H, 5.81; N, 13.45; found: C, 57.70; H, 5.83; N, 13.47.

Synthesis of N-benzylidene-2-(2,6-bis (4-hydroxy-3-methoxyphenyl) piperidin-4-ylidene) hydrazinecarbothioamide (2a) brownish yellow powder (80%); Mp 175°C; IR (KBr) ($cm^{-1}$); 3500 (OH), 3341 (NH), 3042 (CH-Ar ring), 1633 (C=N), 1629 (C=S), 740 (C-N-C, str). $^1$H NMR ($CDCl_3$), (ppm) $J$ (Hz) $\delta$: 11.38 (1H, s, NH), 8.10 (1H, s, N=CH), 7.80 (2H, d, $J$ = 10.4 Hz, Ph), 7.48–7.15 (3H, m, Ph), 6.89, 6.72 (6H, m, Ar-H), 5.33 (2H, s, OH), 4.15 (2H, m, CH in piperidin ring), 3.93 (6H, s, $OCH_3$), 2.95–2.73 (4H, m, $CH_2$ in piperidin ring), 2.10 (s, 1H, NH, in piperidin ring). $^{13}$C NMR ($CDCl_3$) $\delta$ (ppm): 178.20 (1C, C=S), 147.00 (2C, Ar), 146.51 (2C, OH), 144.30, 143.4 (2C, Ar), 142.61 (1C, C=N), 140.50 (1C, N=CH), 136.71, 132.20, 130.61, 128.80, 126.90, 122.30 (6C, Ph), 127.51 (2C, Ar), 126.41 (2C, Ar), 119.51, 118.42 (2C, Ar), 61.20 (2C, CH of piperidin), 56.00 (2C, $OCH_3$), 51.30, 50.71 (2C, $CH_2$ of piperidin). EI-MS $m/z$ 505.19 ($M^+$, 29%). Elemental analysis: anal. $C_{27}H_{28}N_4O_4S$: C, 64.27; H, 5.59; N, 11.10; found: C, 64.29; H, 5.61; N, 11.12.

Synthesis of 2-(2,6-bis (4-hydroxy-3-methoxyphenyl) piperidin-4-ylidene)-N-(2-hydroxy benzylidene) hydrazinecarbothioamide (2b) brown solid (78%); Mp 182°C; IR (KBr) ($cm^{-1}$); 3452 (OH), 3353 (NH), 3047 (CH-Ar), 1636 (C=N), 1468 (C=S), 733 (C-N-C, str). $^1$H NMR ($CDCl_3$), (ppm) $J$ (Hz) $\delta$: 11.40 (1H, s, NH), 9.86 (1H, s, OH-Ph), 8.34

(1H, s, N=CH), 8.22, 7.23, 6.87, 6.78 (4H, m, Ph),6.92, 6.74 (6H, m, Ar), 5.30 (2H, s, OH), 4.14 (2H, m, CH in piperidin ring), 3.85 (6H, s, $OCH_3$), 2.93–2.70 (4H, m, $CH_2$ in piperidin ring), 2.13 (1H, s, NH, in piperidin ring). $^{13}$C NMR ($CDCl_3$) (ppm) $\delta$: 177.50 (1C, C=S), 156.31 (1C, N=CH), 147.60 (2C, Ar), 146.71 (2C, C-OH), 144.72, 143.60 (2C, Ar), 142.70 (1C, C=N), 139.71 (1C, C-OH), 131.20, 125.60, 120.42, 118.71, 116.32 (5C, Ph), 127.30 (2C, Ar), 126.31 (2C, Ar-C), 119.21, 118.60 (2C, Ar-C), 61.51 (2C, CH of piperidin), 56.40 (2C, $OCH_3$), 51.52, 50.61 (2C, $CH_2$ of piperidin). EI-MS $m/z$ 521.18 ($M^+$, 32%). Elemental analysis: anal. $C_{27}H_{28}N_4O_5S$: C, 62.29; H, 5.42; N, 10.76; found: C, 62.31; H, 5.44; N, 10.78.

Synthesis of 2-(2,6-bis (4-hydroxy-3-methoxyphenyl) piperidin-4-ylidene)-N-(4-hydroxy benzylidene) hydrazinecarbothioamide (2c) Brown powder (75%); Mp 187°C; IR (KBr) ($cm^{-1}$); 3456 (OH), 3345 (NH), 3049 (CH-Ar), 1634 (C=N), 1463 (C=S), 730 (C-N-C). $^1$H NMR ($CDCl_3$), $\delta$ (ppm) $J$ (Hz): 11.43 (1H, s, NH), 8.03 (1H, s, N=CH), 7.68 (2H, d, $J = 8.5$ Hz, Ph), 6.89, 6.73 (6H, m, Ar), 6.85 (2H, d, $J = 8.5$ Hz, Ph), 5.40 (1H, s, OH-Ph), 5.32 (2H, s, OH), 4.10 (2H, m, CH in piperidin ring), 3.83 (6H, s, $OCH_3$), 2.95–2.72 (4H, m, $CH_2$ in piperidin), 2.17 (1H, s, NH, in piperidin). $^{13}$C NMR ($CDCl_3$) $\delta$ (ppm): 177.80 (1C, C=S), 159.41 (1C, N=CH), 147.20 (2C, Ar), 146.42 (2C, C-OH), 144.70, 143.21 (2C, Ar), 142.72 (1C, C=N), 139.30 (1C, C-OH), 139.21, 124.70, 120.41, 118.50, 115.71 (5C, Ph), 127.52 (2C, Ar), 126.91 (2C, Ar), 119.42, 118.30 (2C, Ar), 61.30 (2C, CH of piperidin), 56.51 (2C, $OCH_3$), 51.72, 50.40 (2C, $CH_2$ of piperidin). EI-MS $m/z$ 521.18 ($M^+$, 32%). Elemental analysis: anal. $C_{27}H_{28}N_4O_5S$: C, 62.29; H, 5.42; N, 10.76; found: C, 62.27; H, 5.40; N, 10.74.

Synthesis of 2-(2,6-bis (4-hydroxy-3-methoxyphenyl) piperidin-4-ylidene)-N-(4-chlorobenzylidene) hydrazinecarbothioamide (2d) light brown (70%); Mp 190°C; IR (KBr) ($cm^{-1}$); 3460 (OH), 3343 (NH), 3044 (CH-Ar), 1632 (C=N), 1432 (C=S), 732 (C-N-C). $^1$H NMR ($CDCl_3$), $J$ (Hz) (ppm) $\delta$: 11.47 (1H, s, NH), 8.01 (1H, s, N=CH), 7.85, 7.45 (4H, m, Ph), 6.92, 6.77 (6H, m, Ar), 5.37 (2H, s, OH), 4.11 (2H, m, CH in piperidin), 3.91 (6H, s, $OCH_3$), 2.97–2.76 (4H, m, $CH_2$ in piperidin), 2.14 (1H, s, NH, in piperidin). $^{13}$C NMR ($CDCl_3$) $\delta$ (ppm): 176.03 (1C, C=S), 147.81 (2C, Ar), 146.70 (2C, C-OH), 144.42, 143.60 (2C, Ar), 142.10 (1C, C=N), 141.41 (1C, N=CH), 137.81, 135.12, 132.50, 130.61, 129.32, 127.30 (6C, Ph), 127.32 (2C, Ar-C), 126.51 (2C, Ar), 119.62, 118.50 (2C, Ar), 61.20 (2C, CH of piperidin), 56.51 (2C, $OCH_3$), 51.42, 50.60 (2C, $CH_2$ of piperidin). EI-MS $m/z$ 539.11 ($M^+$, 29%). Elemental analysis: anal. $C_{27}H_{27}ClN_4O_4S$: C, 60.16; H, 5.05; N, 10.39; found: C, 60.18; H, 5.07; N, 10.41.

Synthesis of 2-(2,6-bis (4-hydroxy-3-methoxyphenyl) piperidin-4-ylidene)-N-(2-chlorobenzylidene) hydrazinecarbothioamide (2e) brown powder (89%); Mp 195°C; IR (KBr) ($cm^{-1}$); 3467 (OH), 3350 (NH), 3038 (CH-Ar ring), 1630 (C=N), 1462 (C=S), 734 (C-N-C). $^1$H NMR ($CDCl_3$), $J$ (Hz) (ppm) $\delta$: 11.42 (1H, s, NH), 8.03 (s, 1H, N=CH), 7.87, 7.48, 7.41, 7.34 (4H, m, Ph), 6.95, 6.74 (6H, m, Ar), 5.34 (2H, s, OH), 4.14 (2H, m, CH in piperidin ring), 3.92 (6H, s, $OCH_3$), 2.94–2.70 (4H, m, $CH_2$ in piperidin ring), 2.13 (1H, s, NH, in piperidin ring). $^{13}$C NMR ($CDCl_3$) (ppm) $\delta$: 176.30 (1C, C=S), 147.50 (2C, Ar), 146.41 (2C, C-OH), 144.22, 143.50 (2C, Ar), 142.31 (1C, C=N), 141.62 (1C, N=CH), 139.10, 136.71, 130.42, 129.70, 127.30, 126.52 (6C, Ph), 127.41 (2C, Ar), 126.62 (2C, Ar), 119.30, 118.21 (2C, Ar), 61.40 (2C, CH of piperidin), 56.31 (2C, $OCH_3$), 51.22, 50.10 (2C, $CH_2$ of piperidin). EI-MS $m/z$ 417.16 ($M^+$, 22%). Elemental analysis: anal. $C_{27}H_{27}ClN_4O_4S$: C, 60.16; H, 5.05; N, 10.39; found: C, 60.14; H, 5.03; N, 10.37.

Synthesis of 2-(2,6-bis (4-hydroxy-3-methoxyphenyl) piperidin-4-ylidene)-N-(4-methoxybenzylidene) hydrazinecarbothioamide (2f) light brown powder (68%); Mp 200°C; IR (KBr) ($cm^{-1}$); 3498 (OH), 3354 (NH), 3040 (CH-Ar), 1632 (C=N), 1432 (C=S), 738 (C-N-C). $^1$H NMR ($CDCl_3$), $J$ (Hz) (ppm) $\delta$: 11.31(1H, s, NH), 7.98 (1H, s, N=CH), 7.74, 7.71, 6.98, 6.94 (4H, m, Ph), 6.87, 6.71 (6H, m, Ar), 5.30 (2H, s, OH), 4.10 (m, 2H, CH in piperidin ring), 3.83 (6H, s, $OCH_3$), 3.79 (3H, s, $OCH_3$-Ar), 2.96–2.73 (4H, m, $CH_2$ in piperidin ring), 2.16 (1H, s, NH, in piperidin ring). $^{13}$C NMR ($CDCl_3$) $\delta$ (ppm): 177.41 (1C, C=S), 160.60, 141.10, 128.90, 126.72, 114.02 (6C, Ph), 147.80 (2C, Ar), 146.51 (2C, C-OH), 144.32, 143.30 (2C, Ar), 142.51 (1C, C=N), 127.41 (2C, Ar), 126.30 (2C, Ar), 119.60, 118.41 (2C, Ar), 61.60 (2C, CH of piperidin), 56.41 (2C, $OCH_3$), 55.22 (1C, $OCH_3$-Ph), 51.40, 50.61 (2C, $CH_2$ of piperidin). EI-MS $m/z$ 535.20 ($M^+$, 30%). Elemental analysis: anal. $C_{28}H_{30}N_4O_4S$: C, 62.90; H, 5.66; N, 10.48; found: C, 62.92; H, 5.68; N, 10.50.

Synthesis of 2-(2,6-bis (4-hydroxy-3-methoxyphenyl) piperidin-4-ylidene)-N-(3-nitrobenzylidene) hydrazinecarbothioamide (2g) Brown color substance (70%); Mp 186°C; IR (KBr) ($cm^{-1}$); 3495 (OH), 3345 (NH), 3048 (CH-Ar), 1634 (C=N), 1461 (C=S), 735 (C-N-C). $^1$H NMR ($CDCl_3$), $J$ (Hz) $\delta$ (ppm): 11.61(1H, s, NH), 8.67, 8.26, 8.15, 7.68 (4H, m, Ph), 8.10 (1H, s, N=CH), 6.94, 6.76 (6H, m, Ar), 5.37 (2H, s, OH), 4.15 (2H, m, CH in piperidin ring), 3.88 (6H, s, $OCH_3$), 2.94–2.71 (4H, m, $CH_2$ in piperidin ring), 2.13 (1H, s, NH, in piperidin ring). $^{13}$C NMR ($CDCl_3$) $\delta$ (ppm): 178.33 (1C, C=S), 148.20, 136.20, 133.41, 130.51, 123.82, 121.90 (6C, Ph), 147.41 (2C, Ar), 146.72 (2C, C-OH), 144.40, 143.21 (2C, Ar), 142.72 (1C, C=N), 139.60 (1C, N=CH), 127.50 (2C, Ar), 126.31 (2C, Ar), 119.41, 118.52 (2C, Ar), 61.70 (2C, CH of piperidin), 56.31 (2C, $OCH_3$), 51.52, 50.23 (2C, $CH_2$ of piperidin). EI-MS $m/z$ 550.17 ($M^+$, 32%). Elemental analysis: anal. $C_{27}H_{27}N_5O_6S$: C, 59.00; H, 4.95; N, 12.74; found: C, 59.02; H, 4.97; N, 12.76.

Synthesis of 2-(2,6-bis (4-hydroxy-3-methoxyphenyl) piperidin-4-ylidene)-N-(4-dmethylami nobenzylidene) hydrazinecarbothioamide (2h) brownish yellow powder (73%); Mp 237°C; IR (KBr) ($cm^{-1}$); 3492 (OH), 3340 (NH), 3046 (CH-Ar), 1632 (C=N), 1461 (C=S), 737 (C-N-C). $^1$H NMR ($CDCl_3$), $J$ (Hz) $\delta$ (ppm): 11.70 (1H, s, NH), 7.98 (1H, s, N=CH), 7.61, 6.75, 6.53 (4H, m, Ph), 6.89, 6.68 (6H, m, Ar), 5.36 (2H, s, OH), 4.15 (2H, m, CH in piperidin ring), 4.05 (6H, m, N $(CH_3)_2$), 3.86 (6H, s, $OCH_3$), 2.97–2.78 (4H, m, $CH_2$ in piperidin ring), 2.19 (1H, s, NH, in piperidin ring). $^{13}$C NMR ($CDCl_3$) $\delta$ (ppm):179.61 (1C, C=S), 162.00 (1C, N=CH), 153.00 (1C, C-N), 147.30 (2C, Ar), 146.51 (2C, C-OH), 144.22, 143.60 (2C, Ar), 142.41 (1C, C=N), 128.52, 123.43, 112.00 (5C, Ph), 127.90 (2C, Ar), 126.51 (2C, Ar), 119.80, 118.31 (2C, Ar), 61.10 (2C, CH of piperidin), 56.41

(2C, $OCH_3$), 51.92, 50.73 (2C, $CH_2$ of piperidin), 41.01 (2C, N-$(CH_3)_2$). EI-MS $m/z$ 548.23 ($M^+$, 31%). Elemental analysis: anal. $C_{29}H_{33}N_5O_4S$: C, 63.60; H, 6.07; N, 12.79; found: C, 63.62; H, 6.09; N, 12.81.

Synthesis of 2-(2,6-bis (4-hydroxy-3-methoxyphenyl) piperidin-4-ylidene)-N-3-phenylallylidene) hydrazinecarbothioamide (2i) Dark Brown powder (74%); Mp 198°C; IR (KBr) ($cm^{-1}$); 3485 (OH), 3338 (NH), 3042 (CH-Ar), 1645 (C=N), 1462 (C=S), 734 (C-N-C). $^1$H NMR ($CDCl_3$), $J$ (Hz) $\delta$ (ppm): 11.82 (1H, s, NH), 7.99 (1H, s, N=CH), 7.63, 7.35, 7.20 (5H, m, Ph), 7.08 (1H, d, $J = 10.5$ Hz, CH=CH), 6.96 (1H, t, $J = 8.5$ Hz, C-CH), 6.87, 6.74 (6H, m, Ar), 5.33 (2H, s, OH), 4.12 (2H, m, CH in piperidin ring), 3.86 (6H, s, $OCH_3$), 2.92–2.70 (4H, m, $CH_2$ in piperidin ring), 2.18 (1H, s, NH, in piperidin ring). $^{13}$C NMR ($CDCl_3$) $\delta$ (ppm): 177.42 (1C, C=S), 147.10 (2C, Ar), 146.41 (2C, C-OH), 145.82 (1C, NH=C), 144.30, 143.61 (2C, Ar), 142.22 (1C, C=N), 141.00, 137.60, 130.33, 130.21 (6C, Ph), 127.81 (2C, Ar), 126.90 (2C, Ar), 126.02, (1C, C=C), 125.20 (1C, C=C), 119.71, 118.20 (2C, Ar), 61.31 (2C, CH of piperidin), 56.42 (2C, $OCH_3$), 51.60, 50.71 (2C, $CH_2$ of piperidin). EI-MS $m/z$ 530.64 ($M^+$, 33%). Elemental analysis: anal. $C_{29}H_{30}N_4O_4S$: C, 65.64; H, 5.70; N, 10.56; found: C, 65.66; H, 5.72; N, 10.58.

Synthesis of 2-(2,6-bis (4-hydroxy-3-methoxyphenyl) piperidin-4-ylidene)-N-(furan-2-ylthylene) hydrazinecarbothioamide (2j) light brown powder (82%); Mp 240°C; IR (KBr) ($cm^{-1}$); 3501 (OH), 3342 (NH), 3043 (CH-Ar), 1634 (C=N), 1425 (C=S), 736 (C-N-C). $^1$H NMR ($CDCl_3$), $J$ (Hz) $\delta$ (ppm): 11.84 (1H, s, NH), 8.06 (1H, s, N=CH), 7.94 (1H, d, $J = 20.2$ Hz, furyl), 6.92, 6.57 (2H, m, furyl), 6.93, 6.74 (6H, m, Ar), 5.31 (2H, s, OH), 4.14 (2H, m, CH in piperidin ring), 3.87 (6H, s, $OCH_3$), 2.95–2.70 (4H, m, $CH_2$ in piperidin ring), 2.13 (1H, s, NH, in piperidin ring). $^{13}$C NMR ($CDCl_3$) $\delta$ (ppm): 192.00 (1C, C=S), 148.41, 145.02, 117.82, 114.0 (4C, furyl), 147.90 (2C, Ar), 146.11 (2C, C-OH), 144.30, 143.01 (2C, Ar), 142.42 (1C, C=N), 135.00 (1C, CH=N), 127.71 (2C, Ar), 126.52 (2C, Ar), 119.80, 118.61 (2C, Ar), 61.20 (2C, CH of piperidin), 56.01 (2C, $OCH_3$), 51.92, 50.43 (2C, $CH_2$ of piperidin). EI-MS $m/z$ 495.17 ($M^+$, 27%). Elemental analysis: anal. $C_{25}H_{26}N_4O_4S$: C, 60.71; H, 5.80; N, 11.33; found: C, 60.73; H, 5.82; N, 11.35.

*2.5. In Vitro Antibacterial Screening.* The antibacterial action of the substances 2a-2j was tested against the various bacterial pathogens using a method previously reported [56]. Every generated compounds the lowest inhibitory concentration was calculated. The DMSO was dissolved in each test sample at a concentration of 64 $\mu$g/mL (dimethyl-sulfoxide). Twofold dilutions were used to create different dilutions (64, 32, and 0.5 $\mu$g/mL). The matching wells were injected with the microbe solutions containing 106 CFU/mL, which were then incubated at 36°C for 24 hours.

## 3. Results and Discussion

*3.1. Characterization of CuO NPs*

*3.1.1. TEM (Transmission Electron Microscopy).* The morphology and particle size of phytosynthesized CuO NPs was described using TEM analysis. Figure 5 is a schematic representation of green synthetic CuO NPs, which exhibit spherical morphology with an average size of 20 nm. The diameters of the nanoparticles, which range from 0 to 25 nm, are uniform. So, it is evident from the TEM study that the CuO NPs are of high quality and are reduced in size.

*3.1.2. X-Ray Diffraction Study.* The XRD (Figure 6) peaks' relative intensities and positions matched those indexed to CuO. (JCPDS file no. 48-1548). Copper oxide was identified by XRD peaks at reaction planes (002), (111), (202), (202), (113), and (311) at 35.47, 38.68, 48.76, 56.23, 61.60, and 66.31° 2$\theta$, respectively [57]. $Cu^{2+}$ was determined to be CuO, a hydrolysis product of $Cu(OAc)_2$, as confirmed by XRD.

*3.1.3. Retrieval of Catalyst.* Catalyst retrieval is crucial in the biosynthetic method. We investigated their recyclability nearly ten times, with a slight loss catalytic action utilised in imine formation of vanillin coupled piperidine derivatives (2a-2j) copper oxide nanoparticle reaction. Figure 7 represent the recovery of catalyst, due to the catalyst's surface area throughout the reaction or partial loss of regeneration/basic sites, the reduced activity might be seen with the regenerate catalyst on salvaging. The yield of several aldehydes employed in the condensation with CuO NPs is shown in Table 1.

*3.2. Chemistry*

*3.2.1. Preparation of Piperidine Analogues.* The $R_F$ value of vanillin derivative is 0.297 using hexane: ethylacetate. A previously published literature approach [14] was used to manufacture the piperidin-4-one derivative of molecule 1. The compound 2 was obtained in excellent yield with a short reaction time using a one-pot two-component condensation reaction of piperidine-4-one derivative (0.01 mol, 3.43 g) and thiosemicarbazide (0.01 mol, 0.91 g) dissolved in aqueous ethanol solvent system, reflux for 2 hours under CuO NPs as a catalyst. The piperidin-4-ylidene hydrazinecarbothioamide derivatives freshly synthesized are given in Scheme 1. The synthesized compounds of (2a-j) showed in Scheme 2, and pathway mechanism of 2a-j given in Scheme 3. All the newly synthesized chemical structures are showed in Figure 8.

*3.3. In Vitro Antibacterial Screening.* Vanillin linked piperidine analogues of 2a-2j were evaluated *in vitro* against *Lactobacillus plantarum* (ATCC-25923), *Listeria innocua* (ATCC 33090), *Pseudomonas aeruginosa* (ATCC-27853), and *Escherichia coli* (ATCC-25922). Erythromycin was used as a reference. Compound 2d (5.0 $\mu$g/mL, *E. coli*) is more active when compared to normal medicine, while compound 2c (4.0 $\mu$g/mL, *L. plantarum*) is extremely active. Figure 9 displays the antibacterial assay images, and Table 2 lists the MIC values.

*3.4. Structure Activity Relationship.* Structure to its antibacterial action. SAR analysis can be used to identify chemical groups that are responsible for the organism's

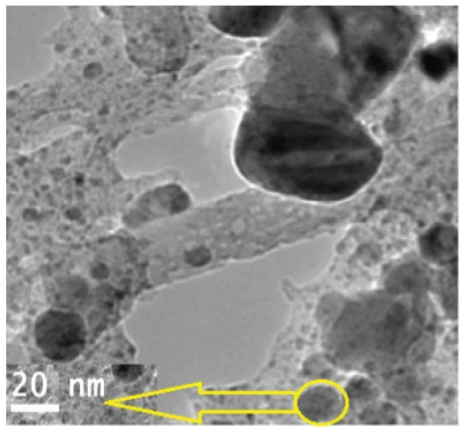


Figure 5: TEM image of CuO NPs at 20 nm.

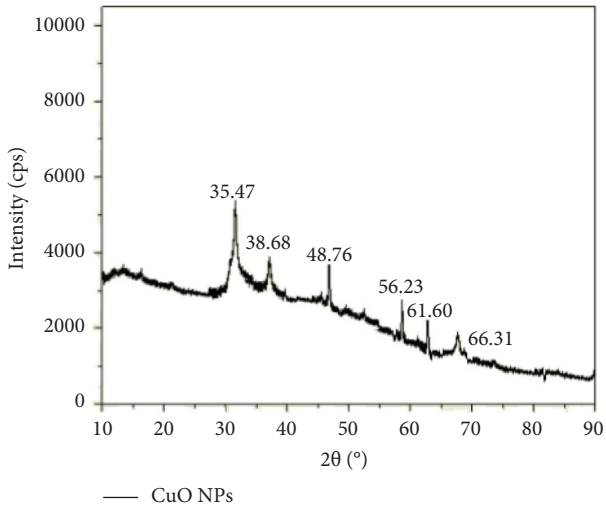


Figure 6: X-ray diffraction study of CuO nanoparticle.

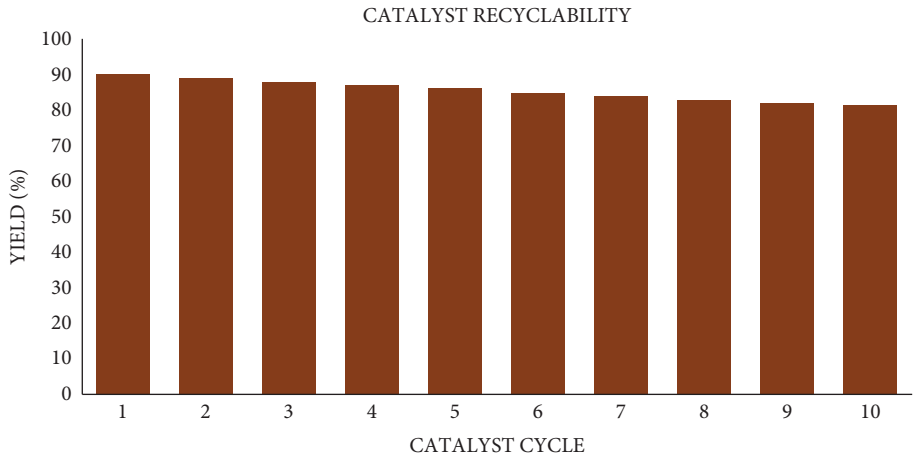


Figure 7: Recyclability of CuO nanoparticles.

Table 1: Catalyst recyclability.

| S. no | Catalyst use | (%) yield |
|---|---|---|
| 1 | 1st | 90 |
| 2 | 2nd | 89 |
| 3 | 3rd | 88 |
| 4 | 4th | 87 |
| 5 | 5th | 86 |
| 6 | 6th | 85 |
| 7 | 7th | 84 |
| 8 | 8th | 83 |
| 9 | 9th | 82 |
| 10 | 10th | 81 |

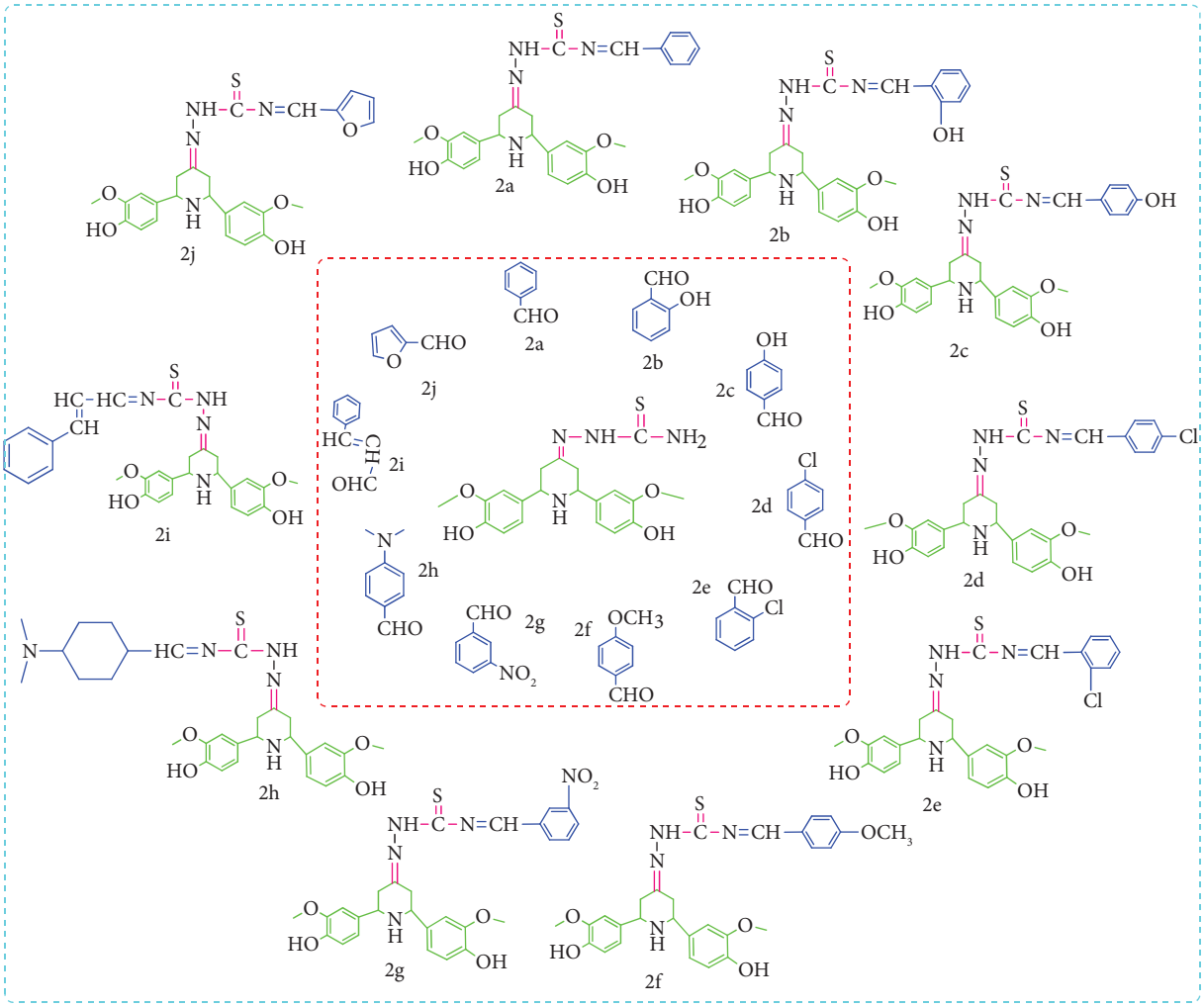


Figure 8: Structure of newly synthesized piperidine-4-ylidene-benzylidene analogues 2a-2j.

antibacterial activity. The SAR was calculated using the antibacterial activity of vanillin linked piperidine derivatives. When compared to the standard erythromycin and others, compounds 2c and 2d are much more active. When compared to standard erythromycin, it was discovered to be extremely active against 2d (5.0 $\mu$g/mL, *E. coli*, Gram −ve) and 2c (4.0 $\mu$g/mL, *L. plantarum*, Gram +ve) bacteria due to the presence of chloro (Cl) and hydroxyl (-OH) groups at para position in the phenyl moiety. The synthesis of imine improves the antibacterial activity of highly active drugs. Figure 10 depicts the SAR of highly active chemicals.

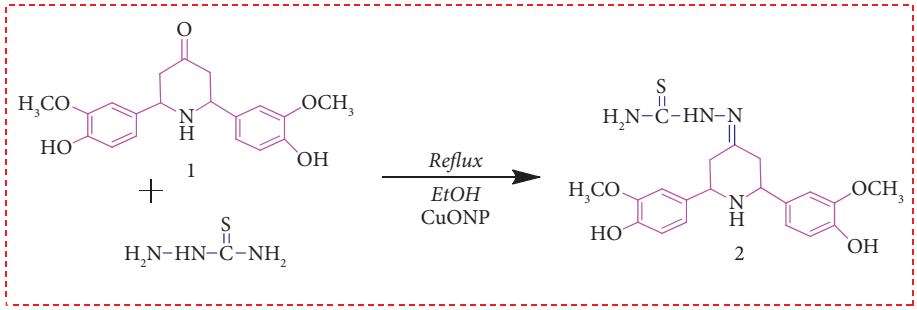


Scheme 1: Synthesis of piperidin-4-ylidene hydrazinecarbothioamide derivatives.

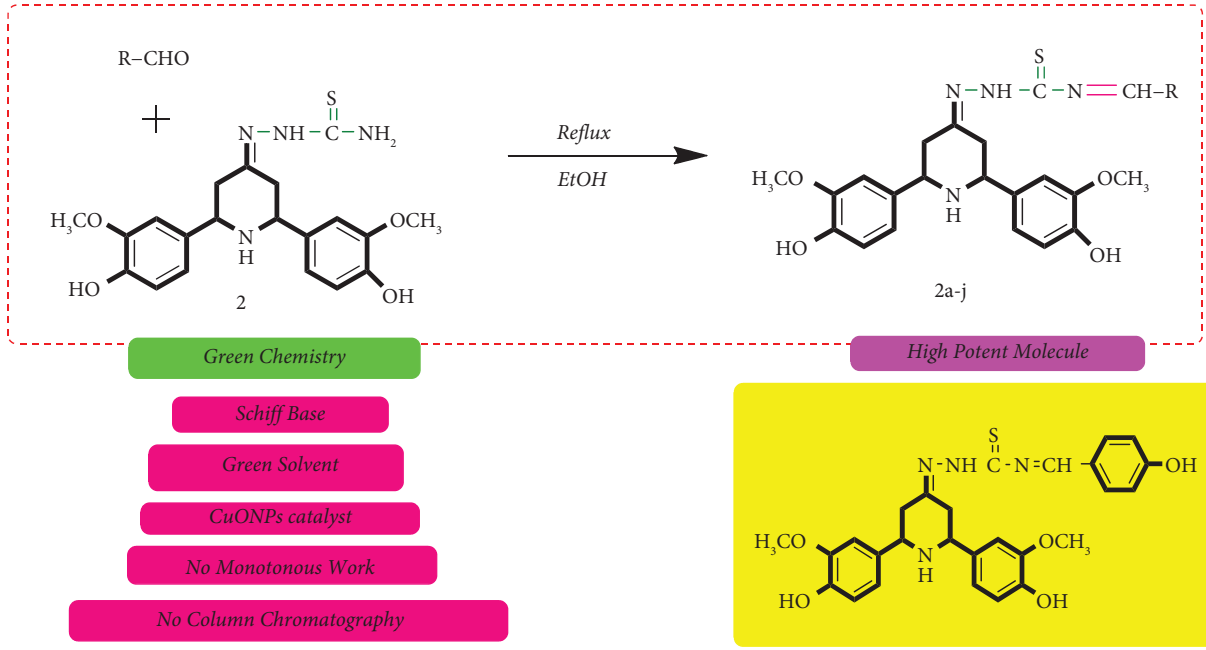


R= $C_6H_5$, 2-OH-$C_6H_4$, 4-OH-$C_6H_4$, 4-Cl-$C_6H_4$, 2-Cl-$C_6H_4$, 4-$OCH_3$-$C_6H_4$, 3-$NO_2$-$C_6H_4$, 4-N $(CH_3)_2$-$C_6H_4$, Ph-CH=CH-CHO, Furfural

Scheme 2: Synthesis of benzylidene derivatives viz. Schiff base method.

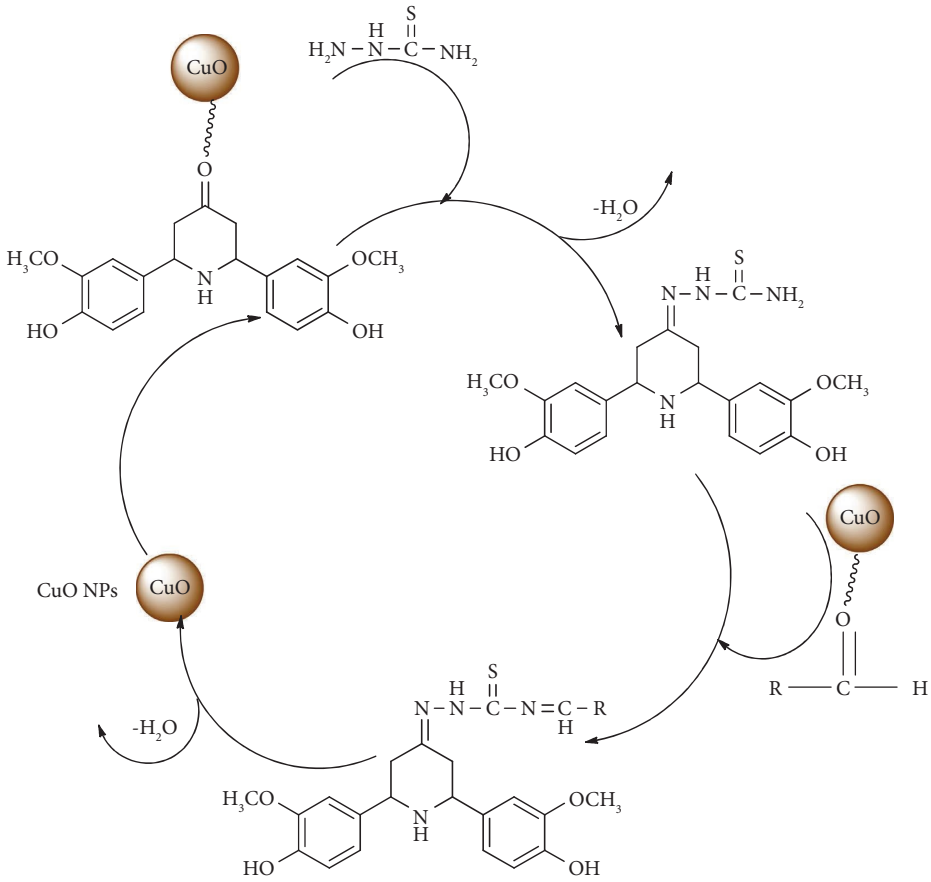


Scheme 3: Proposed mechanism of vanillin derivatives synthesis using a CuO NPs catalyst.

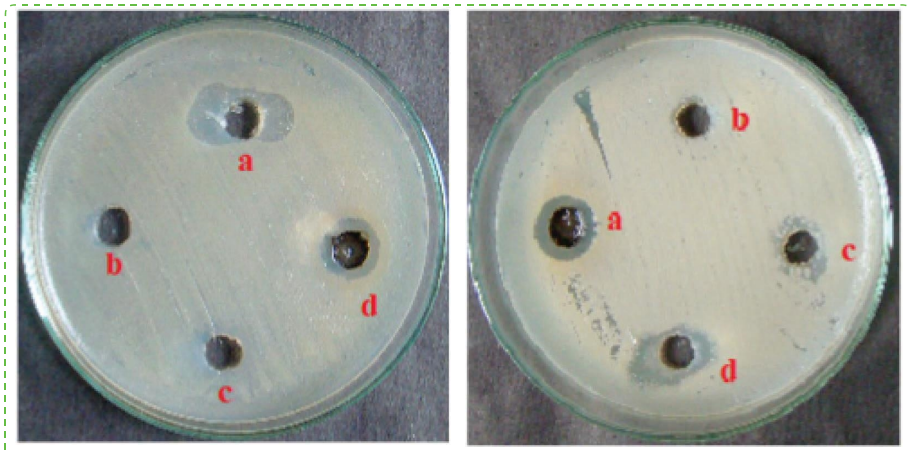


Compound - 2c is highly active in gram positive *L.plantarum*

a = 4.0 μg/mL, *L. plantarum*, b = 32 μg/mL,c = DMSO, d = Standard

Compound - 2d is highly active in gram negative *E. coli*

a = 5.0 μg/mL, *E. coli*, b = 32 μg/mL c = DMSO, d = Standard

Figure 9: Antibacterial assay of highly active compounds with standard.

Table 2: Antibacterial activity of Gram-negative and Gram-positive for compounds 2a-2j with their MIC values.

| | Gram negative ($\mu$g/mL) | | Gram positive ($\mu$g/mL) | |
|---|---|---|---|---|
| Compounds no | *E. coli* | *P. aeruginosa* | *L. plantarum* | *L. innocua* |
| 2a | 10 | 21 | 9 | 30 |
| 2b | 9 | 8 | 14 | 11 |
| **2c** | 11 | 10 | **4** | 17 |
| **2d** | **5** | 12 | 32 | 21 |
| 2e | 13 | 18 | 10 | 12 |
| 2f | 15 | 9 | 7 | 31 |
| 2g | 12 | 20 | 20 | 16 |
| 2h | 16 | 11 | 15 | 10 |
| 2i | 8 | 15 | 23 | 14 |
| 2j | 20 | 17 | 28 | 18 |
| Erythromycin | 7 | 7 | 5 | 9 |

Compounds 2c and 2d are highly active in antibacterial activity.

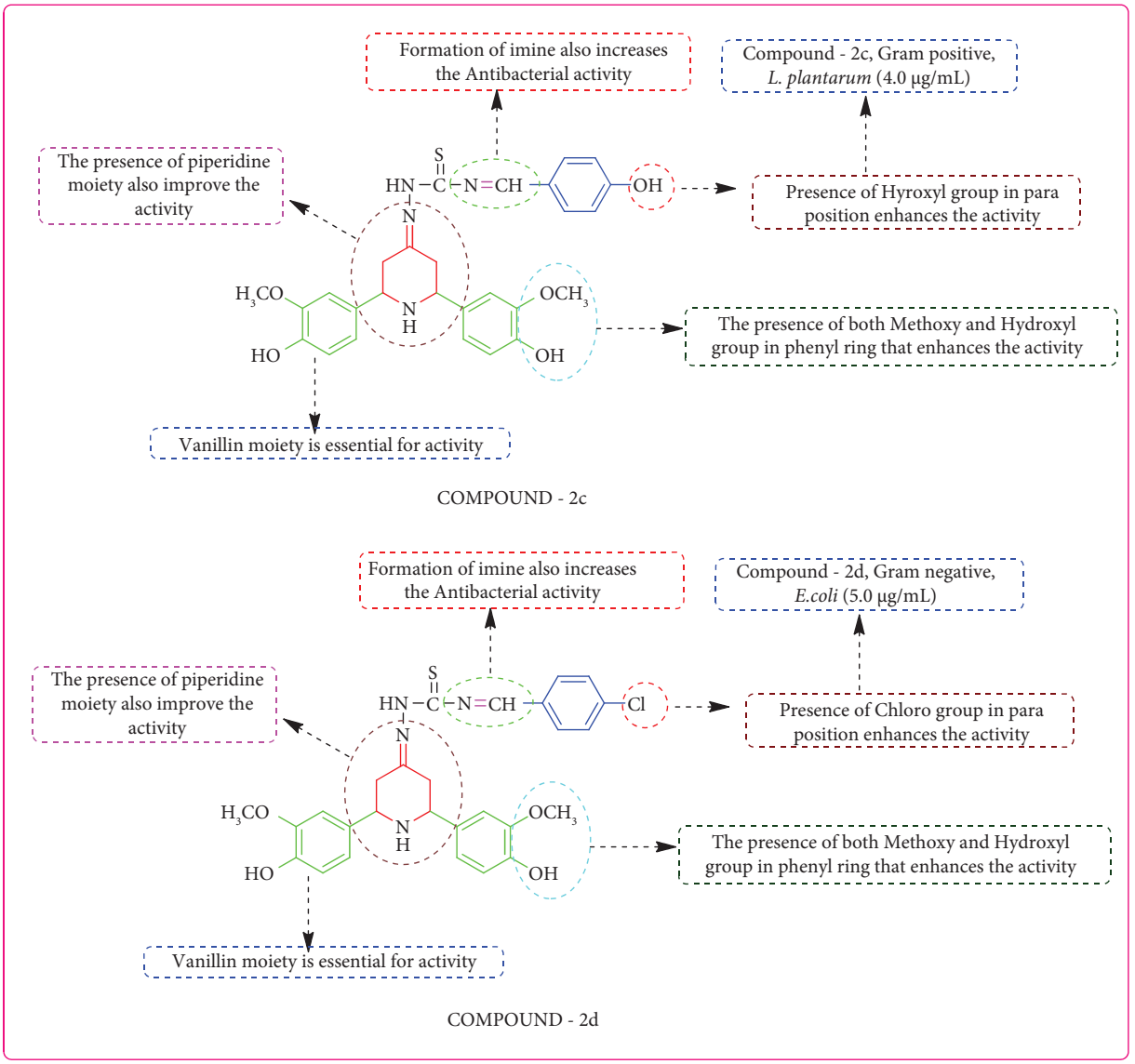


Figure 10: SAR relationship of highly active compounds.

## 4. Conclusions

The goal of this study was to figure out why freshly synthesized Schiff bases of vanillin coupled piperidine analogues have anticancer activity and toxicity. Using a green chemical technique and a CuO nanoparticle as a catalyst, an unique one-pot syn-thesis of Schiff base vanillin linked piperidine derivatives (2, 2a-2j) may be created, with a potential yield in a short reaction time. FT-IR, NMR ($^1$H, $^{13}$C), mass spectra, and elemental analyses were used to evaluate the newly synthesized piperidin-4-ylidene analogues, while morphological analysis was observed using XRD and TEM. Antibacterial activity of the compound 2a-2j was tested against gramme positive and gramme negative bacterial strains. Against normal erythromycin, compound 2c and 2d showed (4.0 $\mu$g/mL, *L. plantarum*), (5.0 $\mu$g/mL, *E. coli*). Finally, when compared to the reference and other compounds, compound 2c, 2d has a high potential activity. As a result, compound 2c and 2d have a lot of action against bacterial strains and could be employed as an antibacterial medicine in the future.

## Data Availability

The data used to support the findings of this study are included within the supplementary information file(s).

## Conflicts of Interest

The authors declare that there are no conflicts of interest.

## Acknowledgments

The authors extend their appreciation to the Deputyship for Research & Innovation, Ministry of Education in Saudi Arabia for funding this research work through the Project no. IFKSURG-2-1565.

## Supplementary Materials

The supplementary material used to support the findings of this study is included within the supplementary information files. (The supplementary file contains FT-IR, 1H-NMR, 13C-NMR and MS spectrum). (*Supplementary Materials*)

## References

[1] B. S. Patil, G. Krishnamurthy, N. D. Shashikumar, M. R. Lokesh, and H. S. BhojyaNaik, "Synthesis and antimicrobial activity of some [1,2,4]-Triazole derivatives," *Journal of Chemistry*, vol. 2013, Article ID 462594, 7 pages, 2013.

[2] R. Yadav, D. Saini, and D. Yadav, "Synthesis and evaluation of vanillin derivatives as antimicrobial agents," *Turkish Journal Of Pharmaceutical Sciences*, vol. 15, no. 1, pp. 57–62, 2018.

[3] M. Leeb, "Antibiotics: a shot in the arm," *Nature*, vol. 431, no. 7011, pp. 892-893, 2004.

[4] S. S. Arya, M. M. Sharma, R. K. Das, J. Rookes, D. Cahill, and S. K. Lenka, "Vanillin mediated green synthesis and application of gold nanoparticles for reversal of antimicrobial resistance in *Pseudomonas aeruginosa* clinical isolates," *Heliyon*, vol. 5, no. 7, pp. 020211–e2111, 2019.

[5] C. F. Bezerra, C. J. Camilo, M. K. do Nascimento Silva, T. S. de Freitas, J. Ribeiro-Filho, and H. D. M. Coutinho, "Vanillin selectively modulates the action of antibiotics against resistant bacteria," *Microbial Pathogenesis*, vol. 113, pp. 265–268, 2017.

[6] M. B. Hocking, "Vanillin: synthetic flavoring from spent sulfite liquor," *Journal of Chemical Education*, vol. 74, no. 9, pp. 1055–1059, 1997.

[7] J. D. Evans and S. A. Martin, "Effects of thymol on ruminal microorganisms," *Current Microbiology*, vol. 41, no. 5, pp. 336–340, 2000.

[8] J. P. Kamat, A. Ghosh, and T. P. A. Devasagayam, "Vanillin as an antioxidant in rat liver mitochondria: inhibition of protein oxidation and lipid per oxidation induced by photosensitization," *Molecular and Cellular Biochemistry*, vol. 209, Article ID 1007048313556, 2000.

[9] L. R. Beuchat and D. A. Golden, "Antimicrobials occurring naturally in foods," *Food Technology*, vol. 43, pp. 134–142, 1989.

[10] J. M. Jay and G. M. Rivers, "Antimicrobial activity of some food flavoring compounds," *Journal of Food Safety*, vol. 6, no. 2, pp. 129–139, 1984.

[11] D. J. Fitzgerald, M. Stratford, M. J. Gasson, J. Ueckert, A. Bos, and A. Narbad, "Mode of antimicrobial action of vanillin against *Escherichia coli*, Lactobacillus plantarum and Listeria innocua," *Journal of Applied Microbiology*, vol. 97, no. 1, pp. 104–113, 2004.

[12] R. M. Cava-Roda, A. Taboada-Rodriguez, M. T. Valverde-Franco, and F. Marín-Iniesta, "Antimicrobial activity of vanillin and mixtures with cinnamon and clove essential oils in controlling Listeria monocytogenes and *Escherichia coli* O157: H7 in milk," *Food and Bioprocess Technology*, vol. 5, no. 6, pp. 2120–2131, 2012.

[13] I. Mourtzinos, S. Konteles, N. Kalogeropoulos, and V. T. Karathanos, "Thermal oxidation of vanillin affects its antioxidant and antimicrobial properties," *Food Chemistry*, vol. 114, no. 3, pp. 791–797, 2009.

[14] S. T. Harini, H. V. Kumar, J. Rangaswamy, and N. Naik, "Synthesis, antioxidant and antimicrobial activity of novel vanillin derived piperidin-4-one oxime esters: preponderant role of the phenyl ester substituents on the piperidin-4-one oxime core," *Bioorganic & Medicinal Chemistry Letters*, vol. 22, no. 24, pp. 7588–7592, 2012.

[15] S. Zukic, E. Veljovic, S. Spirtovic-Halilovic et al., "Antioxidant, antimicrobial and antiproliferative activities of synthesized 2,2,5,5-tetramethyl-9-aryl-3,4,5,6,7,9-hexahydro-1H-xanthene-1,8(2H)-dione derivatives," *Croatica Chemica Acta*, vol. 91, pp. 1–9, 2018.

[16] D. Kumar and V. Singh, "Study of heterocyclic compound piperidine," *International Journal of Scientific & Technology Research*, vol. 3, pp. 25–28, 2014.

[17] S. Przedborski, V. Jackson-Lewis, R. Djaldetti et al., "The parkinsonian toxin MPTP: action and mechanism," *Restorative Neurology and Neuroscience*, vol. 16, no. 2, pp. 135–142, 2000.

[18] G. Aridoss, P. Parthiban, R. Ramachandran, M. Prakash, S. Kabilan, and Y. T. Jeong, "Synthesis and spectral characterization of a new class of N-(N-methylpiperazinoacetyl)-2,6- diarylpiperidin-4-ones: antimicrobial, analgesic and antipyretic studies," *European Journal of Medicinal Chemistry*, vol. 44, no. 2, pp. 577–592, 2009.

[19] M. K. Prashanth, H. D. Revanasiddappa, K. Lokanatha Rai, and B. Veeresh, "Synthesis, characterization, antidepressant and antioxidant activity of novel piperamides bearing piperidine and piperazine analogues," *Bioorganic & Medicinal Chemistry Letters*, vol. 22, no. 23, pp. 7065–7070, 2012.

[20] Z. Kiasalari, M. Khalili, M. Roghani, A. Ahmadi, and M. Mireie, "Antioxidant and antiepileptic activity of 1-[1-(3-Methoxyphenyl) (Tetralyl)] piperidine as a new derivative of phencyclidine on pentylentetrazole-induced kindling mice," *Iranian Journal of Pathology*, vol. 9, pp. 138–148, 2013.

[21] K. Paulrasu, A. Duraikannu, M. Palrasu, A. Shanmugasundaram, M. Kuppusamy, and B. Thirunavukkarasu, "Synthesis of 4-methyl- N'-(3-alkyl-2r, 6C-diaryl piperidin-4-ylidene) - 1,2,3-thiadiazole-5-carbohydrazides with antioxidant, antitumor and antimicrobial activities," *Organic and Biomolecular Chemistry*, vol. 12, no. 31, pp. 5911–5921, 2014.

[22] R. M. D. Freitas, F. D. O. Silva, M. G. D. V. Silva, and D. Feng, "Antioxidant mechanisms of iso-6- cassine in suppressing seizures induced by pilocarpine," *RevistaBrasileira de Farmacognosia*, vol. 21, no. 3, pp. 437–443, 2011.

[23] P. Parthiban, G. Aridoss, P. Rathika, V. Ramkumar, and S. Kabilan, "Synthesis, stereochemistry and antimicrobial studies of novel oxime ethers of aza/diazabicycles," *Bioorganic & Medicinal Chemistry Letters*, vol. 19, no. 24, pp. 6981–6985, 2009.

[24] K. K. Goel, A. Gajbhiye, and N. M. Goel, "Synthesis and antimicrobial activity of piperidin-4-one derivatives," *Biomedical & Pharmacology Journal*, vol. 1, pp. 201–206, 2008.

[25] M. Baroudi, J. Robert, and C. Luu-Duc, "Imidazole derivatives of pyrrolidonic and piperidonic acids as potential inhibitors of human placental aromatase in vitro," *The Journal of Steroid Biochemistry and Molecular Biology*, vol. 57, no. 1-2, pp. 73–77, 1996.

[26] C. Ramalingan, S. Balasubramanian, S. Kabilan, and M. Vasudevan, "Synthesis and study of antibacterial and antifungal activities of novel 1-[2-(benzoxazol-2-yl) ethoxy]-2, 6- diarylpiperidin-4-ones," *European Journal of Medicinal Chemistry*, vol. 39, no. 6, pp. 527–533, 2004.

[27] N. Rameshkumar, A. Veena, R. Ilavarasan, M. Adiraj, P. Shanmugapandiyan, and S. K. Sridhar, "Synthesis and biological activities of 2,6-Diaryl-3-methyl-4-piperidone derivatives," *Biological and Pharmaceutical Bulletin*, vol. 26, no. 2, pp. 188–193, 2003.

[28] Z. Yuxia, Z. Tao, M. Wanshan, Z. Haibin, and C. Suifeng, "Synthesis, structural determination and antibacterial activity of compounds derived from vanillin and 4- aminoantipyrine," *Hauxueshiji*, vol. 24, p. 117, 2002.

[29] F. M. Abdel-Gawad, Y. M. Issa, and S. M. Abd-Alhamid, "Spectrophotometric and potentiometric studies on some salicylidene-sulpha derivatives," *Egyptian Journal of Pharmaceutical Sciences*, vol. 34, p. 219, 1993.

[30] V. V. Mulwad and J. M. Shirodkar, "Synthesis and biological activity of some new Schiff's bases, thiazolidinones and azetidinones of 4-hydroxy coumarin," *Indian Journal of Heterocyclic Chemistry*, vol. 11, pp. 199–202, 2002.

[31] N. Sari, S. Arslan, E. Logoglu, and I. Sariyan, "Antibacterial activites of some new amino acid- schiff bases," *Gazi University Journal of Science*, vol. 16, pp. 283–288, 2010.

[32] P. Parthiban, S. Balasubramanian, G. Aridoss, and S. Kabilan, "Synthesis and NMR spectral studies of some 2,6-diarylpiperidin-4-one O-benzyloximes," *Spectrochimica Acta Part A: Molecular and Biomolecular Spectroscopy*, vol. 70, no. 1, pp. 11–24, 2008.

[33] A. K. Potbhare, R. G. Chaudhary, P. B. Chouke et al., "Phytosynthesis of nearly monodisperse CuO nanospheres using Phyllanthus reticulatus/Conyza bonariensis and its antioxidant/antibacterial assays," *Materials Science and Engineering: C*, vol. 99, pp. 783–793, 2019.

[34] J. A. Tanna, R. G. Chaudhary, V. N. Sonkusare, and H. D. Juneja, "CuO nanoparticles: synthesis, characterization and reusable catalyst for polyhydroquinoline derivatives under ultrasonication," *Journal of the Chinese Advanced Materials Society*, vol. 4, no. 2, pp. 110–122, 2016.

[35] R. G. Chaudhary, V. N. Sonkusare, G. S. Bhusari, A. Mondal, D. P. M. D. Shaik, and H. D. Juneja, "Microwave-mediated synthesis of spinel CuAl2O4 nanocomposites for enhanced electrochemical and catalytic performance," *Research on Chemical Intermediates*, vol. 44, no. 3, pp. 2039–2060, 2018.

[36] K. Rajesh, B. Palakshi Reddy, and V. Vijayakumar, "Ultrasound-promoted synthesis of novel bipodal and tripodalpiperidin-4-ones and silica chloride mediated conversion to its piperidin-4-ols: synthesis and structural confinements," *Ultrasonics Sonochemistry*, vol. 19, no. 3, pp. 522–531, 2012.

[37] F. Zhang, Z. J. Liu, and J. T. Liu, "Michael addition of N-sulfinylmetalloenamines to $\beta$-trifluoromethyl-$\alpha$, $\beta$-unsaturated ester: an efficient access to chiral 4-trifluoromethyl-2-piperidones," *Tetrahedron*, vol. 66, no. 34, pp. 6864–6868, 2010.

[38] X. D. Jia, X. N. Chen, C. De Huo, F. F. Peng, C. Qing, and X. C. Wang, "Cross double Mannich reaction catalyzed by I2: synthesis of highly substituted 4-piperidones," *Chinese Chemical Letters*, vol. 23, no. 3, pp. 309–312, 2012.

[39] A. B. Garcia, C. Valdes, and M. P. Cabal, "An imino-Diels–Alder route to meso-2,6-disubstituted 4-Piperidones," *Tetrahedron Letters*, vol. 45, no. 22, pp. 4357–4360, 2004.

[40] R. W. Hartmann, M. Reichert, and S. Gohring, "Novel 5$\alpha$-reductase inhibitors. Synthesis and structure-activity studies of 5-substituted 1-methyl-2-pyridones and 1-methyl-2-piperidones," *European Journal of Medicinal Chemistry*, vol. 29, no. 11, pp. 807–817, 1994.

[41] K. A. Kumar, K. L. Rai, G. V. Kumar, and B. N. Mylarappa, "A facile route for the synthesis of ethyl N-aryl-2,6-dioxo-piperid-3-ene-4-carboxylates and their biological activity," *International Journal of Pharmacy and Pharmaceutical Sciences*, vol. 4, pp. 564–568, 2012.

[42] K. Ajay Kumar, K. M. Lokanatha Rai, and K. B. Umesha, "Evaluation of antibacterial activity of 3,5-dicyano-4,6-diaryl-4-ethoxycarbonyl-piperid-2-ones," *Journal of Pharmaceutical and Biomedical Analysis*, vol. 27, no. 5, pp. 837–840, 2002.

[43] A. R. Cruz, M. G. Zolotukhin, S. L. Morales et al., "Use of 4-piperidones in one-pot syntheses of novel, high-molecular-weight linear and virtually 100%-hyperbranched polymers," *Chemical Communications*, vol. 29, pp. 4408–4410, 2009.

[44] G. Aridoss, S. Amirthaganesan, N. Ashok Kumar et al., "A facile synthesis, antibacterial, and antitubercular studies of some piperidin-4-one and tetrahydropyridine derivatives," *Bioorganic & Medicinal Chemistry Letters*, vol. 18, no. 24, pp. 6542–6548, 2008.

[45] Y. R. Shah, D. J. Sen, and C. N. Patel, "Schiff's bases of piperidone derivative as microbial growth inhibitors," *Journal of Chemical and Pharmaceutical Research*, vol. 2, pp. 581–589, 2010.

[46] R. B. C. Jagt, J. G. de Vries, B. L. Feringa, and A. J. Minnaard, "Enantioselective synthesis of 2-aryl-4-piperi dones via rhodium/phosphoramidite-catalyzed conjugate addition of

arylboroxines," *Organic Letters*, vol. 7, no. 12, pp. 2433–2435, 2005.

[47] N. Karthik, S. Nithiya, and J. Jayabharathi, "Novel piperidone derivatives: synthesis, spectral and evaluation of antioxidant activity," *International Journal of Drug Development & Research*, vol. 3, pp. 122–127, 2011.

[48] T. Kalai, M. L. Kuppusamy, M. Balog et al., "Synthesis of N-substituted 3, 5-bis (arylidene)-4-piperidones with high antitumor and antioxidant activity," *Journal of Medicinal Chemistry*, vol. 54, no. 15, pp. 5414–5421, 2011.

[49] S. Das, U. Das, H. Sakagami et al., "Dimeric 3,5-bis(benzylidene)-4-piperidones: a novel cluster of tumour selective cytotoxins possessing multidrug resistant properties," *European Journal of Medicinal Chemistry*, vol. 51, pp. 193–199, 2012.

[50] K. Selvendiran, L. Tong, A. Bratasz et al., "Anticancer efficacy of a difluorodiarylidenylpiperidone (HO-3867) in anticancer efficacy of a difluorodiarylidenyl piperidone (HO-3867) in human ovarian cancer cells and tumor xenografts," *Molecular Cancer Therapeutics*, vol. 9, no. 5, pp. 1169–1179, 2010.

[51] S. Kant Sahu, B. Kumar Dubey, A. C Tripathi, M. Koshy, and S. K Saraf, "Piperidin-4-one: the potential pharmacophore," *Mini Reviews in Medicinal Chemistry*, vol. 13, no. 4, pp. 565–583, 2013.

[52] A. C. L. Leite, D. M. L. C. D. Coelho, F. D. de Menezes, and D. J. Brondani, "Synthesis of aryl-hydrazones via ultrasound irradiation in aqueous medium," *Tetrahedron Letters*, vol. 49, no. 9, pp. 1538–1541, 2008.

[53] Y. A. Selim, M. A. Azb, I. Ragab, and M. H M Abd El-Azim, "Green synthesis of zinc oxide nanoparticles using aqueous extract of deverratortuosa and their cytotoxic activities," *Scientific Reports*, vol. 10, pp. 3445–3449, 2020.

[54] D. Mulugeta, B. Abdisa, A. Belay, and M. Endale, "Synthesis of chalcone and flavanone derivatives using ZnO nanoparticle as catalyst for antibacterial activity," *Chemistry and Materials Research*, vol. 10, pp. 2224–3224, 2018.

[55] A. Iqbal, A. U. Haq, G. A. Cerron-Calle, S. A. R. Naqvi, P. Westerhoff, and S. Garcia-Segura, "Green synthesis of flower-shaped copper oxide and nickel oxide nanoparticles via Capparis decidua leaf extract for synergic adsorption-photocatalytic degradation of pesticides," *Catalysts*, vol. 11, no. 7, p. 806, 2021.

[56] R. Surendra Kumar, M. Moydeen, S. S. Al-Deyab, A. Manilal, and A. Idhayadhulla, "Synthesis of new morpholine-connected pyrazolidine derivatives and their antimicrobial, antioxidant, and cytotoxic activities," *Bioorganic & Medicinal Chemistry Letters*, vol. 27, no. 1, pp. 66–71, 2017.

[57] C. Zhou, L. Xu, J. Song et al., "Ultrasensitive non-enzymatic glucose sensor based on three-dimensional network of ZnO-CuO hierarchical nanocomposites by electrospinning," *Scientific Reports*, vol. 4, pp. 7382–7389, 2014.

Hindawi
Journal of Chemistry
Volume 2022, Article ID 9402236, 17 pages
https://doi.org/10.1155/2022/9402236

*Research Article*

# Environmental Hazard of Polypropylene from Disposable Face Masks Linked to the COVID-19 Pandemic and Its Possible Mitigation Techniques through a Green Approach

**Selvakumar Vijayalakshmi**,[1,2] **Preethi Gopalsamy**,[2] **Karnan Muthusamy**,[2,3] **Dinesh Kumar Sundarraj**,[4] **Steffi Pulikondan francis**,[5] **Thiyagarajan Ramesh**,[6] **Deog-Hwan Oh**,[1] **Duong Ly Thi Thuy**,[7] **Tuyet Thi Anh Truong**,[7] **Huu Tap Van**,[8] **and Shankar Karuppannan**[9]

[1]*Food Science and Biotechnology, School of Agriculture and Life Sciences, Kangwon National University, Chuncheon, Republic of Korea*
[2]*Askoscen Probionics (R&D), Thiruchirappalli, Tamilnadu, India*
[3]*Grassland and Forage Division, National Institute of Animal Science, Republic of Korea*
[4]*Applied Phycology and Biotechnology Division, Marine Algal Research Station, CSIR-Central Salt & Marine Chemical Research Institute, Mandapam 623 519, Tamil Nadu, India*
[5]*Department of Microbiology, Cauvery College for Women (Autonomous), Tiruchirappalli-620 024, Tamil Nadu, India*
[6]*Department of Basic Medical Sciences, College of Medicine, Prince Sattam Bin Abdulaziz University, Al-Kharj 11942, Saudi Arabia*
[7]*Faculty of Environment, Thai Nguyen University of Agriculture and Forestry, Thai Nguyen, Vietnam*
[8]*Faculty of Natural Resources and Environment, TNU - University of Sciences, Thai Nguyen, Vietnam*
[9]*Department of Applied Geology, School of Applied Natural Science, Adama Science and Technology University, Adama, Ethiopia*

Correspondence should be addressed to Shankar Karuppannan; shankar.karuppannan@astu.edu.et

Received 16 June 2022; Revised 27 July 2022; Accepted 4 August 2022; Published 2 September 2022

Academic Editor: Balasubramani Ravindran



The COVID-19 outbreak again underlined plastic items' importance in our daily lives. The public has widely utilized disposable face masks constructed of polypropylene polymer materials as effective and inexpensive personal protective equipment (PPE) to inhibit virus transmission. The consequences of this have resulted in millions of tons of plastic garbage littering the environment due to inappropriate disposal and mismanagement. Surgical masks are among them, and this study aimed to assess the biodegrading efficiency of disposable face masks using *Pseudomonas aeruginosa* VJ 1. This work used a bacterial strain, *Pseudomonas aeruginosa* VJ 1, obtained from sewage water-contaminated surface soil in Tiruchirappalli, India, to investigate the biodegradation of polypropylene (PP) face masks. The mask pieces were incubated with *Pseudomonas aeruginosa* VJ 1 culture in three different solid and liquid media for 30 days at 37°C. Surface changes and variations in the intensity of functional groups and carbonyl index variations were confirmed using Field Emission Scanning Electron Microscopy (FE-SEM) and Fourier Transform Infrared Spectroscopy (FTIR) analysis to ensure microbial degradation (up to 5.37% weight reduction of PP films within 30 days). These findings show that *Pseudomonas aeruginosa* VJ 1 could be a good choice for biodegrading PP masks without harming our health or the environment. There is a need for a novel solution for the degradation of PP. The methods and strain presented here reveal the potential biodegrading agents of PP masks.

## 1. Introduction

The rapid global spread of the SARS-CoV-2 pandemic has required essential attempts to reduce transmission, resulting in considerable and widespread socioeconomic damage [1]. According to World Health Organization, as of March 6, more than 445 million cases and 5.99 million deaths were reported.

The coronavirus pandemic has prompted the establishment of emergency solutions and progressive actions targeted at dealing with and defeating COVID-19 while reducing exposures and promoting a healthy lifestyle worldwide. Compulsory use of plastic-based PPE by healthcare staff and face masks for the general public leaving their homes for significant reasons is a preventive step meant to reduce the community spread of COVID-19 transmitted through droplets [2].

At the beginning of the COVID-19 pandemic, the use of medical masks as an infection control measure was widespread in East and South-East Asia, and it later gathered speed in the rest of the world in 2020 and 2021 [3]. Medical mask usage and production are currently at massive levels, and both are anticipated to rise further soon. For instance, China made roughly 450 million medical masks every day as of April 2020. In reality, China, the world's largest producer, was expected to produce 10 billion medical masks annually by 2020, up from 5 billion in 2019 [4]. In the current circumstances, three types of face masks can be used: (i) respirator mask (N95, FFP2), (ii) surgical or medical mask, and (iii) noncertified disposable mask (cloth mask) [5].

The top and bottom layers of disposable (one-time use) face masks were woven fabric, while the center layer was formed of melting polypropylene polymers. Each day, the authors' models are predicted to generate 6.88 billion (about 206,470 t) of material, subsequently disposed of or burnt [6]. Because of their lightweight, used face masks are easily carried into city streets, rivers, and oceans, where they are fragmented into microplastics (MPs) [7, 8]. Furthermore, single-purpose face masks are made of nonbiodegradable materials that take hundreds of years to degrade in the environment [8, 9]. Medical masks come in many styles and materials, including polyurethane, polyacrylonitrile, polyester, polyethylene terephthalate, and polypropylene. The last one, polypropylene, has been used for a very long time and is still by far the most popular material [10].

Poor waste management is the leading environmental risk linked to the growing use of disposable medical masks by the general public [7]. Thermochemical conversion of disposable medical masks into value-added goods has recently been proposed as a potential waste management strategy [11]. However, masks are frequently disposed of improperly in public areas and the environment at large [12]. This adds to the polluting of the world's oceans with plastics, which has harmful effects on the environment [13]. Additionally, as recently discovered, throwaway surgical masks could be a sizable new source of microplastics.

Accordingly, an immediate multidisciplinary approach is required to dispose of the waste generated by the pandemic. Biodegradation is a microorganism's best ability to persuade abiotic deterioration through physical, chemical, or enzymatic action [14].

Microorganisms were well suited for the biodegradation process because they possess enzymes and their small size, allowing them to contact the plastic surface [15]. Exoenzymes from bacteria can break down complex polymers into simpler ones that can pass through semipermeable outer membranes and be used as carbon and energy sources by the microbes [16]. Researchers have identified several bacterial and fungal taxa that may degrade MPs, including *Pseudomonas* sp. [17–20].

Several gut bacterial species were isolated from worms and validated for their potential to facilitate plastic breakdown directly. *Bacillus* sp. YP1 and *Enterobacter asburiae* YT1 are two bacterial strains obtained from wax worms that can depolymerize polyethylene (PE) in vitro [21]. *P. aeruginosa* isolated from the intestines of super worms can biodegrade three different types of plastics in unusual ways (PE, PP, and PPS (polyphenylene sulfide)). Biodegradation efficiency varies from one plastic to the next; the fastest biodegradation happens on PE [22]. *Pseudomonas fluorescens* and *P. aeruginosa* are highly able to degrade polyethylene [23]. This study aimed to assess *Pseudomonas* sp. biodegradation ability on a surgical face mask in an environmentally acceptable manner to safeguard our environment from pandemic-related garbage.

## 2. Materials and Methods

*2.1. Chemicals and Reagents.* The soil sample was taken from *sewage water-contaminated surface soil,* Geetha Nagar, Uyyakondan Thirumalai, Tiruchirappalli, Tamilnadu, South India. It is located at longitude of 78°40′22.01″E (78.672779) and latitude of 10°48′56.12″N (10.81559). The sample was packed with collection bags and then securely transported to our laboratory, where the plastic-degrading *Pseudomonas* sp. was isolated. Due to laboratory norms and regulations in this COVID-19 pandemic, the utilized face masks were not allowed to be employed in our laboratory test. The trials employed clean surgical face masks (ear loops were removed). The HiMedia laboratory in India provided the chemicals used in our research.

*2.2. Isolation of Bacteria from a Soil Sample.* Serially diluted soil samples were put onto a sterile nutrient agar (NA) medium that had previously been prepared and incubated at 37°C for 24–48 hours to isolate bacteria from the sample. Individual colonies were taken after incubation and used to make pure cultures. Gram staining was used to identify the pure colonies for the first time. The isolated bacterium was then kept at 4°C in our laboratory on nutrient agar for the biodegradation experiment in our current investigation.

*2.3. Identification of Bacteria.* Bergey's Manual of Systematic Bacteriology was used to identify the isolated culture based on morphological, staining reaction, culture, and other biochemical properties. Basic biochemical tests were used to determine the isolated bacterial strain. The biochemical

assays were carried out on cultures cultivated on nutrient agar medium for 24 hours at 37°C. According to the supplier's procedure, an indole test was done to verify their use of tryptophan. According to [24], a catalase study was performed. Bacterial colonies were inoculated on Simmons Citrate Agar to study citrate metabolism (according to supplier protocol). The oxidase test determined which bacteria possessed the cytochrome oxidase enzyme. Sugar fermentation tests (glucose, lactose, and sucrose) were investigated (according to supplier protocol). SIM media was used to measure motility and $H_2S$ generation (according to supplier protocol). The MR-VP test was used to determine whether or not the isolate was a facultative anaerobe based on their sugar fermentation patterns. The bacterium was also streaked over selective agar Cetrimide for confirmation. 16S rRNA sequencing was used to identify the isolated bacterial strain ISJ14. For molecular identification, using forward and reverse 16S rRNA primers together with DNTP, buffer, and Taq polymerase, PCR of the extracted genomic DNA was carried out. In order to amplify the 16SrRNA genes, a universal primer sequence was used: CGGTTACCTTGTTACGACTT and AGAGTTTGATCMTGGCTCAG. 100 ng of template DNA is present in the mixture of PCR amplified product. The 16S rRNA sequence was submitted to the GenBank, and accession number was obtained [17].

### 2.4. Investigation of Biodegradation of Polypropylene Mask

*2.4.1. Pretreatment of Polypropylene Mask Pieces.* The masks were stripped of their metal strips and ear loops. The masks were then prepped using the procedure outlined by [17]. The masks were cut into 33 cm sections for this procedure and soaked for 30–60 minutes in a solution containing 7 ml Tween-80. Tween-80 is used as a wetting agent, and it will moisten the mask's surface and cause it to repel air, making the treatment more effective: 10 ml bleach for disinfection and 983 ml sterile water with constant stirring. The mask parts were then washed at room temperature with distilled water. The pieces were then sterilized with 70% ethanol for 30 minutes before drying at 45°C. The mask parts were weighed using a weighing balance after drying, and the initial weight of the pieces was recorded.

*2.4.2. Biodegradation Experiment.* *Pseudomonas aeruginosa* VJ 1 was aseptically inoculated on nutrient agar (NA), Bushnell Haas agar medium (BHM), and Mineral Salt agar medium (MSM) plates using the carpet culture method. Pretreatment polypropylene mask pieces (about 0.1 g) were aseptically placed over the inoculated plates using sterile forceps and incubated for one month at 30°C and 37°C, respectively, following inoculation (30 days). The negative control agar plates, which contained the same number of mask pieces but were not inoculated with bacteria, were kept at the same temperature as the positive control agar plates. In addition, the pretreated mask pieces were incubated with *Pseudomonas aeruginosa* VJ 1 in Nutrient Broth (NB), BH (Bushnell Haas broth), and MS (Mineral Salt broth) as well as liquid media containing the same quantity of mask pieces but no culture, for the same amount of time as the control.

*2.4.3. Experimental Setup*

T1A: 0.1 g of pretreated mask pieces + *Pseudomonas aeruginosa* VJ 1 (in NA plates)

T1B: 0.1 g of pretreated mask pieces + *Pseudomonas aeruginosa* VJ 1 (in NB)

C1A: 0.1 g of pretreated mask pieces in NA plates (without inoculums)

C1B: 0.1 g of pretreated mask pieces in NB (without inoculums)

T2A: 0.1 g of pretreated mask pieces + *Pseudomonas aeruginosa* VJ 1 in BHM plates

T2B: 0.1 g of pretreated mask pieces + *Pseudomonas aeruginosa* VJ 1 (in BH)

C2A: 0.1 g of pretreated mask pieces in BHM plates (without inoculums)

C2B: 0.1 g of pretreated mask pieces in BH broth (without inoculums)

T3A: 0.1 g of pretreated mask pieces + *Pseudomonas aeruginosa* VJ 1 in MSM plates

T3B: 0.1 g of pretreated mask pieces + *Pseudomonas aeruginosa* VJ 1 (in MS)

C3A: 0.1 g of pretreated mask pieces in MSM plates (without inoculums)

C3B: 0.1 g of pretreated mask pieces in MS (without inoculums)

*2.4.4. Monitoring the Planktonic Growth of Pseudomonas aeruginosa VJ 1 Strain.* The growth of *Pseudomonas aeruginosa* VJ 1 in liquid and solid media such as NB, BHM, and MSM was studied for 30 days (1 month), with a 15-day interval due to the presence of a PP film and the properties of the biofilm generated on the polymer surface. Before analyzing the biofilm, sterile forceps were used to remove polymer samples from the media, which were then carefully rinsed with sterilized distilled water to remove the loosely adhered bacteria. The biofilm was then cleaned off the surface of the polymer by using a gentle water bath sonication for 4 minutes at 1-minute intervals in 1 ml of 0.85 percent saline solution. The resulting saline solution was serially diluted up to $10^{-7}$, and aliquots were disseminated on nutrient agar, with the number of colonies calculated as CFU/$\mu$L [25].

*2.4.5. Viability Testing of Surface-Attached Bacteria.* The survivability of bacterial strains adhered to the surface of PP films was calculated [26]. PP films were removed from the media at 10-day intervals and rinsed with sterile distilled water before being subjected to mild bath sonication with a 0.85 percent saline solution. The resulting solution was serially diluted, plated on NA, and incubated for 48 hours at

35°C. CFU/ml was used to calculate the number of viable bacteria species.

*2.4.6. Assessment of Cell Surface Hydrophobicity of Pseudomonas aeruginosa VJ 1.* The BATH test was used to measure the hydrophobicity of the bacterial cell surface with minor adjustments [27], which was explained as follows: The bacteria were grown in NB media until they reached the mid-log stage of growth. It was then centrifuged and twice rinsed with phosphate urea buffer (PUM containing 17 g $K_2HPO_4$, 7.26 g $KH_2PO_4$, 1.8 g urea, and 0.2 g $MgSO_4.7H_2O$ per liter). Following washing, the cells were suspended in PUM buffer with an OD 400 of 1.0–1.2. To facilitate phase separation, aliquots of 1.2 ml of the above-obtained suspension were introduced to a series of test tubes containing escalating quantities of xylene (ranges from 0 to 0.2 ml) and shaken well for 10 minutes before being left to stand for 2 minutes. The lower aqueous phase's OD 400 nm was measured and recorded as OD 1. The percentage of xylene-bound cells reported as the fraction of cells expelled from the aqueous phase calculated the cell surface hydrophobicity. The blank was a plain PUM buffer. Therefore, the percentage of adhering cells is represented using the following formula: cell surface hydrophobicity (%) = $((OD_0 - OD_{10})/OD_0) \times 100$ ($OD_0$ is the initial OD of the aqueous phase).

*2.4.7. Determination of Dry Weight of the Recovered Mask Pieces.* After a month of incubation, the remaining mask parts were collected from the culture plates. The bacterial biomass that had adhered to the polypropylene mask surface was rinsed for 2 hours with a sodium dodecyl sulfate (SDS) solution (2 percent v/v). After that, the pieces were cleaned with distilled water to remove any contaminants from the surface and dried at 45°C overnight. Then, the degraded mask pieces were weighed using a weighing balance, and the percentage of biodegradation (weight loss) was estimated using the following formula:

$$\text{biodegradation}\,(\%) = \frac{\text{initial weight} - \text{final weight}}{\text{initial weight}} \times 100. \quad (1)$$

*2.4.8. Surface Analysis of Mask Pieces*

*(1) Scanning Electron Microscopy*. The mask pieces were taken from the media and exposed to FE-SEM to observe biofilm growth and surface degradation after being infected with *Pseudomonas aeruginosa* VJ 1 for 30 days. The bacterial morphology of a biofilm on the surface of a PP mask was examined. Before the observation, the treated mask pieces were rinsed for 2 minutes in a 0.01 M phosphate buffer solution to eliminate any excess media that had adhered to the bacterial colonies. The treated mask pieces were washed with 2 percent SDS and warm water for 10–20 minutes to aid in the complete removal of bacterial biomass and to observe surface modification. After the process, the mask parts were fixed in 4% glutaraldehyde at 4°C for 2 hours and dehydrated in 50% ethanol for 30 minutes. The recovered mask parts were treated in 70% ethanol at room temperature overnight. The pieces were dried, mounted, and sputter-coated with gold for 40 seconds before scanning with an FE-SEM.

*2.4.9. Fourier Transform Infrared Spectroscopy (FTIR Analysis).* PP mask films were washed with 2 percent SDS and warm distilled water for 10 to 20 minutes to remove bacterial biomass. The PP films were then fixed in 4% glutaraldehyde at 4°C for 2 hours after being dehydrated with 50% ethanol for 30 minutes. The PP films were treated with 70% ethanol at room temperature overnight before being dried. Small pieces of dried mask pieces were analyzed using FTIR spectra in the 4000–400 $cm^{-1}$ which were employed at a 1 $cm^{-1}$ resolution to investigate the structural and functional group modifications. The following formula was used to calculate the relative absorbance intensities of the keto carbonyl bond, ester carbonyl bond, terminal double bond (vinyl), and internal double bond with methyl bond: keto carbonyl bond index (KCBI) = I1715/I1465, ester carbonyl bond index (ECBI) = I1740/I1465, vinyl bond index (VBI) = I1650/I1465, and the internal double bond index (IDBI) = I908/I1465. The carbonyl index was used to determine the degree of biodegradation because its value depends on the degree of degradation. The percentage of crystallinity of the polypropylene mask film was determined using the previously described method by Zerbi et al. (1989).

## 3. Results

*3.1. Isolation and Identification of Pseudomonas aeruginosa VJ 1.* Typical bacterial isolate colonies were subcultured on nutrient agar and incubated for 24 hours at 37°C. *Pseudomonas aeruginosa* VJ 1 was recognized as a Gram-negative rod based on a presumptive identification of bacteria using Gram's staining procedure. The isolated bacteria were identified as a *Pseudomonas aeruginosa* VJ 1 strain based on various biochemical characteristics (Figure 1(a)). A *Pseudomonas aeruginosa* VJ 1 specific substrate for isolation was further validated by streaking the strain onto cetrimide agar. After incubation, the isolates had a green-pigmented, round, and opaque colony shape.

Further, the isolate was identified through 16S rRNA sequence analysis. The 16S rRNA was compared with the other sequences in GenBank (NCBI). The results indicated that the isolate was identified as *Pseudomonas aeruginosa* VJ 1. Also, the nucleotide sequence of the isolates was deposited in NCBI and obtained the accession number (ON626420).

*3.2. Cell Surface Hydrophobicity of Bacteria.* Bacteria's capacity to exploit any substrate is determined by their development and adherence to that substrate. Several physical factors, including the pressures that help bacteria adhere to solid substrates, the substrate's qualities, and the bacteria's nature, influence bacteria's ability to stick to either hydrophilic or hydrophobic surfaces. The hydrophobicity of mid-log phase *Pseudomonas aeruginosa* VJ 1 cells at 0.2 mL

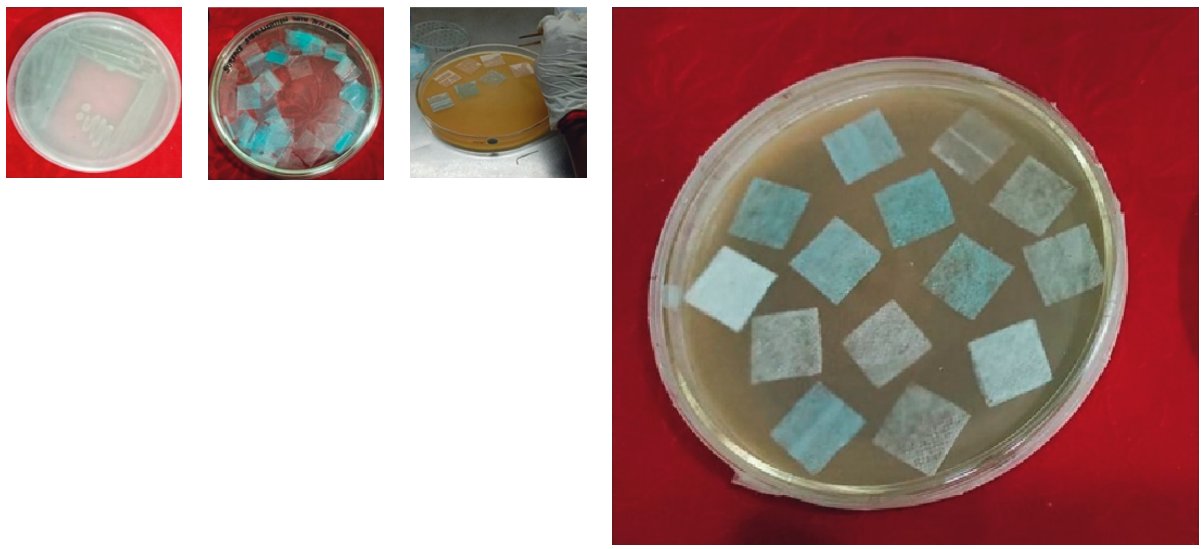

(a) (b) (c) (d)

Figure 1: (a) Pure culture of *Pseudomonas* sp. strain. (b) Pretreated PP mask pieces. (c) PP mask placed on the culture-inoculated nutrient agar plate. (d) PP mask pieces on nutrient agar after 30 days.

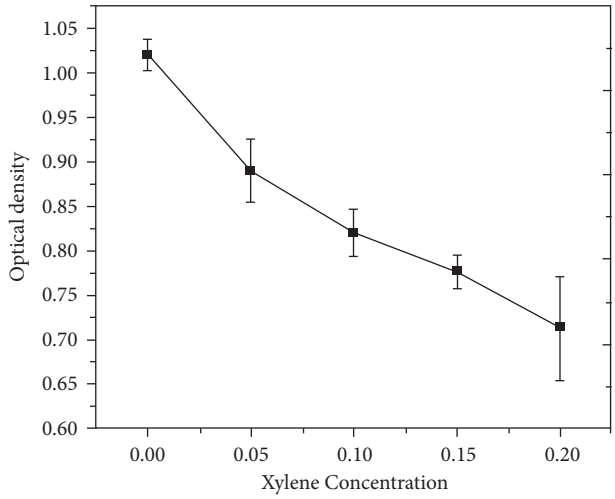


Figure 2: Cell surface hydrophobicity of *Pseudomonas* sp.

xylene revealed a considerable rise in hydrophobicity in this study (30.39 percent) (Figure 2).

*3.3. Growth of Pseudomonas aeruginosa VJ 1 and Surface-Attached Cells on PP Films.* After 15 and 30 days of incubation, the bacterial cell development was characterized by a rapid increase in planktonic cells and the surface-attached bacterial mass. In all of the liquid media employed, *Pseudomonas aeruginosa* VJ 1 reached a consistent growth rate of about $10^7$ CFU/ml after 15–20 days of incubation (Table 1). Biofilm production patterns were similar to planktonic cell growth in all three mediums (Table 2). According to the findings, *Pseudomonas aeruginosa* VJ 1 cells showed more significant colonization, biofilm formation, and fractional biodegradation of PP film in all three conditions. These findings indicate that *Pseudomonas aeruginosa* VJ 1 cell is a high affinity for the PP film. Still, they also suggest that *Pseudomonas aeruginosa* VJ 1 cultures can form biofilms through hydrophobic contacts even when carbon is limited.

Table 1: Viability of *Pseudomonas* sp. on different day intervals.

| S. no. | Days | NB (CFU/$\mu$L) | BHM (CFU/$\mu$L) | MSM (CFU/$\mu$L) |
|---|---|---|---|---|
| 1 | 0 | $1.07 \times 10^5$ | $0.8 \times 10^5$ | $0.92 \times 10^5$ |
| 2 | 10 | $2.01 \times 10^6$ | $1.9 \times 10^6$ | $1.92 \times 10^6$ |
| 3 | 20 | $2.02 \times 10^7$ | $1.95 \times 10^7$ | $1.99 \times 10^7$ |
| 4 | 30 | $1.97 \times 10^7$ | $1.98 \times 10^7$ | $1.98 \times 10^7$ |

Table 2: Monitoring the planktonic growth of *Pseudomonas* sp.

| Media | Day 0 (CFU/$\mu$L) | 15th day (CFU/$\mu$L) | 30th day (CFU/$\mu$L) |
|---|---|---|---|
| NB | $0.9 \times 10^5$ | $2.0 \times 10^5$ | $2.08 \times 10^5$ |
| BHM | $1.1 \times 10^7$ | $1.9 \times 10^7$ | $2.07 \times 10^7$ |
| MSM | $1.2 \times 10^7$ | $2.0 \times 10^7$ | $2.12 \times 10^7$ |

On the other hand, this situation is not necessarily known to all biofilm-forming bacterial species. PP sheets served as a substrate for attachment and biofilm production and a carbon source for our study's *Pseudomonas aeruginosa* VJ 1. The incubation of *Pseudomonas aeruginosa* VJ 1 with PP films for an extended period resulted in forming a solid biofilm on the PP surface, leading to the fractional depletion of this polymer. Similarly, using low molecular mass elements in the polymer may aid in creating and maintaining active biofilm throughout the 30-day incubation period.

*3.4. Dry Weight Determination of Recovered Polypropylene Mask Pieces.* After a month (30 days) of incubation, the remaining polypropylene mask strips were retrieved from the media. The adhering media and bacterial biomass were rinsed and left to air dry after cleaning with suitable solutions. Table 3 shows the final weight loss for *Pseudomonas*

Table 3: Weight reduction percentage of PP mask pieces after 30-day treatment with *Pseudomonas* sp. on different media sources.

| Media sources | Incubation period | | |
|---|---|---|---|
| | 10 days (%) | 20 days (%) | 30 days (%) |
| Nutrient agar | 1.88 | 2.3 | 3.28 |
| Nutrient broth | 2.88 | 4.13 | 5.37 |
| BHM agar | 1.3 | 1.95 | 2.20 |
| BHM broth | 1.87 | 2 | 2.45 |
| MSM agar | 1.2 | 1.76 | 1.84 |
| MSM broth | 1.63 | 1.90 | 2.1 |

*aeruginosa* VJ 1 in various culture media (NA, NB, BHM agar, BHM broth, MSM agar, and MSM broth). The *Pseudomonas aeruginosa* VJ 1 strain's growth kinetics in media revealed colonization on the Surface of PP mask pieces, resulting in a weight reduction due to using PP mask film as a nutrition source.

After one month, our study found a 5.37 and 3.28 percent weight decrease in the case of PP films placed in NB and NA, 2.20 and 2.45 percent weight reduction in BHM and BH, and 1.84 and 2.1 percent weight reduction in MSM and MS (30 days).

*3.5. Surface Change Analysis.* The surface morphology changes on the PP mask pieces before and after biotic exposure were investigated with the help of a Field Emission Scanning Electron Microscope (FE-SEM). Figures 3(a), 3(b), and 3(c) show that the surface changes recorded during FE-SEM analysis were for *Pseudomonas aeruginosa* VJ 1 (T1A, T1B, T2A, T2B, T3A, and T3B) and untreated negative control (C1A, C1B, C2A, C2B, C3A, and C3B) after 30 days of treatment. It was observed that signs of surface deterioration appeared on the PP mask films treated with *Pseudomonas aeruginosa* VJ 1 after 30 days of incubation. On the other hand, the control film (untreated with *Pseudomonas aeruginosa* VJ 1 strain) kept a smooth surface under the same incubation conditions.

*3.6. Structural Analysis Using FTIR.* Structural changes in biologically treated PP mask films were further analyzed with the help of FTIR. This investigation of the degraded PP films has shown the stretching of numerous functional groups after incubation with the *Pseudomonas aeruginosa* VJ 1 strain. The differences were found in the FTIR spectra peaks of the control and test samples in all media used. Tables 4–6 summarize the functional group implicated in stretching by the role of *Pseudomonas aeruginosa* VJ 1, the wave number, and IR band position on the PP films. A considerable reduction in the carbonyl index (CI) was observed in the samples incubated with *Pseudomonas aeruginosa* VJ 1 for 30 days. Spectrophotometric variations of PP mask films and the value of CI determine the maximum degradation when compared to an untreated negative control.

In this study, FTIR analysis affords a close view of the N-H stretching of the aldehydes group at 3190.18 $cm^{-1}$. The C-C absorption peaks were shifted at 1255.18, 1302.34, 1794.87, 2427.49, and 2617.26 $cm^{-1}$. The conformational changes on PP mask film were supported by the changes in almost all functional groups (Figures 4(a)–4(l)).

## 4. Discussion

This study revealed that the isolated strain was *Pseudomonas aeruginosa* VJ 1 by biochemical and selective agar screening methods. Another author reported that the isolated bacteria were cultured in milk agar with cetrimide for the preliminary detection of *Pseudomonas* sp., which is similar to our findings [28]. Based on the results, it was reasonable to identify the isolated bacterium belonging to *Pseudomonas aeruginosa* VJ 1.

In this present investigation, the hydrophobicity was high in mid-log phase cells of *Pseudomonas aeruginosa* VJ 1. In most cases, a hydrophobic bacterium prefers a hydrophobic surface for adhesion, whereas the inverse is true for bacteria with hydrophilic qualities [17]. These results agree with previous reports [17], which observed that bacterial cells in the log phase are more hydrophobic. A previous investigation found similar results, with the isolates *Kocuria palustris* M16 and *Bacillus subtilis* H1584 showing a maximum increase in hydrophobicity of 24 percent turbidity reduction at 0.25 l and a maximum decrease of 32 percent turbidity at 150 l of hydrocarbon like hexadecane. [27]. Another recent study found that the hydrophobicity of *L. monocytogenes* strain CICC 21332 was the lowest (12.5%), and the strain FSIS 57034 had the highest percentage of CSH (74.81%) at 1 ml of xylene concentration [29].

This investigation showed high affinity of *Pseudomonas aeruginosa* VJ 1 cells for the PP film. Similarly, in planktonic cells, the growth pattern of bacteria attached to the surface of PP film was investigated as well as the viability of surface-attached bacterial species [26, 30]. According to the concurrence model, the process of microbes forming biofilms begins when planktonic cell growth reaches a high density, allowing for the attachment of bacterial cells to a surface via cell signaling and the formation of microcolonies that will eventually frame the mature biofilms [31]. This biofilm population is diverse and stable and ideal for extended periods [32].

*Pseudomonas* sp. isolated from the soil of the Sisdol landfill site and the Sanothimi household garbage site in Nepal displays similar biochemical features [33]. *Pseudomonas* sp. ISJ14 was highly efficient at degrading low-density polyethylene (LDPE) in BHM [17]. On the other hand, this work is the first to show that a *Pseudomonas aeruginosa* VJ 1 can biodegrade a surgical face mask constructed of a rigid PP-like polymer.

Similar findings were recorded in earlier studies such as the biodegradation of untreated films of polyethylene by *Pseudomonas putida* IRN22, *Micrococcus luteus* IRN20, *Acinetobacter pittii* IRN19 [34], and other bacterial genera, including *Delftia, Stenotrophomonas*, and *Comamonas* [35], and *Galleria mellonella* isolated from the gut of the wax worm also have been establishing the capabilities of PE degradation [36]. Similar findings were reported by several other researchers on the LDPE surface [37–39]. The LDPE

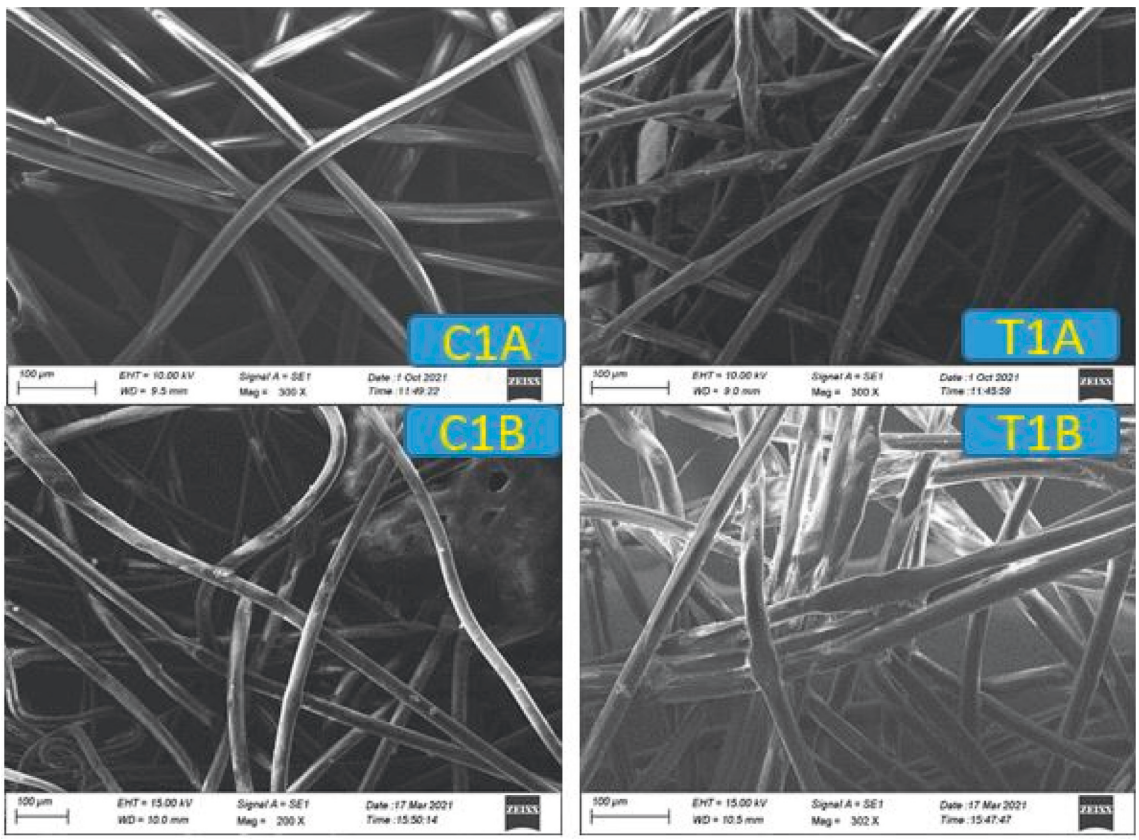


(a)

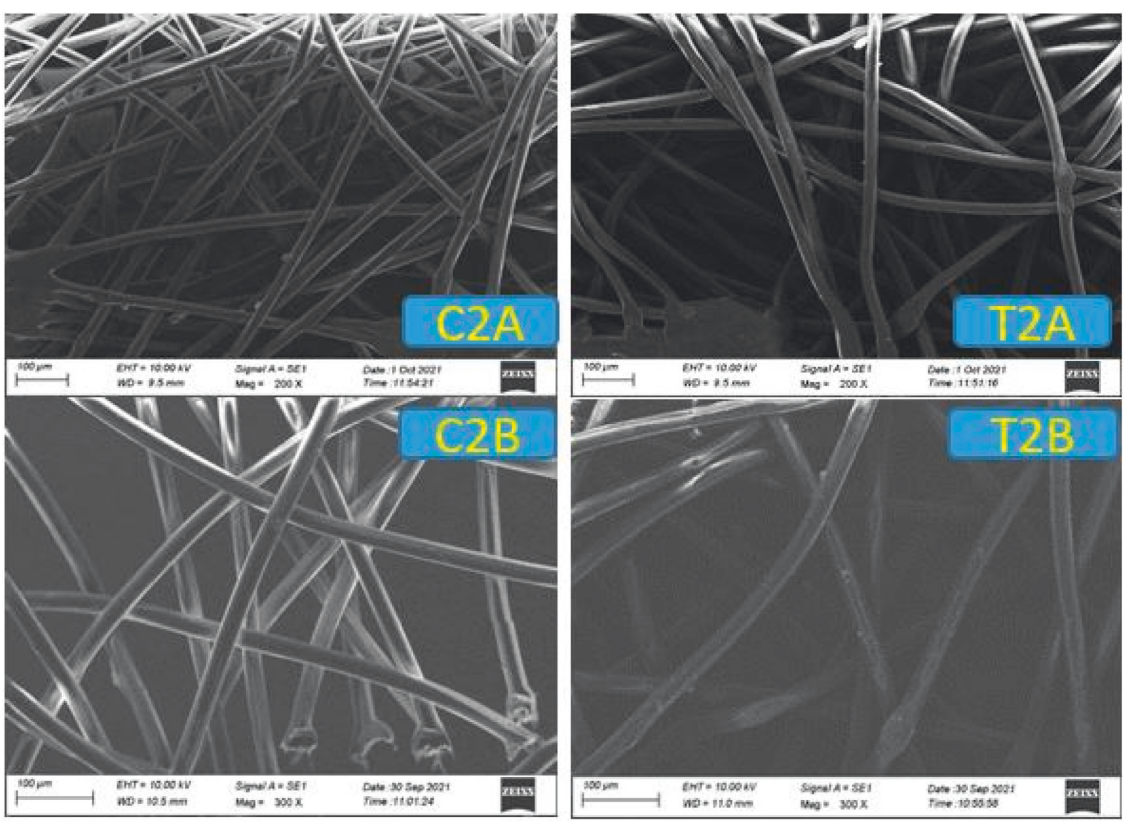


(b)

Figure 3: Continued.

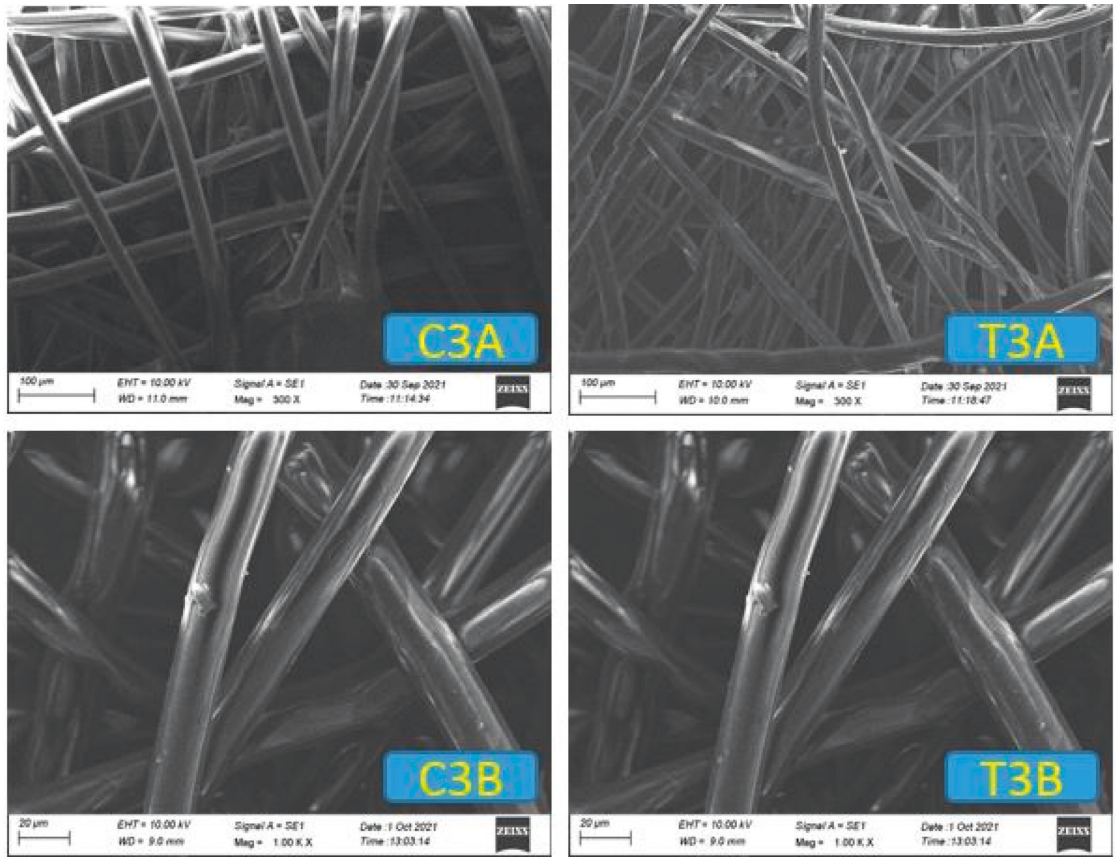


(c)

Figure 3: (a) SEM images of PP films placed in nutrient medium: C1A and C1B, control; T1A and T1B, treated with *Pseudomonas* sp. NA and NB media, respectively. (b) SEM images of PP films placed in BHM: C2A and C2B, control; T2A and T2B, treated with *Pseudomonas* sp. in BHM agar and broth, respectively. (c) SEM images of PP films placed in MSM: C3A and C3B, control; T3A and T3B, treated with *Pseudomonas* sp. in MSM agar and broth, respectively.

Table 4: Comparison of IR band position in the PP films after incubation with *Pseudomonas* sp. in NB and NA (both control and test).

| S. no. | Incubation period | IR band position in NB control-test ($cm^{-1}$) | IR band position in NA control-test ($cm^{-1}$) | Functional group involved |
|---|---|---|---|---|
| 1 | 30 days | 459.12–458.59 | 458.78–455.96 | C-X stretching |
| 2 | | 1104.03–1102.10 | 1102.65–1101.96 | C-H stretching |
| 3 | | 2722.14–2721.10 | 2722.18–2721.97 | C-H stretching |
| 4 | | 3763.83–3761.66 | 3763.18–2911.74 | O-H stretching |

Table 5: Comparison of IR band position in the PP films after incubation with *Pseudomonas* sp. in BHM broth and BHM agar (both control and test).

| S. no. | Incubation period | IR band position in BHM broth control-test ($cm^{-1}$) | IR band position in BHM agar control-test ($cm^{-1}$) | Functional group involved |
|---|---|---|---|---|
| 1 | 30 days | 572.18–460.23 | 1002.24–808.93 | C-X stretching |
| 2 | | 2950.10–2838.92 | 2918.97–2917.61 | C-H stretching |
| 3 | | 2916.61–2722.13 | 2947.73–2838.92 | C-H stretching |
| 4 | | 3762.08–3189.68 | 3761.52–3189.68 | O-H stretching |

film treated with *Pseudomonas* sp. showed a 20% reduction after 120 days of treatment, which has also been reported [40]. Several other studies on the LDPE surface have reported similar results [37–39]. The LDPE film treated with *Pseudomonas* sp. showed a 20% reduction after 120 days of treatment, which has also been reported [40]. However, a recent study provided strong evidence for PP microplastic degradation by *Rhodococcus* sp.36 with 6.4% degradation

Table 6: Comparison of IR band position in the PP films after incubation with *Pseudomonas* sp. in MSM broth and MSM agar (both control and test).

| S. no. | Incubation period | IR band position in MSM broth control-test ($cm^{-1}$) | IR band position in MSM agar control-test ($cm^{-1}$) | Functional group involved |
|---|---|---|---|---|
| 1 | 30 days | 562.12–458.98 | 460.00–459.35 | C-X stretching |
| 2 | | 2839.02–2722.15 | 2839.57–2838.65 | C-H stretching |
| 3 | | 2916.76–2838.83 | 2918.00–2917.14 | C-H stretching |
| 4 | | 3760.91–3346.85 | 3351.15–3190.32 | O-H stretching |

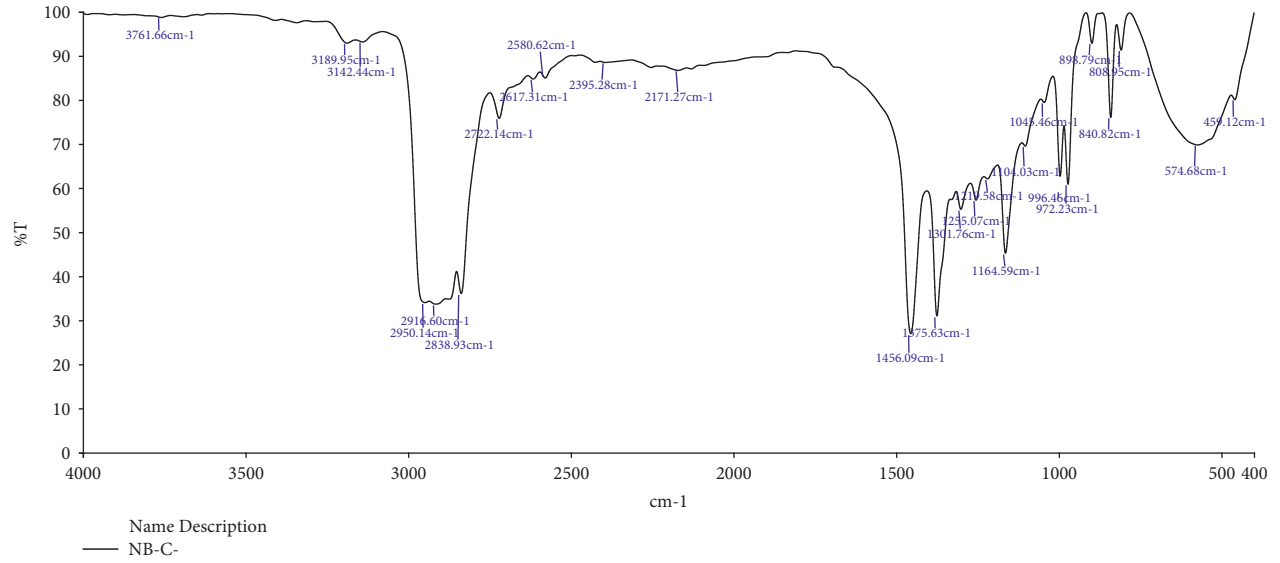


(a)

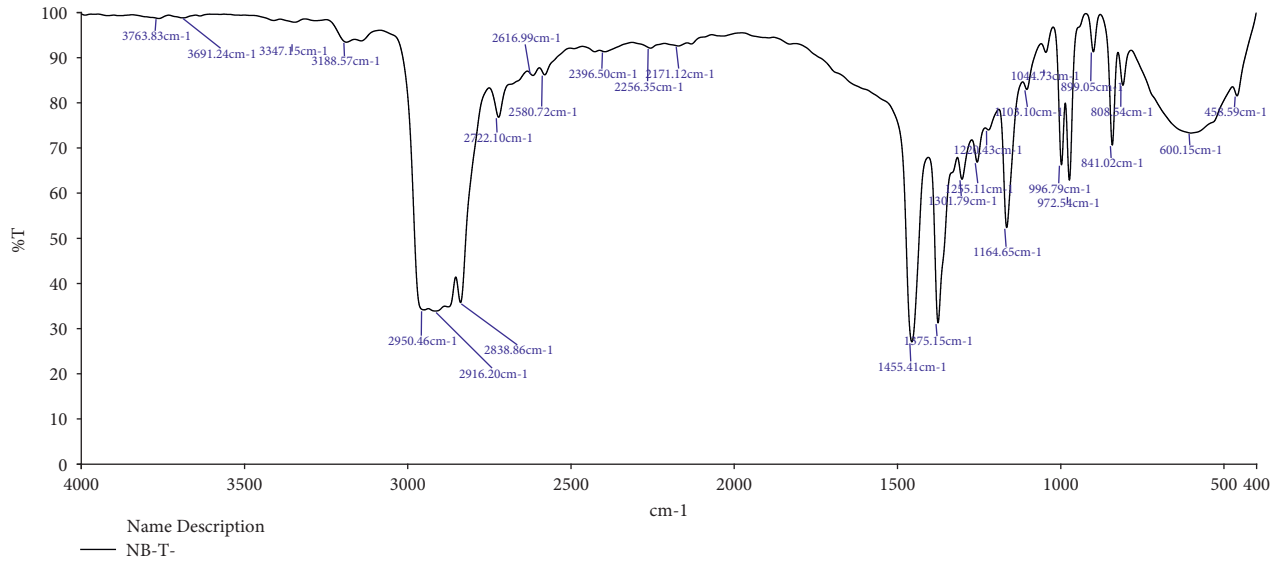


(b)

Figure 4: Continued.

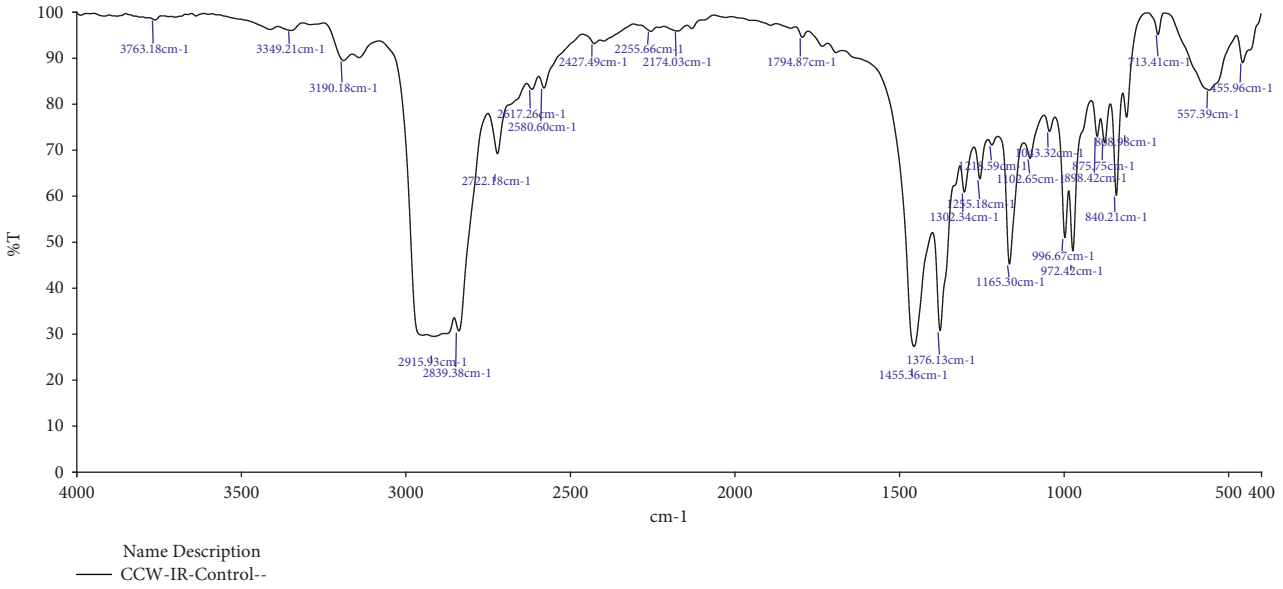


(c)

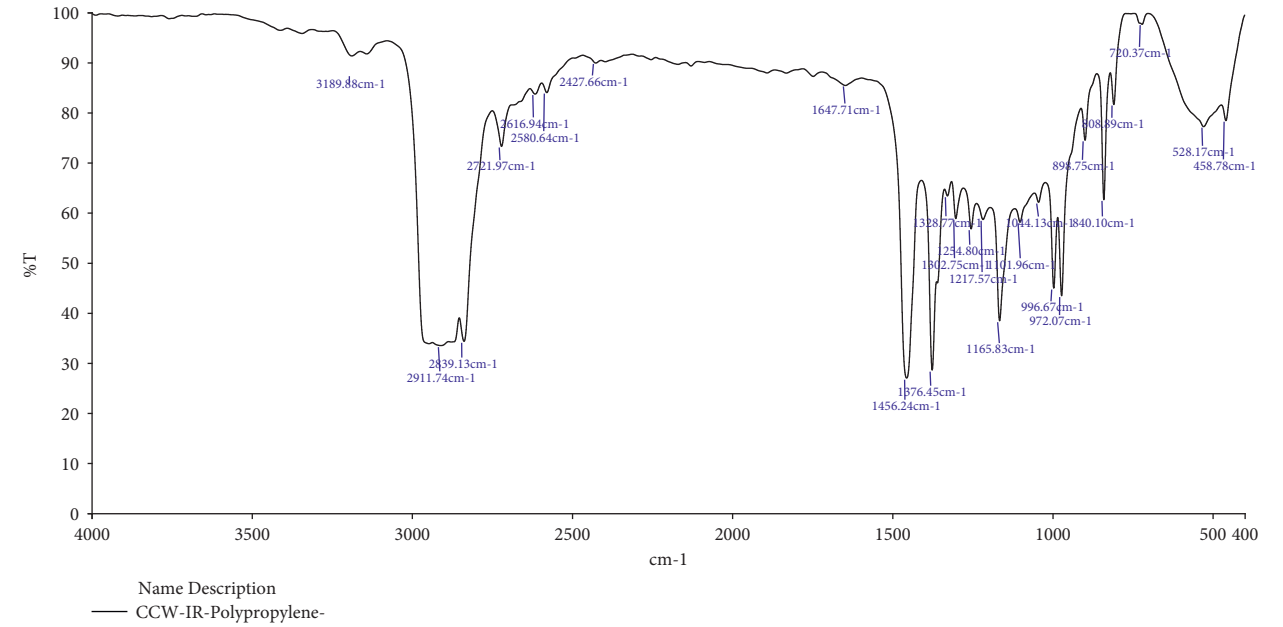


(d)

Figure 4: Continued.

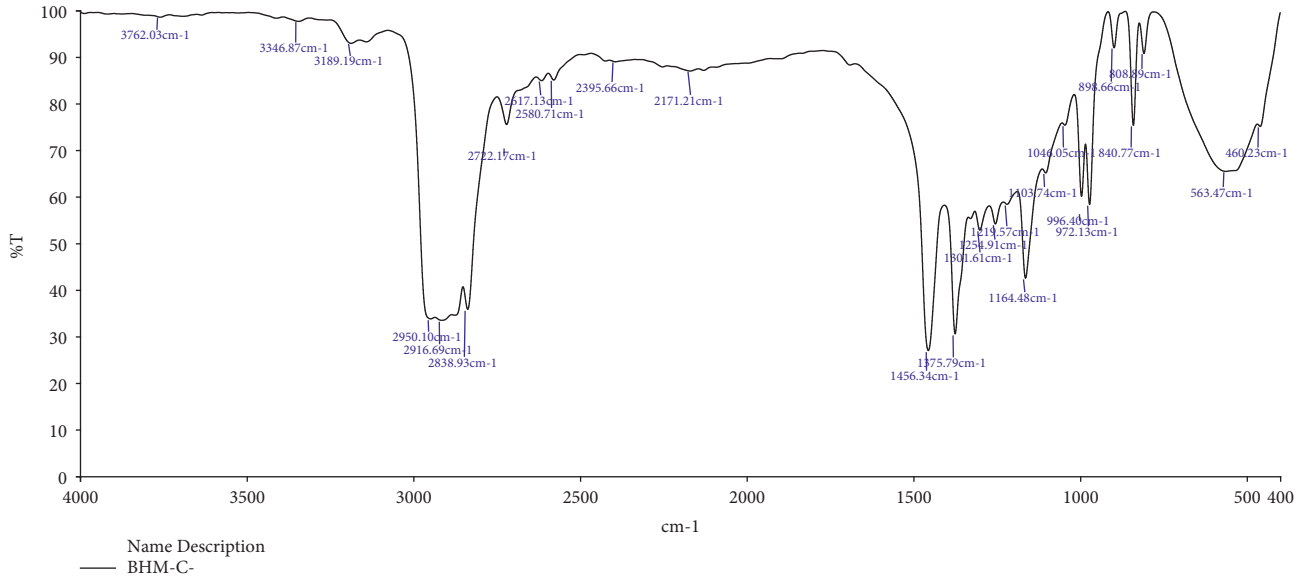


(e)

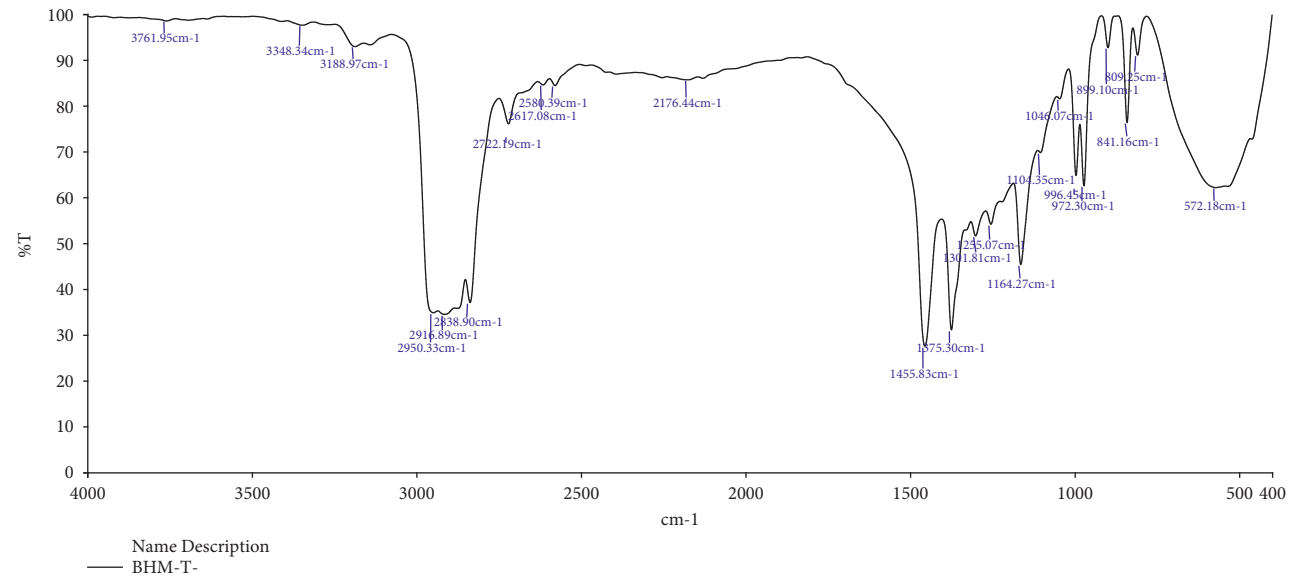


(f)

Figure 4: Continued.

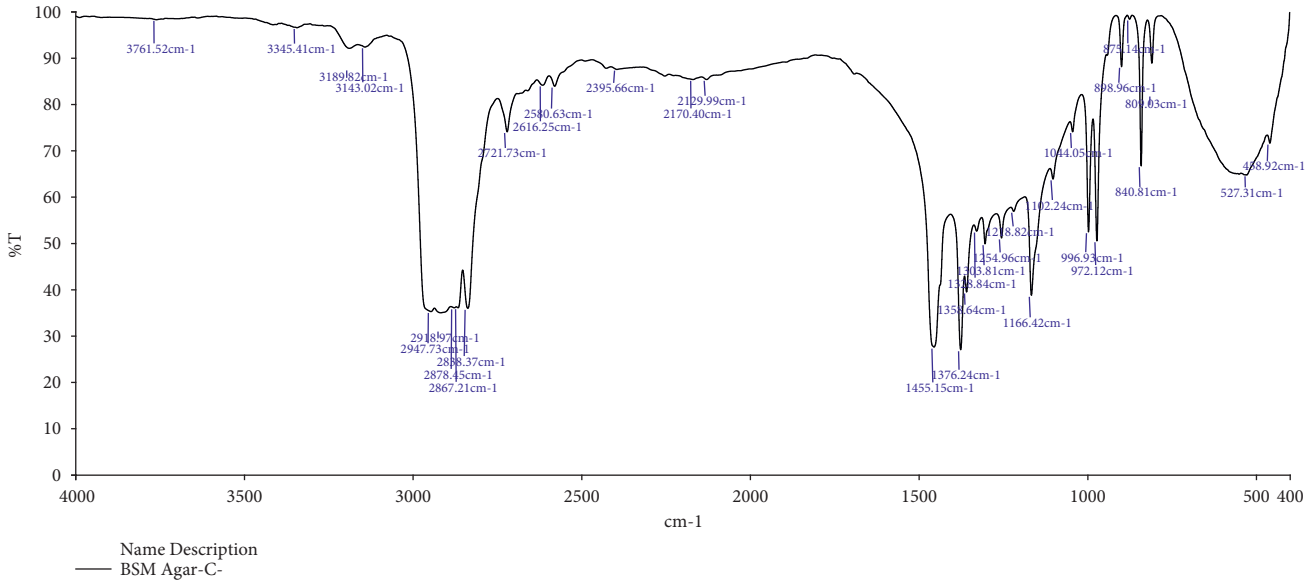


(g)

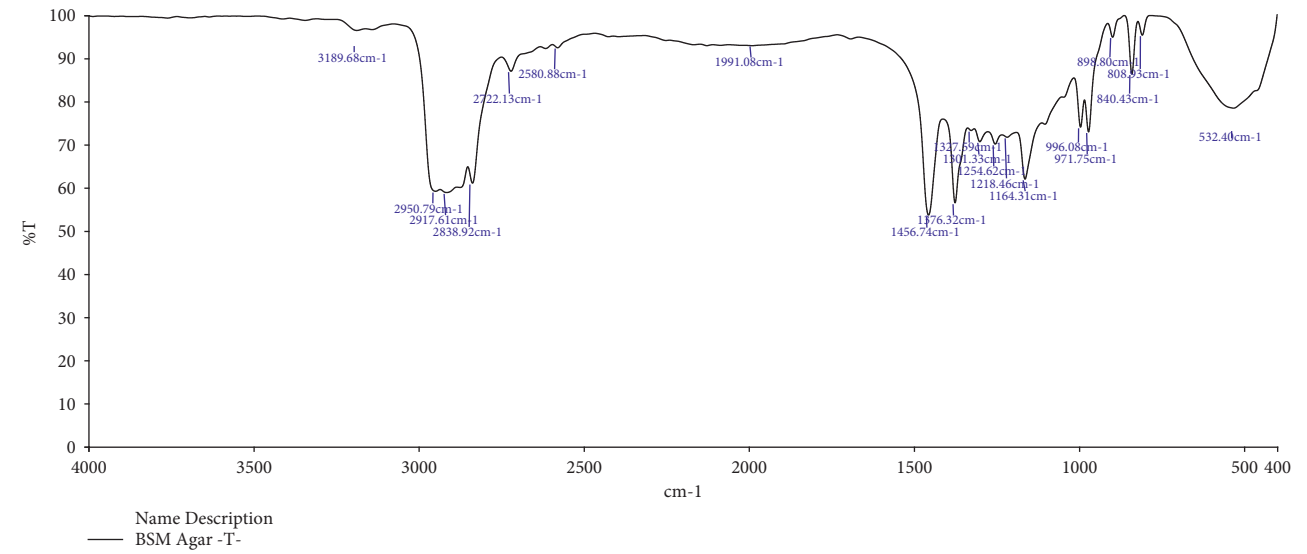


(h)

Figure 4: Continued.

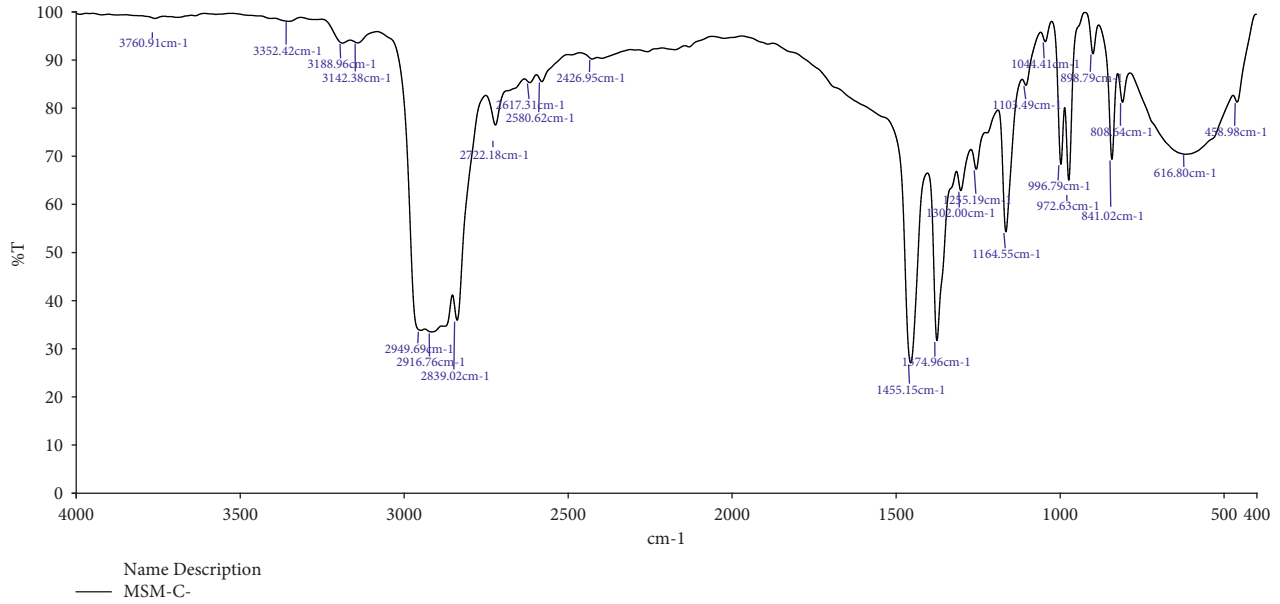


(i)

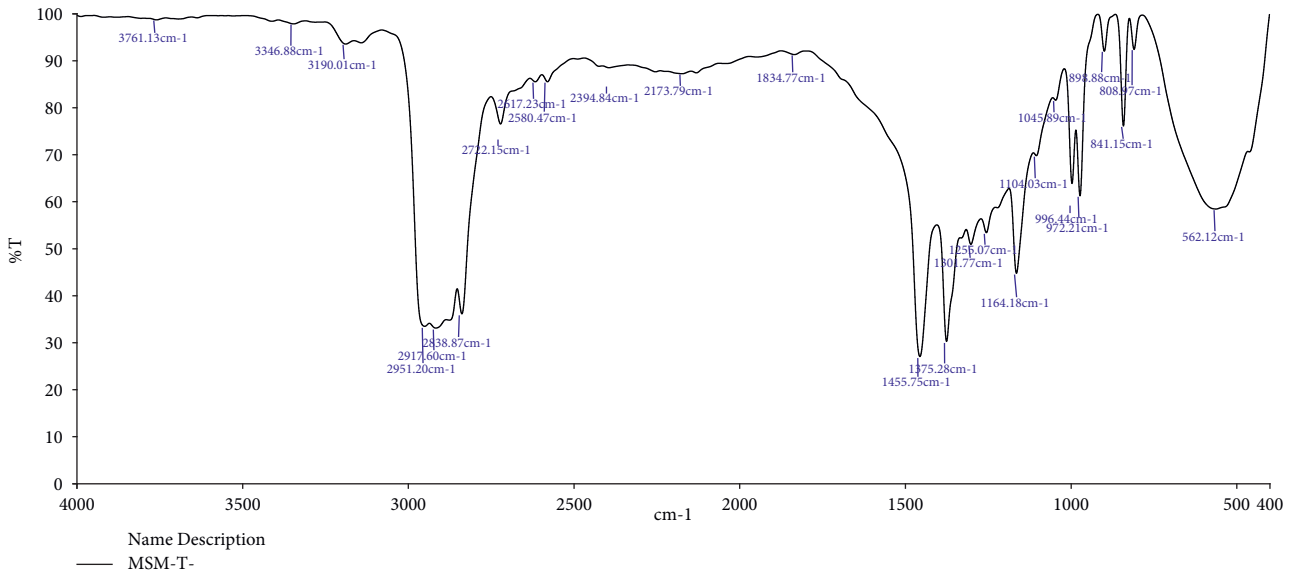


(j)

Figure 4: Continued.

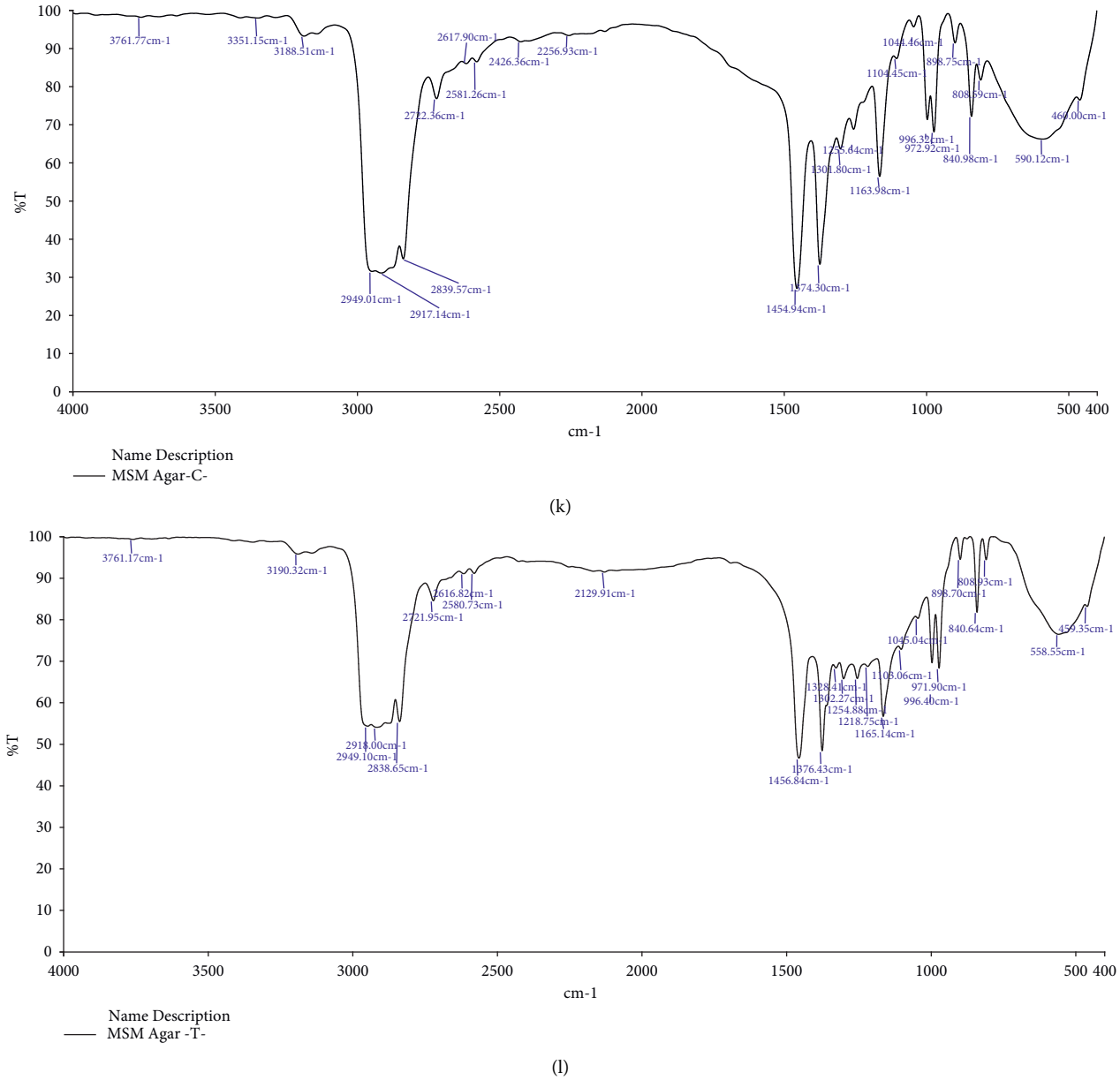


Figure 4: (a) IR spectra of PP films in NB (control). (b) IR spectra of PP films in NB (treated). (c) IR spectra of PP films in NA (control). (d) IR spectra of PP films in NA (treated). (e) IR spectra of PP films in BHM broth (control). (f) IR spectra of PP films in BHM broth (treated). (g) IR spectra of PP films in BHM agar (control). (h) IR spectra of PP films in BHM agar (treated). (i) IR spectra of PP films in MSM broth (control). (j) IR spectra of PP films in MSM broth (treated). (k) IR spectra of PP films in MSM agar (control). (l) IR spectra of PP films in MSM agar (treated).

and *Bacillus* sp.27 with 4%, demonstrating the excellent degradation capacity of bacterial strains [41].

Similar findings were reported in the surface morphology of the LDPE films treated with *Pseudomonas* sp. by SEM after 40, 80, and 120 days of incubation [40]. Another study also reported that the *P. aeruginosa* ISJ14 used to treat LDPE film showed maximum deterioration after 60 days of treatment when observed under the FE-SEM [17]. In a cross-reference to the earlier research studies on LDPE biodegradation, many authors have reported similar morphological changes in LDPE degradation by *Aspergillus* spp. [42], as well as *A. clavatus JASK1* [43]. The LDPE film incubated with *P. aeruginosa* PAO1 showed a maximum reduction in CI, as reported by [40, 44]. Based on our findings, a significant reduction of the carbonyl index was detected in the samples incubated with *Pseudomonas aeruginosa* VJ 1 for 30 days. A similar observation was reported by several authors [45]. Our results were supported by various previous research studies that noticed the formation of functional groups and the loss of these groups in the LDPE degradation using the strain *Bacillus amyloliquefaciens* [46]. In our study [43], we noticed visible modifications in the synthetic polymers that undergo biodegradation before and after exposure to microbes by FTIR analysis. Thus, our results

suggest that the *Pseudomonas aeruginosa* VJ 1 has a notable ability to degrade the PP mask films.

## 5. Conclusion

This work offered a versatile biological process to evaluate the degradation of disposable face masks used in this SARS-CoV-2 pandemic. The *in vitro* biodegradation of the *Pseudomonas aeruginosa* VJ 1 in three different solid and liquid mediums reflects the eco-friendly approach. We observed a tremendous biodegradation efficiency of our isolates towards the PP-based disposable face mask, whose molecular weight was as high as 228,000. The isolate can form biofilm on the PP surface and utilize it as a sole nutrient source for growth. The weight reduction of PP mask films relative to untreated control films reflects within 30 days (up to 5.37 percent weight reduction). Based on the FE-SEM and FTIR analysis results, the *Pseudomonas aeruginosa* VJ 1 is suitable for PP degradation without UV treatment. However, further studies on the enzyme-based metabolic passages of *Pseudomonas aeruginosa* VJ 1 are also recommended to better understand its tremendous role in biodegradation.

## Data Availability

The data supporting the findings of this study are included within the article.

## Disclosure

A preprint of this manuscript is available on Research Square and the link is https://www.researchsquare.com/article/rs-1002388/v1.

## Conflicts of Interest

The authors declare no conflicts of interest.

## Authors' Contributions

Selvakumar Vijayalakshmi contributed to conceptualization, methodology, data curation, original draft writing, and review and editing; Preethi Gopalsamy contributed to methodology, data curation, initial draft writing, and review and editing; Karnan Muthusamy contributed to formal analysis; Dinesh Kumar Sundarraj contributed to software provision, data curation, and review and editing; Steffi Pulikondan francis, Ly Thi Thuy Duong, Tuyet Thi Anh Truong, Huu Tap Van, Shankar Karuppannan, and Thiyagarajan Ramesh contributed to review and editing; Deog-Hwan Oh contributed to conceptualization, methodology, supervision, project administration, and review and editing.

## Acknowledgments

The authors are thankful to Askoscen Probionics (R&D), Thiruchirappalli, Tamilnadu, India, for the support.

## References

[1] C. Sohrabi, Z. Alsafi, N. O'Neill et al., "World Health Organization declares global emergency: a review of the 2019 novel coronavirus (COVID-19)," *International Journal of Surgery*, vol. 76, pp. 71–76, 2020.

[2] N. U. Benson, O. H. Fred-Ahmadu, D. E. Bassey, and A. A. Atayero, "COVID-19 pandemic and emerging plastic-based personal protective equipment waste pollution and management in Africa," *Journal of Environmental Chemical Engineering*, vol. 9, no. 3, Article ID 105222, 2021.

[3] C. J. Worby and H.-H. Chang, "Face mask use in the general population and optimal resource allocation during the COVID-19 pandemic," *Nature Communications*, vol. 11, no. 1, 2020.

[4] A. Jemec Kokalj, A. Dolar, D. Drobne et al., "Environmental hazard of polypropylene microplastics from disposable medical masks: acute toxicity towards Daphnia magna and current knowledge on other polypropylene microplastics," *Microplastics and nanoplastics*, vol. 2, no. 1, pp. 1–15, 2022.

[5] S. Dharmaraj, V. Ashokkumar, S. Hariharan et al., "The COVID-19 pandemic face mask waste: a blooming threat to the marine environment," *Chemosphere*, vol. 272, Article ID 129601, 2021.

[6] C. Nzediegwu and S. X. Chang, "Improper solid waste management increases potential for COVID-19 spread in developing countries," *Resources, Conservation and Recycling*, vol. 161, Article ID 104947, 2020.

[7] J. C. Prata, A. L. Silva, T. R. Walker, A. C. Duarte, and T. Rocha-Santos, "COVID-19 pandemic repercussions on the use and management of plastics," *Environmental Science & Technology*, vol. 54, no. 13, pp. 7760–7765, 2020.

[8] M. Saberian, J. Li, S. Kilmartin-Lynch, and M. Boroujeni, "Repurposing of COVID-19 single-use face masks for pavements base/subbase," *Science of the Total Environment*, vol. 769, Article ID 145527, 2021.

[9] R. Dhawan, B. M. S. Bisht, R. Kumar, S. Kumari, and S. Dhawan, "Recycling of plastic waste into tiles with reduced flammability and improved tensile strength," *Process Safety and Environmental Protection*, vol. 124, pp. 299–307, 2019.

[10] K. O'Dowd, K. M. Nair, P. Forouzandeh et al., "Face masks and respirators in the fight against the COVID-19 pandemic: a review of current materials, advances and future perspectives," *Materials*, vol. 13, no. 15, 2020.

[11] S. Jung, S. Lee, X. Dou, and E. E. Kwon, "Valorization of disposable COVID-19 mask through the thermo-chemical process," *Chemical Engineering Journal*, vol. 405, Article ID 126658, 2021.

[12] X. Chen, X. Chen, Q. Liu, Q. Zhao, X. Xiong, and C. Wu, "Used disposable face masks are significant sources of microplastics to environment," *Environmental Pollution*, vol. 285, Article ID 117485, 2021.

[13] M. Sigler, "The effects of plastic pollution on aquatic wildlife: current situations and future solutions," *Water, Air, & Soil Pollution*, vol. 225, no. 11, pp. 2184–2189, 2014.

[14] A.-C. Albertsson, S. O. Andersson, and S. Karlsson, "The mechanism of biodegradation of polyethylene," *Polymer Degradation and Stability*, vol. 18, no. 1, pp. 73–87, 1987.

[15] R. S. Devi, R. K. Velu, N. Krishnan et al., "The role of microbes in plastic degradation," *Environmental and Waste Management*, vol. 341, 2016.

[16] J. D. Gu, "Microbiological deterioration and degradation of synthetic polymeric materials: recent research advances,"

*International Biodeterioration & Biodegradation*, vol. 52, no. 2, pp. 69–91, 2003.

[17] K. K. Gupta and D. Devi, "Characteristics investigation on biofilm formation and biodegradation activities of *Pseudomonas aeruginosa* strain ISJ14 colonizing low density polyethylene (LDPE) surface," *Heliyon*, vol. 6, no. 7, Article ID e04398, 2020.

[18] M. Vague, G. Chan, C. Roberts, N. A. Swartz, and J. L. Mellies, *Pseudomonas Isolates Degrade and Form Biofilms on Polyethylene Terephthalate (PET) Plastic*, BioRxiv, Laurel Hollow, NY, USA, 2019.

[19] E. Munir, R. S. M. Harefa, N. Priyani, and D. Suryanto, "Plastic degrading fungi Trichoderma viride and Aspergillus nomius isolated from local landfill soil in Medan," *IOP Conference Series: Earth and Environmental Science*, IOP Publishing, Bristol, UK, 2018.

[20] C. Roberts, S. Edwards, M. Vague et al., "Environmental consortium containing pseudomonas and bacillus species synergistically degrades polyethylene terephthalate plastic," *mSphere*, vol. 5, no. 6, Article ID e01151, 2020.

[21] J. Yang, Y. Yang, W. M. Wu, J. Zhao, and L. Jiang, "Evidence of polyethylene biodegradation by bacterial strains from the guts of plastic-eating waxworms," *Environmental Science & Technology*, vol. 48, no. 23, pp. 13776–13784, 2014.

[22] H. M. Lee, H. R. Kim, E. Jeon et al., "Evaluation of the biodegradation efficiency of four various types of plastics by *Pseudomonas aeruginosa* isolated from the gut extract of superworms," *Microorganisms*, vol. 8, no. 9, Article ID 1341, 2020.

[23] A. A. Hussaïn, S. H. Khudhair, and I. K. Al-Mayaly, "Optimum conditions for LDPE strips biodegradation by local bacterial isolates," *Journal of International Environmental Application & Science*, vol. 10, no. 4, pp. 399–407, 2015.

[24] N. Kumari, A. Vashishtha, P. Saini, and E. Menghani, "Isolation, identification and characterization of oil degrading bacteria isolated from the contaminated sites of Barmer, Rajasthan," *International Journal of Biotechnology and Bioengineering Research*, vol. 4, no. 5, pp. 429–436, 2013.

[25] J. Arutchelvi, M. Sudhakar, A. S. Arkatkar, M. Doble, S. Bhaduri, and P. V. Uppara, "Biodegradation of polyethylene and polypropylene," *Indian Journal of Biotechnology*, vol. 7, 2008.

[26] D. Andes, J. Nett, P. Oschel, R. Albrecht, K. Marchillo, and A. Pitula, "Development and characterization of an in vivo central venous catheter Candida albicans biofilm model," *Infection and Immunity*, vol. 72, no. 10, pp. 6023–6031, 2004.

[27] K. Harshvardhan and B. Jha, "Biodegradation of low-density polyethylene by marine bacteria from pelagic waters, Arabian Sea, India," *Marine Pollution Bulletin*, vol. 77, no. 1-2, pp. 100–106, 2013.

[28] G. Szita, V. Tabajdi, A. Fabian, G. Biro, O. Reichart, and P. S. Kormoczy, "A novel, selective synthetic acetamide containing culture medium for isolating *Pseudomonas aeruginosa* from milk," *International Journal of Food Microbiology*, vol. 43, no. 1-2, pp. 123–127, 1998.

[29] Y. Fan, J. Qiao, Z. Lu et al., "Influence of different factors on biofilm formation of Listeria monocytogenes and the regulation of cheY gene," *Food Research International*, vol. 137, Article ID 109405, 2020.

[30] A. Arkatkar, J. Arutchelvi, S. Bhaduri, P. V. Uppara, and M. Doble, "Degradation of unpretreated and thermally pretreated polypropylene by soil consortia," *International Biodeterioration & Biodegradation*, vol. 63, no. 1, pp. 106–111, 2009.

[31] J. W. Costerton, P. S. Stewart, and E. P. Greenberg, "Bacterial biofilms: a common cause of persistent infections," *Science*, vol. 284, no. 5418, pp. 1318–1322, 1999.

[32] G. Bødtker, T. Thorstenson, B. L. P. Lillebo et al., "The effect of long-term nitrate treatment on SRB activity, corrosion rate and bacterial community composition in offshore water injection systems," *Journal of Industrial Microbiology & Biotechnology*, vol. 35, no. 12, pp. 1625–1636, 2008.

[33] G. Badahit, J. Kumar, and A. Singh, "Screening of plastic degrading Pseudomonas spp. from soil," *International Journal of Scientific Engineering and Research*, vol. 9, pp. 484–489, 2018.

[34] Z. Montazer, M. B. Habibi Najafi, and D. B. Levin, "Microbial degradation of low-density polyethylene and synthesis of polyhydroxyalkanoate polymers," *Canadian Journal of Microbiology*, vol. 65, no. 3, pp. 224–234, 2019.

[35] J. Peixoto, L. P. Silva, and R. H. Krüger, "Brazilian Cerrado soil reveals an untapped microbial potential for unpretreated polyethylene biodegradation," *Journal of Hazardous Materials*, vol. 324, pp. 634–644, 2017.

[36] B. J. Cassone, H. Grove, O. Elebute, S. Villanueva, and C. M. R. LeMoine, "Role of the intestinal microbiome in low-density polyethylene degradation by caterpillar larvae of the greater wax moth, Galleria mellonella," *Proceedings of the Royal Society B*, vol. 287, Article ID 20200112, 2020.

[37] A. Kapri, M. Zaidi, A. Satlewal, and R. Goel, "SPION-accelerated biodegradation of low-density polyethylene by indigenous microbial consortium," *International Biodeterioration & Biodegradation*, vol. 64, no. 3, pp. 238–244, 2010.

[38] A. A. Shah, A. Nawaz, L. Kanwal, F. Hasan, S. Khan, and M. Badshah, "Degradation of poly (ε-caprolactone) by a thermophilic bacterium Ralstonia sp. strain MRL-TL isolated from hot spring," *International Biodeterioration & Biodegradation*, vol. 98, pp. 35–42, 2015.

[39] A. Sah, A. Kapri, M. G. H. Zaidi, H. Negi, and R. Goel, "Implications of fullerene-60 upon in-vitro LDPE biodegradation," *Journal of Microbiology and Biotechnology*, vol. 20, no. 5, pp. 908–916, 2010.

[40] B. M. Kyaw, R. Champakalakshmi, M. K. Sakharkar, C. S. Lim, and K. R. Sakharkar, "Biodegradation of low density polythene (LDPE) by Pseudomonas species," *Indian Journal of Microbiology*, vol. 52, no. 3, pp. 411–419, 2012.

[41] H. S. Auta, C. Emenike, B. Jayanthi, and S. Fauziah, "Growth kinetics and biodeterioration of polypropylene microplastics by Bacillus sp. and Rhodococcus sp. isolated from mangrove sediment," *Marine Pollution Bulletin*, vol. 127, pp. 15–21, 2018.

[42] S. Zahra, S. S. Abbas, M. T. Mahsa, and N. Mohsen, "Biodegradation of low-density polyethylene (LDPE) by isolated fungi in solid waste medium," *Waste Management*, vol. 30, no. 3, pp. 396–401, 2010.

[43] A. Gajendiran, S. Krishnamoorthy, and J. Abraham, "Microbial degradation of low-density polyethylene (LDPE) by Aspergillus clavatus strain JASK1 isolated from landfill soil," *3 Biotech*, vol. 6, no. 1, pp. 52–56, 2016.

[44] S. Skariyachan, M. Megha, M. N. Kini, K. M. Mukund, A. Rizvi, and K. Vasist, "Selection and screening of microbial consortia for efficient and ecofriendly degradation of plastic

garbage collected from urban and rural areas of Bangalore, India," *Environmental Monitoring and Assessment*, vol. 187, no. 1, pp. 4174–4214, 2015.

[45] G. Howard and N. Hilliard, "Use of Coomassie blue-polyurethane interaction inscreening of polyurethanase proteins andpolyurethanolytic bacteria," *International Biodeterioration & Biodegradation*, vol. 43, no. 1-2, pp. 23–30, 1999.

[46] M. P. Das and S. Kumar, "An approach to low-density polyethylene biodegradation by Bacillus amyloliquefaciens," *3 Biotech*, vol. 5, no. 1, pp. 81–86, 2015.

Hindawi
Journal of Chemistry
Volume 2022, Article ID 1591703, 9 pages
https://doi.org/10.1155/2022/1591703

*Research Article*

# Thermochemical Recycling of Solid Biomass Materials for Achieving Sustainable Goal: A Complete Characterization Study on Liquid Yield Products

**Ashok Kumar Koshariya**,[1] **J. Madhusudhanan**,[2] **Harishchander Anandaram**,[3] **J. Isaac JoshuaRamesh Lalvani**,[9] **L. Natrayan**,[4] **Praveen Bhai Patel**,[5] **P. Jayaraman**,[6] **Ezhakudiyan Ravindran**,[7] **and Palanisamy Rajkumar**[8]

[1]*Department of Plant Pathology, School of Agriculture, Lovely Professional University, Jalandhar 144411, Punjab, India*
[2]*Department of Biotechnology, Anand Institute of Higher Technology, Kazhipattur, Chennai 603103, Tamil Nadu, India*
[3]*Centre for Excellence in Computational Engineering and Networking, Amrita Vishwa Vidyapeetham, Coimbatore 641112, Tamil Nadu, India*
[4]*Department of Mechanical Engineering, Saveetha School of Engineering, SIMATS, Chennai 602105, Tamil Nadu, India*
[5]*Department of Chemical Engineering, University Institute of Engineering and Technology, C S J M University, Kanpur 208024, Uttar Pradesh, India*
[6]*Department of Mechanical Engineering, Prathyusha Engineering College, Aranvoyalkuppam, Tiruvallur 602025, Tamil Nadu, India*
[7]*Organic Electronic Materials Laboratory, Department of Information Display, Kyung Hee University, Dongdaemoon-Gu, Seoul 02447, Republic of Korea*
[8]*Department of Chemical Engineering, Kunsan National University, Gunsan 54150, Jeonbuk, Republic of Korea*
[9]*Faculty of Mechanical Engineering, Arba Minch Institute of Technology, Arba Minch University, PO Box 21, Arba Minch, Ethiopia*

Correspondence should be addressed to J. Isaac JoshuaRamesh Lalvani; isaac.jrl@amu.edu.et and L. Natrayan; natrayan07@gmail.com

Received 18 July 2022; Revised 1 August 2022; Accepted 16 August 2022; Published 31 August 2022

Academic Editor: Balasubramani Ravindran



In order to achieve sustainability goals, biomass is a renewable energy source that lowers emissions of greenhouse gases and other hazardous gases. Biochemical and thermochemical methods are both used to produce bioenergy from biomass. Pyrolysis is an effective thermochemical conversion technique used for the conversion of biomass into energy-rich bio-oil. In this study, the pyrolysis characteristics and bio-oil obtained from the residues of *Ricinus communis* were investigated. The experimental run was designed to analyze the impact of bed temperature on product yield by varying the process temperature from 350°C to 750°C. In this study, a maximum of 46.5 wt% of bio-oil was produced at 500°C. The maximum conversion was recorded at temperatures ranging from 450°C to 550°C. The bio-oil obtained at maximum yield conditions was analyzed using different analytical techniques. The Fourier transform infrared spectroscopy (FT-IR) and gas chromatography and mass spectroscopy (GC-MS) analyses of the bio-oil revealed that the oil has a significant amount of phenol derivatives, oxygenated chemicals, acids, and esters. The physical properties of the bio-oil showed that it is viscous and has a medium heating value compared with commercial fossil fuel.

## 1. Introduction

During the 1970s, the energy crisis in the world raised many questions and uncertainty that could depend on the economy and abundant supply of fossil fuels. Therefore, the scientific work on fossil fuels has focused a lot of attention and effort on developing a more sustainable resource that could replace conventional energy sources. Renewable energy comes from natural sources that replace themselves more quickly. Renewable energy, often known as clean energy, is derived from renewable natural resources or processes. By supplying domestic clean energy sources, bioenergy can help to create a safe and sustainable environment. The production of bioenergy and biomass creates new, decentralized, and diverse income streams that support regional economic growth and employment [1].Compared with other renewable sources, the development of carbon-neutral and less polluting green fuels from renewable resources like biomass is getting interest more [2]. Biomass is medium energy biological matter obtained directly or indirectly from living or recently living organisms, most commonly plants [3]. Resources made of biomass are abundant in nature. The estimated annual production of biomass around the world is 100 billion tonnes [4]. Almost all the developed countries in the world have initiated the production of market goods from waste raw materials, which is necessary for the transition to a cleaner and sustainable economy. In this row, growing interest is being shown in waste-to-energy activities as a means of improving the sustainability [5].

The handling of waste items is referred to as waste management. It involves the gathering, moving, processing, and disposal of trash. Some important developed waste management systems reduce the strain on landfills by protecting natural resources. Compared with fossil fuels, biofuel production utilizing biomass offers substantial environmental benefits [6]. The emissions of carbon dioxide ($CO_2$) during the combustion of petro-diesel are polluting the environment severely. The technologies to reduce $CO_2$ emissions are limited. It is necessary for plants to grow in order to create biomass feedstock, and this removal of $CO_2$ from the environment offsets the increase in air pollution due to burning of biomass fuels [7]. Currently, various methods, including biological and thermochemical conversion methods, have been established to transform lignocellulosic feedstock into fuels or value-added chemicals. Biomass feedstock can quickly alter biological conversion, which typically takes more time. Thermochemical conversion is another technique to convert any type of biomass into fuels or chemicals without any constraints [8]. This method is the most convenient and does not require any preprocessing. In the olden days, charcoal was the main product produced by pyrolysis, which was used for heating applications. The primary drawback of this technology was poor energy yields. Therefore, research is being done to develop technology to give the highest output of energy from biomass. Pyrolysis of lignocellulosic material is a somewhat complicated process. Without the presence of air or oxygen, pyrolysis begins by thermally degrading the organic components. Pyrolysis is generally classified as conventional slow pyrolysis, fast pyrolysis, and flash pyrolysis. Slow pyrolysis is an old technique used for millennia for the production of char. Fast and flash pyrolysis is the advanced technology used for producing more liquid and gas products. Fast pyrolysis offers various appealing qualities, including more bio-oil production. It is simple and efficient, and no feedstocks can be lost during the process. In this process, the majority of the feedstock can be converted into a fuel product. The most suitable pyrolysis process temperature is around 350°C to 550°C, and it can sometimes extend up to 800°C. Due to its prolonged residence period and low heat transfer rates, slow pyrolysis requires additional energy inputs. The fast-pyrolysis process is gaining importance due to the yield of higher liquid fuels. These liquid fuels are easy to transport and store [9]. Fast pyrolysis is a more cost-effective and efficient process compared with the slow pyrolysis process. As pyrolysis technology continues to advance, many reactor designs have been investigated in an effort to improve pyrolysis efficiency and produce maximum bio-oil [10]. The pyrolysis experiments are generally performed by various reactors such as fixed bed, fluidized bed, circulating fluidized bed, vacuum reactor, ablative reactor, vortex reactor, and solar reactor. Fixed bed reactors are widely used for slow pyrolysis processes. Fluidized bed and circulating fluidized bed reactors are used for maximizing liquid products. In an ablative reactor, the feedstock needs not be crushed any more. So, a large particle can be processed with the help of an ablative reactor.

*Ricinus communis* is called the castor oil plant. The plant is native to India, which is grown in gardens and fields as well as in waste areas. In India, almost more than 50% of the tree is found in Gujarat followed by Andhra Pradesh and Rajasthan. The average production of seeds from the tree is 1.2 MT. This production is accounts for 75.6% of the world total production. It is a type of perennial flowering plant that belongs to the Euphorbiaceae family. It is a green plant that can reach a height of 10 m. *Ricinus communis* produces seeds, stems, and leaves used for various purposes. At one tonne of waste plant more than 450 kg of seeds, 350 kg of stems and 150 kg of leaves can be extracted [11]. The tree is widely spread over Eastern Africa and India. Previously, Kaur et al. [12] conducted hydrothermal liquefaction experiments on *Ricinus communis* for the conversion of biofuels and hydrocarbons. The study conducted experiments at different temperatures and produced 15.8 wt% of bio-oil at 300°C. The pressed seed cake obtained from this plant was pyrolyzed by Santos et al. [13]. In another study, the residues of *Ricinus communis* were examined for biofuels and chemicals extraction through a pyrolysis process [14]. According to the findings of the research, the residues from the plant can be used for various processes.

The characterization of the bio-oil acquired through the pyrolysis of *Ricinus communis* residues is the focus of the current research activity. Pyrolysis of residues from the tree was carried out in a fluidized bed reactor at different temperatures from 350°C to 750°C. The work is novel in terms of the selection of new materials for pyrolysis. To the knowledge of the authors, no work has been reported using

the selected feedstock. The experiments were carried out to analyze the impact of bed temperature on the yield of the pyrolysis products. The bio-oil acquired at maximum yield point was characterized using different analytical procedures such as FT-IR and GC-MS, and the physical characteristics were also found as per ASTM protocol. The main goal of this study was to analytically check the subtractions of the liquid products and find their suitability for industrial usage. The feed material used for the analysis represents the novelty of the work. Additionally, the bio-oil underwent testing in its raw, unpurified state to find its natural quality.

## 2. Materials and Methods

*2.1. Materials.* The residues of the *Ricinus communis* tree were obtained from the agricultural fields in and around Coimbatore, India. The residues are the combination of leaves, stems, and wood wastes. The sample was ground using a crusher and sieve shaker to get a uniform size of 0.5–0.7 mm. The powdered feedstock was also used for basic analysis. Prior to the experiments, the basic analysis on the sample was conducted to find its suitability for the thermochemical conversion process. The test results are shown in Table 1. These tests were conducted by following appropriate ASTM protocols. From the initial tests, it can be understood that the material has a higher percentage of volatiles. The higher volatiles in the material give confident for higher volatile release. The lower amount of ash in the material is another positive point for yielding high quality bio-oil. Due to lower ash content, the problems related to burning and corrosion can be minimized. The material has 46.3 wt% C, 5.12 wt% H, 4.01 wt% N, 0.08 wt% S, and 44.4 wt % O. The fixed carbon and oxygen in the sample were found by the difference. The lower amount of sulfur in the material means it is suitable for conversion without emitting hazardous pollutants. The increased amount of oxygen is a disadvantage in the production of high-energy bio-oils such as petroleum diesel.

*2.2. Characterization Methods.* The ultimate analysis of the samples was found by Elementar Vario EL-III (N2410650, PerkinElmer Ltd, US). The thermogravimetric analysis (TGA) of the samples to find the thermal behavior was found by the TGA701 analyzer (LECO Corporation, St. Joe, Michigan, US). TGA was performed to analyze the thermal stability of the feedstock. This analysis was performed in a closed furnace in a nitrogen environment. The material was heated from room temperature to 700°C until it was completely decomposed. The bio-oil produced after the pyrolysis reaction was characterized by the energy-dispersive X-ray analyzer (Model 6587 EDX). The standard redwood viscometer (Neminath Instruments, Ahmedabad, Gujarat), pH meter (Lutron pH meter, Sunshine Instruments, Coimbatore, India), and Pensky-Martens Flash Point apparatus (EIE Instruments, Ahmedabad, India) are used to find its physical properties. The heating value was found by the Parr reactor (model 6772). The functional group of the bio-oil was found by FT-IR and GC-MS analyzers. A FT-IR (BRUKER Optik GmbH, TENSOR 27 Bruker Corporation) spectrometer was used for the FT-IR study. The spectra were captured between 400 and 4000 $cm^{-1}$. The organic fraction was subjected to GC-MS studies (Thermo GC-TRACE Ultra ver: 5.0, Thermo MS DSQ II) using DB-35 with a HP-1 capillary column (30 m length, 0.25 mm diameter, and 0.25 $\mu$m film thickness). In a splitless mode, 0.3 mL of bio-oil was injected. For carrier gas, helium was employed and supplied at the rate of 1 mL/min. The temperature program for the analysis was as follows: heating from 60°C (holding period- 2 min) to 270°C (5°C/min and holding period-5 min).

Table 1: Characteristics of *Ricinus communis*.

| Parameters | Value (wt%) | Standard |
|---|---|---|
| Proximate analysis | | |
| Volatile matter | 75.3 | ASTM D3175 |
| Fixed carbon | 11.8 | By difference |
| Moisture content | 7.5 | ASTM D3173 |
| Ash | 5.4 | ASTM D3174 |
| Ultimate analysis (ash-free basis) | | |
| Carbon | 46.3 | ASTM D5373 |
| Hydrogen | 5.12 | ASTM D5373 |
| Nitrogen | 4.01 | ASTM D5373 |
| Oxygen | 44.4 | By difference |
| Sulfur | 0.08 | ASTM D5373 |

*2.3. Apparatus and Procedure.* A fluidized bed reactor of diameter 50 mm was employed in this study for pyrolysis experiments. The equipment consists of a system for feeding fuel samples. The required amount of quartz sand of 0.5 mm was used as a fluidization medium within the reactor. The material feeding system supplies the feedstock into the bed using a variable speed motor at 20 g/min. For fluidization, nitrogen gas was provided at 1.75 $m^3$/hr. The flow rate of the nitrogen was measured by rotameter and controlled by a control valve. The reactor is provided with five thermocouples located at five different positions. The cyclone separator was attached to separate solid particles. Initially, compressed air was used for the fluidization purpose until the material reached the desired temperature. The air and nitrogen were admitted through the distributor plate attached at the bottom of the reactor. Once the reactor reached the desired temperature, the flow of air was stopped and nitrogen was admitted. For better fluidization, 500 grams of sand of 0.5 mm in diameter was kept inside the reactor. The evolved gas coming out of the reactor is sent via the cold water condenser to cool. Due to the condensation process, the bio-oil was collected. The condensed bio-oil is then stored in a separate vessel for additional analysis. In this study, the yield at different temperature was analyzed by conducting pyrolysis experiments at different temperatures from 350°C to 750°C. The maximum yield condition was identified and set for additional bio-oil production. Each experimental run was conducted up to 45 min until complete volatilization. After conducting each experiment, the reactor and cyclone separator were cleaned. The produced bio-oil and char were physically weighed using an electronic balancing machine. Reaming material balance was used to determine the release of gaseous fraction at each run.

## 3. Results and Discussion

*3.1. Thermogravimetric Analysis.* TGA is an analytical technique used to evaluate the thermal stability and the percentage of volatile components in a material. This analysis was performed by observing the weight changes. The TGA/DTG analysis of *Ricinus communis* residue is shown in Figure 1. The heating of the material was done at the heating rate of 10 K/min. The results show thermal degradation behavior of the material occurred at three different zones, such as initial moisture removal, active zone, and passive zone. The evaporation of moisture and light volatiles occurred in the first stage of the pyrolysis experiment, which started at a temperature of 30°C and extended until it reached 120°C [15]. The initial moisture loss tends to the weight loss of the material up to 11.0 wt% [16]. The decomposition of the material initiated at 75°C and sustained up to 550°C with major weight loss. This is called major pyrolysis zone where the decomposition of hemicellulose and cellulose occurs with minor lignin decomposition [17]. During maximum devolatilization, maximum of condensable volatiles was released. Very minimal mass loss is seen in the third zone, primarily between 550°C and 700°C, which is likely owing to the decomposition of carbonaceous in the residues. The DTG curve made obvious the breakdown of biomass components at various temperatures. The breakdown of hemicellulose is represented by the first shoulder obtained at temperature, whereas the breakdown of cellulose in the material is represented by the next shoulder. The degradation of lignin occurs in the tailing portion, often referred to as passive pyrolysis, which operates between 160°C and 700°C. Char is formed as a byproduct of passive pyrolysis [18].

*3.2. Effect of Temperature on Product Yield.* Figure 2 displays the product yields produced by pyrolyzing *Ricinus communis* residue at different temperatures. The temperature of the bed has a considerable impact on the yields and its characteristics [19]. The product of interest from traditional slow pyrolysis is higher charcoal content, whereas the production of higher bio-oil is the interest from fast pyrolysis [20]. The yields of bio-oil products increased in general as the bed temperature increases. The production of bio-oil varies from 18.3 wt% to 46.5 wt%. The production of bio-oil has gone up to 46.5 wt% at 500°C. In this analysis, up to 250°C of bed temperature, there was no bio-oil obtained. A little drop of bio-oil was collected at 350°C. Temperatures below 400°C encourage the production of char products. Below 400°C, the heat transfer to the biomass is sluggish, related to the reaction kinetics [21]. Therefore, the yield of pyrolysis products is very close to the heat carrier capacity of the biomass. After 450°C, the heat transfer was enhanced to release more volatiles from the reactor. The higher temperature inside the bed breaks the heat transfer resistance and helps to achieve complete decomposition. From 350°C to 750°C, the yield of char is observed as a decreased pattern and gas in an increased pattern. But the bio-oil production is observed as increased decreased pattern. The lower heat to

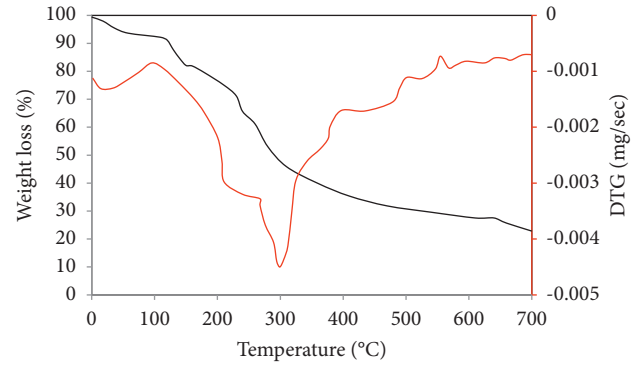


Figure 1: TGA and DTG analysis of *Ricinus communis* residue.

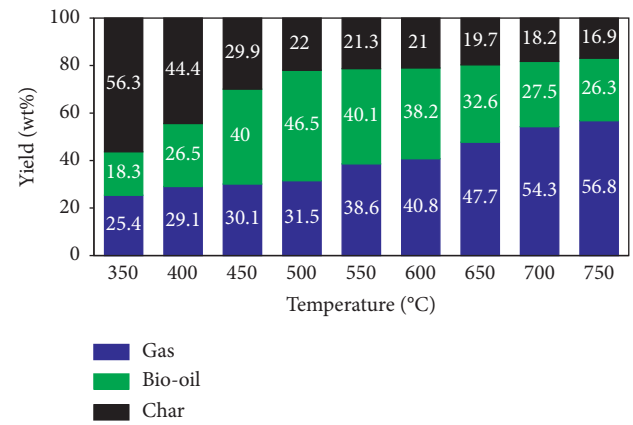


Figure 2: Effect of temperate on product distribution.

the material is favorable for the production of higher char. At 350°C, the char yield was 56.3 wt%, which is decreased to 16.9 at 750°C. After 500°C, there was no rapid decrease in char yield. However, after 500°C, the gas yield increased dramatically. The production of gas was increased by 80.3% at 750°C compared with 500°C. From this, it can be known that the higher temperature is favored for gas production rather than char and oil. The yield of gas at 350°C was 25.4 wt %, and it attained 56.8 wt% at 700°C. In this work, the maximum conversion of biomass into bio-oil ensued between 450°C and 550°C. In the previous literature, it is also reported that the effective pyrolysis temperatures were in the range of 470°C and 530°C [22, 23]. Table 2 shows pyrolysis of different feedstocks under different operating conditions and its outcome.

### 3.3. Bio-Oil Characterization

*3.3.1. Physical Analysis.* The physical characteristics of pyrolysis oil vary subjected to the method of pyrolysis and quality of the feed material, and this has been documented by various authors. The pyrolysis oils contain more oxygenated elements and are denser than fossil fuels. The physical properties of the bio-oil got at 500°C are enumerated in Table 3. The bio-oil is much denser compared with neat diesel. The density is identified as 980 $m^3$/kg. The heating value of the bio-oil is recorded as half that of fossil

Table 2: Pyrolysis under different operating conditions.

| Feedstock | Reactor tyre | Operating condition | Quantity of the bio-oil (wt%) | Heating value of the bio-oil (MJ/kg) | Reference |
|---|---|---|---|---|---|
| Fiber board | Fixed bed | Temperature 450°C, heating rate 20 °C/min | 41.9 | 17.14 | [24] |
| Albizia odoratissima | Fluidized bed | Temperature 450°C, sweep gas flow rate 1.75 $m^3$/hr | 18.15 | 23.47 | [25] |
| Wheat straw | Bubbling fluidized bed | Temperature 480°C | # | 22 | [26] |
| Oak wood | Auger reactor | Temperature 125°C to 175°C | 47 | # | [27] |
| Saw dust | Bubbling fluidized bed | Temperature 500°C, sweep gas flow rate 1.8 $m^3$/hr | 57.8 | # | [28] |
| Garlic stem | Packed tube | Temperature 500°C | 39.6 | 7.5 | [29] |
| Pepper stem | Packed tube | Temperature 480°C | 45.8 | 5.01 | [29] |
| Douglas fir sawdust | Microwave | Temperature 480°C | 40.25 | 17 | [30] |
| Mallee wood | Fluidized bed | Temperature 300°C to 600°C, particle size 100 to 600 $\mu$m | 12 | 22 | [31] |
| Corn stover | Fluidized bed | Temperature 400°C, residence time 1 s | 60 | 22.1 | [32] |
| Lemon grass | Fluidized bed | Temperature 450°C, particle size 1 mm, sweep gas flow rate 1.75 $m^3$/hr | 50.6 | 19.4 | [33] |
| Pressmud | Fixed bed | Temperature 300°C to 600°C | 65 | 34.5 | [34] |
| Hardwood | Vacuum | Temperature 450°C, Particle size 10 mm | 16.8 | 16 | [35] |
| Rice husk | Fixed bed | Temperature 400°C to 800°C, particle size 0.5 mm, sweep gas flow rate 500 to 1500 $cm^3$/min | # | 7.6 | [36] |
| Ficus religiosa wood bark | Fluidized bed | Temperature 450°C, particle size 1.0 mm, sweep gas flow rate 2 $m^3$/hr | 47.5 | 18.3 | [37] |
| Sunflower shell | Fixed bed | Temperature of 450°C, particle size 1.0 mm | 46.4 | # | [38] |
| Tea wastes | Fluidized bed | Temperature 400°C, particle size 1.0 mm, sweep flow rate 1.75 $m^3$/hr. | 46.3 | 21.34 | [39] |
| Soybean cake | Circulating fluidized bed | Temperature 550°C, heating rate 5 °C/min, sweep gas flow rate 50 to 400 $cm^3$/min | — | 21.4 | [40] |
| Neem wood bark | Fluidized bed | Temperature 450°C, particle size 1.0 mm | 49.5 | 22.7 | [41] |
| Napier grass | Fixed bed | Temperature 300°C to 600°C | 74 | 40.1 | [42] |

#Not reported.

Table 3: Physical characterization of the bio-oil.

| | Density (kg/$m^3$) | Viscosity (cSt) | Flash point (°C) | pH | Heating value (MJ/kg) |
|---|---|---|---|---|---|
| Bio-oil [this study] | 980 | 7.8 | 135 | 4.2 | 23.12 |
| Palmyra bunch [43] | 1010 | 8.6 | 160 | 3.9 | 14.5 |
| Waste paper [44] | 1205 | 20 | 200 | 1.5 | 13.10 |
| Hard wood [45] | 1220 | 13 | 66 | $ | 17.5 |
| *Albizia amara* [46] | 1050 | 4.2 | 160 | 3.6 | 18.6 |
| Diesel [47] | 850 | 3.9 | 57 | - | 43.60 |
| Standard | ASTM D4052 | ASTM D445 | ASTM D92 | ASTM D92 | ASTM D240 |

$Not reported.

diesel due to higher oxygen content [48]. The heating value of the bio-oil was recorded with the help of Parr-7662 calorimetric thermometer. The pH value of was found as 4.2. Acidic chemicals are thought to be the cause of the low pH. The physical properties of the bio-oil obtained in this study were compared with other selected pyrolysis bio-oils. Compared with other bio-oils, the bio-oil obtained from *Ricinus communis* has a lower density. The lower density aid allows the fuel sprayer to flow freely. Compared with other pyrolysis oils, the bio-oil has more energy content and it is accepted to be enough for agricultural feedstock [47].

*3.3.2. FT-IR Analysis.* The existence of distinct functional groups is identified by FT-IR analysis, which is utilized to investigate the basic vibrations and related vibrational transitions [49]. In this study, major functional absorption bands were identified in the FT-IR spectrum (Figure 3). The broad band O-H stretching vibration at 2881.4 $cm^{-1}$ represents the existence of carboxylic acids. The C≡C stretch vibrations at 2140.2 $cm^{-1}$ represent the occurrence of alkynes. A broad N-O stretching appeared at 1535.8 $cm^{-1}$, showing the occurrence of nitro compounds. C-O groups can be identified at 1115.6 $cm^{-1}$. The peak detected at

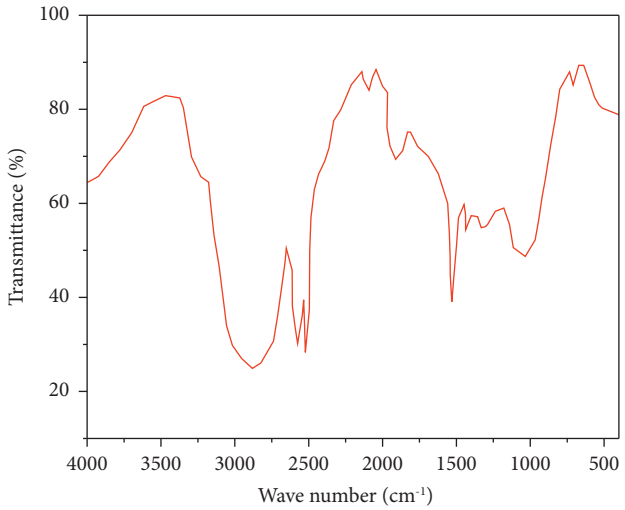


Figure 3: FT-IR analysis of *Ricinus communis* bio-oil.

Table 4: GC-MS analysis of *Ricinus communis* bio-oil.

| Compound name | Retention time/min | Molecular name | Molecular weight | % area |
|---|---|---|---|---|
| 2,5-Piperazinedione, 3-benzyl-6-isopropyl- | 8.31 | $C_{14}H_{18}N_2O_2$ | 246.30 | 3.31 |
| Phenol, 4-ethyl- | 8.53 | $C_8H_{10}O$ | 122.16 | 4.01 |
| Phenol | 9.01 | $C_6H_6O$ | 94.11 | 12.75 |
| Phenol, 4-amino- | 10.11 | $C_6H_7NO$ | 109.12 | 3.75 |
| 3,4-Dimethylthiophene | 11.93 | $C_6H_8S$ | 112.19 | 0.94 |
| p-Cresol | 12.42 | $C_7H_8O$ | 108.13 | 4.71 |
| Di-(2-ethylhexyl) phthalate | 13.11 | $C_{24}H_{38}O_4$ | 390.60 | 1.27 |
| Phenol, 2-methoxy | 14.44 | $C_7H_8O_2$ | 124.13 | 2.39 |
| 2-Methyl-5-(1-butyn-1-yl) pyridine | 15.01 | $C_{10}H_{11}N$ | 145.20 | 1.80 |
| Hydroquinone | 15.20 | $C_6H_6O_2$ | 110.11 | 9.34 |
| Benzene, 1,3,5-trimethoxy- | 15.57 | $C_9H_{12}O_3$ | 168.19 | 3.91 |
| 3-Pyridinol | 18.90 | $C_5H_5NO$ | 95.09 | 4.20 |
| Phenylethyl alcohol | 19.11 | $C_8H_{10}O$ | 122.16 | 1.22 |
| d-Mannose | 20.20 | $C_6H_{12}O_6$ | 180.15 | 3.93 |
| 2,2′-Dioxospirilloxanthin | 21.57 | $C_{42}H_{56}O_4$ | 624.90 | 1.87 |
| 2(1H)-Pyridinethione, 3-hydroxy- | 22.41 | $C_5H_5NOS$ | 127.16 | 0.88 |
| 2-Cyclopenten-1-one, 2,3-dimethyl- | 23.50 | $C_7H_{10}O$ | 122.16 | 1.72 |
| 1-Methyl-1,3,3-triphenylindan-2-one | 23.59 | $C_{28}H_{22}O$ | 374.10 | 2.28 |
| Kaempferol | 23.85 | $C_{15}H_{10}O_6$ | 286.23 | 1.32 |
| 2-Propenenitrile, 3-phenyl-, (E)- | 24.08 | $C_9H_7N$ | 129.15 | 0.74 |
| 2-Isopropyl-2,5-dihydrofuran | 24.51 | $C_7H_{12}O$ | 112.02 | 2.08 |
| 2-Acetylfuran | 28.63 | $C_6H_6O_2$ | 110.11 | 2.40 |
| Phenol, 2,6-dimethyl | 24.87 | $C_8H_{10}O$ | 122.16 | 3.30 |
| Butanoic acid | 25.18 | $C_4H_8O_2$ | 88.11 | 0.83 |
| N-Methyldodecanamide | 26.71 | $C_{13}H_{27}NO$ | 213.36 | 3.47 |
| 4,5-Dimethoxy-2-(2-propenyl)phenol | 27.24 | $C_{11}H_{14}O_3$ | 194.23 | 2.26 |
| 1,2-Benzenediol | 29.36 | $C_6H_6O_2$ | 110.11 | 3.12 |
| N-Benzylpiperidone | 30.04 | $C_{12}H_{15}NO$ | 189.02 | 1.08 |
| Squalene | 30.75 | $C_{30}H_{50}$ | 410.71 | 0.33 |
| Benzhydryl vinyl ether | 31.08 | $C_{15}H_{14}O$ | 210.21 | 2.31 |
| (E)-1,2-Dibromo-1-nonene | 32.34 | $C_9H_{16}Br_2$ | 282.34 | 1.94 |
| 1H-Indole, 4-methyl- | 34.55 | $C_9H_9N$ | 131.17 | 0.84 |
| $\gamma$-Sitosterol | 35.61 | $C_{29}H_{50}O$ | 414.70 | 6.70 |
| Asarone | 37.30 | $C_{12}H_{16}O_3$ | 208.25 | 0.95 |
| Cyclopentanol | 38.18 | $C_5H_{10}O$ | 86.13 | 2.02 |

733.6 $cm^{-1}$ signifies the C-H stretch that displays the presence of aromatics.

*3.3.3. GC-MS Analysis.* GC is a versatile technique used by most of the authors for the detection of thermally stable chemicals with suitable volatility. Quantification by GC has a number of advantages and is regarded as being extremely precise. Several researchers have reported using GC-MS to find various chemical components in liquid and gaseous products. Table 4 shows the analysis of GC-MS of the bio-oil. From this analysis, it can be known that phenols and their derivatives occupied the majority of the portions in the bio-oil. Phenol was identified as a single element with a total area percentage of 12.75. Next to phenol, hydroquinone is identified with a total area percentage of 9.34. The total area percentage of phenols is 28.46. The majority of the chemicals identified in bio-oil are used for numerous engineering and chemical industries. Phenol is also called carbolic acid. It is an important chemical used in many engineering industries. Phenols are frequently utilized in everyday goods and as synthesis intermediates in industry. It is a good ingredient for the production of polymers, explosives like picric acid and medications like aspirin. The component of photographic developer known as common phenol hydroquinone turns exposed silver bromide crystals into black metallic silver. They are also used as a feedstock for cosmetic industries for manufacturing sunscreens, skin creams, and hair coloring agents. They were originally extracted from coal tar, but now they are produced in huge quantities from feedstocks supplied by petroleum. Due to its role as a precursor to numerous minerals and beneficial chemicals, it is a crucial industrial commodity [50]. Production of polycarbonates, bakelite, nylon, and a variety of pharmaceutical industries requires phenol and its chemical derivatives. Hydroquinone is an aromatic organic compound. It is also a type of phenol. It can be used as a reducing agent as well as in the photographic industry. The oxidation of different phenols can also be used to create hydroquinone and its derivatives. Apart from that, many of the chemicals identified in GC are combustible and identified as good hydrocarbon elements. Another chemical substance found in bio-oil is gamma sitosterol. *Achillea santolina*, *Clerodendrum infortunatum*, and other plants contain the natural gamma sitosterol.

*3.3.4. EDX Analysis.* The elements of *Ricinus communis* pyrolysis bio-oil are presented in Table 5. The outcome of this investigation made it very evident that, when compared to other elements, carbon is identified as a major one with 43.63 wt%. The presence of oxygen is almost equal to carbon with 41.37 wt%. The higher percentage of oxygen on the other side improves its combustibility during combustion. But the higher oxygen has a negative impact on its shelf life, while it is being stored. The presence of the least amount of sulfur in the bio-oil can reduce the production of sulfur oxides while burning at higher temperatures. Due to contamination in the residues, the formed pyrolysis oil comprises a minuscule quantity of chlorine. The risk of corrosion during storage of the bio-oil can be decreased by the absence of salts. The bio-antibacterial properties and shelf life are improved by the existence of boron in the bio-oil.

Table 5: EDX analysis of bio-oil.

| Element | wt% |
|---|---|
| Aluminum | 1.01 |
| Antimony | 0.74 |
| Boron | 1.11 |
| Carbon | 43.63 |
| Chlorine | 0.08 |
| Hydrogen | 10.22 |
| Iron | 0.18 |
| Magnesium | 0.10 |
| Molybdenum | 0.37 |
| Oxygen | 41.37 |
| Potassium | 0.40 |
| Silicon | 0.77 |
| Sulfur | 0.05 |

## 4. Conclusion

Pyrolysis has been shown to be a hopeful method for valuing waste biomass as a source of renewable energy. Fast pyrolysis of *Ricinus communis* residues was conducted in a fluidized bed by changing bed temperature from 350°C to 750°C. The preliminary analysis of the feedstock revealed a greater amount of volatile materials for maximum bio-oil yield. A large quantity of bio-oil production of 46.5 wt% was acquired at 500°C. A maximum conversion of biomass into bio-oil ensued between 450°C and 550°C. The analytical study of the bio-oil showed the presence of phenolic components, oxygenated chemicals, acids, and esters. The heating value of the bio-oil is recorded as half that of fossil fuel. The bio-oil produced in this study has more energy content, and it is accepted to be enough for agricultural feedstock. The chemical components identified through GC-MS are used in various engineering and chemical industries as precursors, favoring agents, and reducing agents. In summary, by being aware of the pyrolysis mechanisms, the choice of an appropriate pyrolysis method and feedstock can maximize the production of the required biofuel.

## Abbreviations

ASTM: American Society for Testing and Materials
$CO_2$: Carbon dioxide
cSt: Centistokes
DTG: Differential thermogravimetry
EDX: Energy-dispersive X-ray analysis
FT-IR: Fourier transform infrared spectroscopy
GC-MS: Gas chromatography and mass spectroscopy
TGA: Thermogravimetric analysis.

## Data Availability

The data used to support the findings of this study are included within the article.

## Conflicts of Interest

The authors declare that there are no conflicts of interest regarding the publication of this article.

## References


[1] A. Ramesh, B. M. Ali, R. Manigandan, C. T. Da, and M. T. Nguyen-Le, "Hydrogenolysis of glycerol to 1, 2-propanediol on MgO/Ni3C catalysts fabricated by a solid-state thermal synthesis," *Molecular Catalysis*, vol. 525, 2022.

[2] S. Wang, G. Dai, H. Yang, and Z. Luo, "Lignocellulosic biomass pyrolysis mechanism: a state-of-the-art review," *Progress in Energy and Combustion Science*, vol. 62, pp. 33–86, 2017.

[3] H. Long, X. Li, H. Wang, and J. Jia, "Biomass resources and their bioenergy potential estimation: a review," *Renewable and Sustainable Energy Reviews*, vol. 26, pp. 344–352, 2013.

[4] R. A. Sheldon, "Green and sustainable manufacture of chemicals from biomass: state of the art," *Green Chem.*vol. 16, no. 3, pp. 950–963, 2014.

[5] C. S. Dhanalakshmi, M. Mathew, and P. Madhu, "Biomass material selection for sustainable environment by the application of multi-objective optimization on the basis of ratio analysis (MOORA)," in *Materials, Design, and Manufacturing for Sustainable Environment*, pp. 345–354, Springer, Singapore, 2021.

[6] A. Patel, B. Agrawal, and B. R. Rawal, "Pyrolysis of biomass for efficient extraction of biofuel," *Energy Sources, Part A: Recovery, Utilization, and Environmental Effects*, vol. 42, no. 13, pp. 1649–1661, 2020.

[7] D. Mohan, C. U. Pittman, and P. H. Steele, "Pyrolysis of wood/biomass for bio-oil: a critical review," *Energy and Fuels*, vol. 20, no. 3, pp. 848–889, 2006.

[8] W. H. Beattie, R. Berjoan, and J. P. Coutures, "High-temperature solar pyrolysis of coal," *Solar Energy*, vol. 31, no. 2, pp. 137–143, 1983.

[9] J. G. Brammer, M. Lauer, and A. V. Bridgwater, "Opportunities for biomass-derived "bio-oil" in European heat and power markets," *Energy Policy*, vol. 34, no. 17, pp. 2871–2880, 2006.

[10] M. I. Jahirul, M. G. Rasul, A. A. Chowdhury, and N. Ashwath, "Biofuels production through biomass pyrolysis—a technological review," *Energies*, vol. 5, no. 12, pp. 4952–5001, 2012.

[11] H. Bateni and K. Karimi, "Biodiesel production from castor plant integrating ethanol production via a biorefinery approach," *Chemical Engineering Research and Design*, vol. 107, pp. 4–12, 2016.

[12] R. Kaur, P. Gera, M. K. Jha, and T. Bhaskar, "Reaction parameters effect on hydrothermal liquefaction of castor (RicinusCommunis) residue for energy and valuable hydrocarbons recovery," *Renewable Energy*, vol. 141, pp. 1026–1041, 2019.

[13] N. A. V. Santos, Z. M. Magriotis, A. A. Saczk, G. T. A. Fássio, and S. S. Vieira, "Kinetic study of pyrolysis of castor beans (Ricinuscommunis L.) presscake: an alternative use for solid waste arising from the biodiesel production," *Energy and Fuels*, vol. 29, no. 4, pp. 2351–2357, 2015.

[14] R. Kaur and T. Bhaskar, "Potential of castor plant (Ricinuscommunis) for production of biofuels, chemicals, and value-added products," in *Waste Biorefinery*, pp. 269–310, Elsevier, Amsterdam, Netherlands, 2020.

[15] A. Ramesh, C. T. Da, R. Manigandan, P. B. Bhargav, and M. T. Nguyen-Le, "Selectivity oxidation of benzyl alcohol using mesoporous g-C3N4 catalysts prepared by hard template method," *Colloid and Interface Science Communications*, vol. 48, 2022.

[16] V. Dhyani, M. Kumar Awasthi, Q. Wang et al., "Effect of composting on the thermal decomposition behavior and kinetic parameters of pig manure-derived solid waste," *Bioresource Technology*, vol. 252, pp. 59–65, 2018.

[17] Z. Chen, M. Hu, X. Zhu et al., "Characteristics and kinetic study on pyrolysis of five lignocellulosic biomass via thermogravimetric analysis," *Bioresource Technology*, vol. 192, pp. 441–450, 2015.

[18] D. S. Scott, J. Piskorz, M. A. Bergougnou, R. Graham, and R. P. Overend, "The role of temperature in the fast pyrolysis of cellulose and wood," *Industrial and Engineering Chemistry Research*, vol. 27, no. 1, pp. 8–15, 1988.

[19] C. Vibhakar, R. S. Sabeenian, S. Kaliappan et al., "Production and optimization of energy rich biofuel through co-pyrolysis by utilizing mixed agricultural residues and mixed waste plastics," *Advances in Materials Science and Engineering*, vol. 2022, Article ID 8175552, 9 pages, 2022.

[20] B. M. Lakshmi, M. Mathew, A. M. J. Kinol et al., "An integrated CRITIC-TOPSIS-and Entropy-TOPSIS-based informative weighting and ranking approach for evaluating green energy sources and its experimental analysis on pyrolysis," *Environmental Science and Pollution Research International*, pp. 1–13, 2022.

[21] S. R. G. Oudenhoven, C. Lievens, R. J. M. Westerhof, and S. R. Kersten, "Effect of temperature on the fast pyrolysis of organic-acid leached pinewood; the potential of low temperature pyrolysis," *Biomass and Bioenergy*, vol. 89, pp. 78–90, 2016.

[22] V. Kothari and M. J. Antal, "Numerical studies of the flash pyrolysis of cellulose," *Fuel*, vol. 64, no. 11, pp. 1487–1494, 1985.

[23] J. Piskorz, P. Majerski, D. Radlein, A. Vladars-Usas, and D. S. Scott, "Flash pyrolysis of cellulose for production of anhydro-oligomers," *Journal of Analytical and Applied Pyrolysis*, vol. 56, no. 2, pp. 145–166, 2000.

[24] S. Thirugnanam, R. Srinivasan, K. Anand et al., "Utilisation possibilities of waste medium-density fiberboard: a material recycling process," *Materials Today: Proceedings*, vol. 59, pp. 1362–1366, 2022.

[25] C. Sowmya Dhanalakshmi, S. Kaliappan, H. Mohammed Ali, S. Sekar, and S. Socrates, "Habtewolde ababu birhanu, flash pyrolysis experiment on albizia odoratissima biomass under different operating conditions: a comparative study on bio-oil, biochar, and noncondensable gas products," *Journal of Chemistry*, vol. 2022, Article ID 9084029, 9 pages, 2022.

[26] C. E. Greenhalf, D. J. Nowakowski, A. B. Harms, J. O. Titiloye, and A. V. Bridgwater, "A comparative study of straw, perennial grasses and hardwoods in terms of fast pyrolysis products," *Fuel*, vol. 108, pp. 216–230, 2013.

[27] T. P. Vispute and G. W. Huber, "Production of hydrogen, alkanes and polyols by aqueous phase processing of wood-derived pyrolysis oils," *Green Chemistry*, vol. 11, no. 9, pp. 1433–1445, 2009.

[28] H. S. Choi, Y. S. Choi, and H. C. Park, "Fast pyrolysis characteristics of lignocellulosic biomass with varying reaction conditions," *Renewable Energy*, vol. 42, pp. 131–135, 2012.

[29] Y. K. Park, M. L. Yoo, H. W. Lee et al., "Effects of operation conditions on pyrolysis characteristics of agricultural residues," *Renewable Energy*, vol. 42, pp. 125–130, 2012.

[30] S. Ren, H. Lei, L. Wang et al., "The effects of torrefaction on compositions of bio-oil and syngas from biomass pyrolysis by

microwave heating," *Bioresource Technology*, vol. 135, pp. 659–664, 2013.

[31] M. Garcia-Perez, X. S. Wang, J. Shen et al., "Fast pyrolysis of oil mallee woody biomass: effect of temperature on the yield and quality of pyrolysis products," *Industrial and Engineering Chemistry Research*, vol. 47, no. 6, pp. 1846–1854, 2008.

[32] C. A. Mullen, A. A. Boateng, N. M. Goldberg, I. M. Lima, D. A. Laird, and K. B. Hicks, "Bio-oil and bio-char production from corn cobs and stover by fast pyrolysis," *Biomass and Bioenergy*, vol. 34, no. 1, pp. 67–74, 2010.

[33] P. Madhu, T. S. Livingston, and H. Kanagasabapathy, "Flash pyrolysis of lemon grass (Cymbopogonflexuosus) for bio-oil production in an electrically heated fluidized bed reactor," *Waste and Biomass Valorization*, vol. 9, no. 6, pp. 1037–1046, 2018.

[34] K. B. Ansari and V. G. Gaikar, "Pressmud as an alternate resource for hydrocarbons and chemicals by thermal pyrolysis," *Industrial and Engineering Chemistry Research*, vol. 53, no. 5, pp. 1878–1889, 2014.

[35] J. V. Ortega, A. M. Renehan, M. W. Liberatore, and A. M. Herring, "Physical and chemical characteristics of aging pyrolysis oils produced from hardwood and softwood feedstocks," *Journal of Analytical and Applied Pyrolysis*, vol. 91, no. 1, pp. 190–198, 2011.

[36] W. T. Tsai, M. K. Lee, and Y. M. Chang, "Fast pyrolysis of rice husk: product yields and compositions," *Bioresource Technology*, vol. 98, no. 1, pp. 22–28, 2007.

[37] Y. K. S. S. Rao, C. S. Dhanalakshmi, D. K. Vairavel et al., "Investigation on forestry wood wastes: pyrolysis and thermal characteristics of Ficusreligiosa for energy recovery system," *Advances in Materials Science and Engineering*, vol. 2022, Article ID 3314606, 9 pages, 2022.

[38] A. N. Arularasan, M. Mathew, M. Sudhakar et al., "A holistic framework for environment conscious based material selection and experimental assessment using digraph-based expert system," *Scientific Programming*, vol. 2022, Article ID 2112683, 10 pages, 2022.

[39] I. Kathir, K. Haribabu, A. Kumar et al., "Utilization of tea industrial waste for low-grade energy recovery: optimization of liquid oil production and its characterization," *Advances in Materials Science and Engineering*, vol. 20229 pages, Article ID 7852046, 2022.

[40] A. E. Pütün, E. Apaydin, and E. Pütün, "Bio-oil production from pyrolysis and steam pyrolysis of soybean-cake: product yields and composition," *Energy*, vol. 27, no. 7, pp. 703–713, 2002.

[41] C. S. Dhanalakshmi and P. Madhu, "Recycling of wood bark of Azadirachtaindica for bio-oil and chemicals by flash pyrolysis," *Indian Journal of Ecology*, vol. 46, no. 2, pp. 347–353, 2019.

[42] K. B. Ansari and V. G. Gaikar, "Investigating production of hydrocarbon rich bio-oil from grassy biomass using vacuum pyrolysis coupled with online deoxygenation of volatile products over metallic iron," *Renewable Energy*, vol. 130, pp. 305–318, 2019.

[43] P. Madhu, H. Kanagasabapathy, and I. N. Manickam, "Flash pyrolysis of palmyra palm (Borassus flabellifer) using an electrically heated fluidized bed reactor," *Energy Sources, Part A: Recovery, Utilization, and Environmental Effects*, vol. 38, no. 12, pp. 1699–1705, 2016.

[44] M. Nurul Islam, M. Nurul Islam, M. Rafiqul Alam Beg, and M. Rofiqul Islam, "Pyrolytic oil from fixed bed pyrolysis of municipal solid waste and its characterization," *Renewable Energy*, vol. 30, no. 3, pp. 413–420, 2005.

[45] Y. Solantausta, N. O. Nylund, M. Westerholm, T. Koljonen, and A. Oasmaa, "Wood-pyrolysis oil as fuel in a diesel-power plant," *Bioresource Technology*, vol. 46, no. 1-2, pp. 177–188, 1993.

[46] C. Sowmya Dhanalakshmi and P. Madhu, "Utilization possibilities of Albiziaamara as a source of biomass energy for bio-oil in pyrolysis process," *Energy Sources, Part A: Recovery, Utilization, and Environmental Effects*, vol. 41, no. 15, pp. 1908–1919, 2019.

[47] D. Raguraman, A. Kumar, S. Prasanna Raj Yadav et al., "Performance and emission characteristics of pyrolysis oil obtained from neem de Oiled cake and waste polystyrene in a compression ignition engine," *Advances in Materials Science and Engineering*, vol. 202110 pages, Article ID 3728852, 2021.

[48] S. Czernik and A. V. Bridgwater, "Overview of applications of biomass fast pyrolysis oil," *Energy & Fuels*, vol. 18, no. 2, pp. 590–598, 2004.

[49] A. Ramesh, R. Manigandan, B. M. Ali, K. Dhandapani, C. T. Da, and M. T. Nguyen-Le, "Selective oxidation of benzyl alcohol over sulphated zirconia incorporated ordered mesoporous carbon by a hard template method," *Journal of Alloys and Compounds*, vol. 918, 2022.

[50] M. Weber, M. Weber, and M. Kleine-Boymann, "Ullmann's encyclopedia of industrial chemistry," 2000, https://onlinelibrary.wiley.com/doi/book/10.1002/14356007.

Hindawi
Journal of Chemistry
Volume 2022, Article ID 2215883, 9 pages
https://doi.org/10.1155/2022/2215883

*Research Article*

# Valorization of Hazardous Materials along with Biomass for Green Energy Generation and Environmental Sustainability through Pyrolysis

**Sarika Chhabria,[1] A. V. Raghavendra Rao,[2] V. Naga Lakshmi,[3] Pravin P. Patil,[4] Harishchander Anandaram,[5] Sumanta Bhattacharya,[6] D. Francisca Kalavathi,[7] A. Dhivya,[8] and Solomon Neway Jida[9]**

[1]*Department of Chemistry, Smt. Chandibai Himathmal Mansukhani College, Kalyan, Thane, Maharashtra 421003, India*
[2]*Department of Chemical Engineering, B V Raju Institute of Technology, Narsapur, Medak, Telangana 502313, India*
[3]*Department of Chemistry, Ch.S.D. St Theresa's College for Women (A), Eluru, Andhra Pradesh 530003, India*
[4]*Department of Mechanical Engineering, Graphic Era Deemed to be University, Bell Road, Clement Town Dehradun, Uttarakhand 248002, India*
[5]*Centre for Excellence in Computational Engineering and Networking, Amrita Vishwa Vidyapeetham, Coimbatore, Tamil Nadu 641112, India*
[6]*Research Scholar, Department of Textile Technology, Maulana Abul Kalam Azad University of Technology, Kolkata, West Bengal 700064, India*
[7]*PG Department of Environmental Science, Holy Cross College, Tiruchirappalli, Tamil Nadu 620002, India*
[8]*Department of Biotechnology, PSGR Krishnammal College for Women, Coimbatore, Tamil Nadu 641004, India*
[9]*Faculty of Mechanical Engineering, Arba Minch Institute of Technology, Arba Minch University, P.O. Box 21, Arba Minch, Ethiopia*

Correspondence should be addressed to Solomon Neway Jida; solomon.neway@amu.edu.et

Received 16 June 2022; Revised 26 July 2022; Accepted 1 August 2022; Published 25 August 2022

Academic Editor: Balasubramani Ravindran



Increased population growth, industrialization, and modern culture create a variety of consequences, including environmental pollution, heavy metal accumulation, and decreasing energy resources. This perilous position necessitates the development of long-term energy resources and strategies to address environmental threats and power shortages. In this study, an investigation into the use of castor seed oil cake and waste tyres as a feed material for the copyrolysis process for yielding maximum oil production was performed. The copyrolysis experiments were performed by changing the mass percentage of waste tyres with oil cake to make different ratios of 100 : 0, 75 : 25, 50 : 50, 25 : 75, and 0 : 100. At 50 : 50 ratio, the maximum positive synergy on oil production was obtained. At that condition, a maximum of 59.8 wt% oil was produced and characterized to analyze its physiochemical properties. The coprocessing of the selected two feed materials enables the stabilization of the oil, as the produced oil has a lower oxygen content with a maximum heating value of 38.72 MJ/kg. The Fourier transform infrared spectroscopy (FTIR) and gas chromatography-mass spectrometry (GC-MS) analysis of the oil showed the existence of aromatic hydrocarbons and phenolic elements. Adding waste tyres to the biomass improved the quality of the oil by increasing carbon content with reduced oxygen content.

## 1. Introduction

Biofuels and biochemicals made from renewable resources are a crucial driver for sustainable societies. The use of waste material valorization has been growing fast for the past three decades due to increased global warming, the negative environmental impact of fossil fuel consumption, energy demand, and the availability of waste materials [1]. In this background, it is essential to analyze how to develop current energy recovery processes with minimum environmental effect.

Energy is the essential one for the growth of industries and global economy. It supports the operation of industries and transportation for the development of the nation. The depletion of fossil fuel resources, the growing population, and environmental concerns have all prompted research into alternative fuels [2]. The consumption of biofuel is increasing steadily from 2% to 27% by 2050. Biomass is cheap and abundant. It is a renewable and cost-effective resource that emits very little $CO_2$ into the environment. Generally, it is a clean alternative source. The $CO_2$ generated by burning biomass can be captured during the photosynthesis process. Hence, the sustainability of the world can be achieved by minimizing global warming [3]. Biomass conversion can be accomplished using a variety of processes, which are broadly classified as thermochemical and biochemical conversion [4]. Pyrolysis of biomass provides a viable option for producing energy-rich medium-to-high grade liquid fuels. Pyrolysis has received a lot of attention due to its higher efficiency [5]. Pyrolysis oil is a key product of the pyrolysis process [6]. Despite its potential as a renewable energy source, bio-oil confronts a number of technical challenges, such as higher acidity, higher viscosity, higher water content, higher corrosive nature, and lower calorific value [7]. Due to these unfavourable properties, the bio-oil is unstable during storage [8].

Castor seed oil cake is considered as a solid biomass left over from the process of extraction of castor oil in a huge amount. India is a major producer of castor oil. 96% of India's total castor seed production comes from Gujarat, Rajasthan, and Andhra Pradesh. It is the most useful vegetable oil, having almost 90% ricinoleic acid [9, 10]. Castor seed oil cake is generally unsuitable for animal feed since it has some toxic chemicals and allergens [11]. Despite the fact that numerous ways have been identified to recycle these cakes [12], their usage as fertilizer is still restricted. In this context, pyrolysis of these wastes for bio-oil production has been identified as a promising method due to its high global output. Previously, a lot of literature focused on the usage of various pressed oil cakes obtained from sunflower [13], rapeseed [14], safflower [15], soybean [16], mustard [17], and neem [18] for bio-oil production. Gercel [13] conducted pyrolysis experiments on sunflower oil cake. The author investigated the impact of sweep flow rate and reaction temperature on the yield. In this study, a maximum of 48.69 wt% bio-oil was obtained at 550°C, 100 $cm^3$/min sweep gas flow rate, and 5°C/s heating rate. David and Kopač [19] produced bio-oil from rapeseed cake through a catalytic pyrolysis process. The produced oil has higher fractions of aromatic and phenolic elements. The catalytic pyrolysis produced bio-oil with lower oxygen content. Previously, castor seed oil cake has been used by various authors for producing oil [20], char [21], chemicals [22], and functional materials [23]. Recently, Silva et al. [24] derived biochar from castor seed oil cake to be used as an absorber material for the treatment of waste water. The study also recommended the derived bio-oil to use as a fuel of the production of power [25].

Waste tyres on the other hand have become a major issue for the clean environment. The accumulation of waste tyres has been accumulating every year for the past two decades due to the dynamic growth of the automotive industries. Each year, around 1.5 billion tyres are produced, which ultimately end up in the trash. The waste volume is increasing at a rate of 12% per annum. In India, it is believed that 60% of waste tyres are disposed of through illegal dumping. The growing number of discarded tyres is posing a major hazard to the atmosphere. Waste tyres that have been illegally discarded or stacked pose a risk of uncontrolled combustion [26]. Pyrolysis of waste tyres is an effective method for sustainable development. Recycling waste tyres through pyrolysis is familiar and widely discussed by various authors [27–29]. Czajczyńska et al. [30] pyrolyzed waste tyres at different temperatures of 400, 500, and 600°C. The study produced pyrolysis oil with a low heavy metal level and recommended to use these oils for safe environment. Yazdani et al. [31] found the impact of temperatures on tyre pyrolysis. At 550°C, the higher liquid oil yield of 55 wt% was reached. Abdallah et al. [32] used an industrial-scale system to pyrolyze waste tyres, reporting maximum production of liquid oil of 45 wt%. Martnez [33] conducted waste tyre pyrolysis experiments on a twin-auger reactor to examine the process variables on yields. During this study, 45 wt% of liquid oil was acquired at 475°C under the feedstock flow rate of 1.16 kg/hr and sweep gas flow rate of 300 mL/min. The study discovered that temperature, rather than feeding rate, swept gas flow rate, and residence time, is the significant factor in determining the maximum yield of liquid oil. In a conical spouted reactor, truck tyres were pyrolyzed by Lopez et al. [34]. The authors found that 475°C was the ideal temperature for complete decomposition of tyres to produce higher liquid oil. Williams [35] studied the liquid, char, and gas qualities produced through the pyrolysis of used tyres. The study focused on reaction conditions, product distribution, and its characterization. The study also suggested that it is important to emphasize the pyrolysis behavior, reaction kinetics, and mechanism to gain maximum material conversion.

Apart from individual pyrolysis, copyrolysis of lignocellulosic material with tyres gives a solution for waste management. Copyrolysis of biomass with other materials that are widely available could be a cost-effective way to produce biofuels. Copyrolysis adjusts the carbon, hydrogen, and oxygen contents of the feedstock and produces a favorable synergistic effect on improving the quality of the bio-oil [36]. Khan et al. [37] discovered that copyrolysis of cotton stalk and waste tyre at 550°C yielded the most carbon and hydrogen-rich bio-oil. Wang et al. [38] carried out

copyrolysis experiments with pine wood bark and waste tyres by changing the weight ratio of the tyres from 0 to 100%. The study found that the biogas produced at a higher biomass weight ratio had a higher concentration of $H_2$ and CO. Sanahuja-Parejo et al. [39] performed pyrolysis experiments on grape seeds and waste tyres with calcium oxide catalyst. The author found a synergistic effect on bio-oil yield. The oil content produced in this study had favorable aromatics and hydrocarbons. The above findings also matched with Cao et al. [40] who produced bio-oil through copyrolysis of wood and tyre with enhanced quality due to the positive synergistic effect. Martínez et al. [41] also looked into the copyrolysis characteristics of pine wood chips mixed with scrap tyres. When comparing biomass bio-oil and the bio-oil made by the copyrolysis process, the characteristics of the bio-oil made by copyrolysis increased dramatically. By varying the blend ratio, Uçar and Karagöz [42] copyrolyzed pine nut shells with waste tyres at 500°C. In this study, increased tyre fractions increased the carbon content in the produced oil.

The goal of this paper is to find the sustainable way to the waste tyre recycling process. In this path, this study was planned to investigate the copyrolysis of castor seed oil cake and waste tyres with an emphasis of higher liquid yield. The synergistic effect is basically dependent on the feedstock used for the process. According to the author's knowledge, there has been no work published with the combination of castor seed oil cake and waste tyres. The effect of the addition of tyre during pyrolysis of castor seed oil cake was investigated in this study with respect to yield. The yield was analyzed by increasing tyre material at the ratios of 75 : 25, 50 : 50, and 25 : 75 (biomass: tyre).

## 2. Materials and Methods

*2.1. Materials.* The castor seed oil cake was obtained from local oil mill in Coimbatore, India. The waste tyres were collected from a local vulcanizing centre in Coimbatore. Both materials were available in plenty at a very low cost. The seed cakes were dried initially for one week under direct sunlight and then crushed to reduce their size. The steel wires and fabrics were removed carefully from the collected waste tyres and cut into small pieces. Both feedstocks were maintained at uniform sizes of 0.5–2 mm.

*2.2. Characterization Study.* In order to find the volatile matter in both feedstocks, proximate and ultimate analyses were carried out according to ASTM standards. The thermogravimetric analysis (TGA701, LECO Corporation, Michigan) was used to find the pyrolysis behavior of the materials using the TGA701 thermogravimetric analyzer. The ultimate analysis of the sample was carried out by using a CHNS analyzer and the heating value of the samples was found by using a Paar-6772 bomb calorimeter. The functional groups in the bio-oil are analyzed by BRUKER Optik GmbH TENSOR 27 FT-IR spectroscopy. The spectra were obtained in the range of 400–4000 $cm^{-1}$ with 4 $cm^{-1}$ resolution. The THERMO GC-TRACE ULTRA VER: 5.0 and THERMO MS DSQ II were used to qualitatively identify and quantify the organic elements in bio-oil. The column temperature is initially set to 60°C and heated to 250°C. Helium is used as a carrier gas for the analysis. The capillary column has a length of 30 m and a diameter of 0.25 mm. The ion source temperature is 220°C, and the peak corresponding to the element was obtained with reference to the NIST 11 library.

*2.3. Pyrolysis Reactor.* The fixed bed reactor has an internal diameter of 50 mm and a height of 30 cm. The reactor has a capacity of 200 grams per batch and 30 grams of the feed material was filled for each experiment. The reactor is heated electrically and can withstand up to 1200°C. The reactor is fully covered with insulating material (Chromel Alumel) to resist unwanted energy loss from the reactor bed. Two K-type thermocouples were fixed at the bottom and middle of the reactor. The heat input to the reactor is controlled by an autotransformer with a voltmeter and ammeter set-up. The exit of the reactor is connected to a water-cooled condenser, whereas the cooling water was supplied at 5°C.

*2.4. Experimental Procedure.* All the experiments in this study were conducted at 500°C. The process was carried out by changing the mass percentage of castor seed oil cake and waste tyre ratios such as 100 : 0, 75 : 25, 50 : 50, 25 : 75, and 0 : 100. Initially, individual feedstocks were pyrolyzed, and then, copyrolysis experiments were performed by changing the biomass tyre ratio. For each run, 30 g of sample was loaded and the yield was analyzed. All the experiments were carried out by heating the reactor at a rate of 20 K/min. Each run was conducted till no vapour was released from the reactor. At the end of each experiment, the reactor was cleaned. The condensable volatiles that pass through the reactor have condensed and converted into liquid form. The bio-oil was collected and stored. After the reactor reached atmospheric temperature, the char was collected. The collected samples were weighed and the gas fractions were found by remaining material balance.

*2.5. Synergistic Effect.* The synergistic effect on product yields was observed by comparing theoretical and experimental yields. The theoretical yield during the copyrolysis process was calculated by additivity rule [43] shown in the following equation:

$$YT = \left(W_1 \times \alpha_1 + W_2 \times \alpha_2\right), \quad (1)$$

where $Y_T$ is the theoretical yield, $W_1$ and $W_2$ are the mass proportions of castor seed oil cake and waste tyres, and $\alpha_1$ and $\alpha_2$ are the experimental yields.

## 3. Results and Discussion

*3.1. Material Characterization.* Table 1 shows the basic characteristics of the castor seed oil cake and waste tyres. The caster seed oil cake and waste tyres have a higher amount of volatile matters. The higher volatiles in the material give

Table 1: Feedstock characteristics.

| Parameters | Castor seed oil cake | Waste tyres | Standard |
|---|---|---|---|
| Volatile matter | 68.3 | 64.1 | ASTM D3175 |
| Fixed carbon | 14.3 | 23.4 | By difference |
| Moisture content | 8.12 | 0.9 | ASTM D3173 |
| Ash | 9.28 | 11.6 | ASTM D3174 |
| Carbon | 51.20 | 80.60 | ASTM D5373 |
| Hydrogen | 7.11 | 7.23 | ASTM D5373 |
| Nitrogen | 2.93 | 0.44 | ASTM D5373 |
| Oxygen[#] | 38.73 | 9.91 | By difference |
| Sulphur | 0.03 | 1.82 | ASTM D5373 |
| Heating value (MJ/kg) | 28.10 | 37.20 | ASTM D445 |

[#]By difference.

confidence in the yielding of more bio-oil during volatilization. The presence of higher volatiles in the inveterate burning of fuel would be expedient. The moisture content of the material is within the permissible range (less than 10%). The ash content of both materials is high. Generally, the ash particle in the sample reduces the yield and quality of oil [40]. The ultimate analysis of the samples and products was done on an ash-free basis. The feedstocks are having higher amount of carbon (51.20% and 80.60%) and a lower amount of nitrogen (2.93% and 0.44%). Because there was low nitrogen and sulphur, the formation of SOx and NOx during pyrolysis would be reduced. In energy content point of view, the waste tyres have higher calorific value (37.20 MJ/kg) than castor seed oil seed cake (28.10 MJ/kg).

*3.2. Thermogravimetric Analysis.* This analysis is used to evaluate the thermal behavior of castor seed oil cake and waste tyres under a pyrolysis environment. For this, the feedstocks were heated from atmospheric temperature to 800°C in a nitrogen environment at 20°C/min heating rate. The biomass devolatilization begins earlier than waste tyres. The initial degradation started at 50°C, which represents the evaporation of moisture from the material. Around 10% of the weight was lost due to the moisture removal process. The decomposition of the oil cake took place in three stages [44]. At first, the lignin starts to decompose till 500°C. A major mass loss (70%) occurred between 225°C and 450°C representing the breakdown of cellulose and hemicellulose. At this temperature range, the cellulose and hemicellulose of the biomass material have decomposed rapidly and released a greater number of volatiles. After 500°C, castor seed oil cake is converted to carbon residue. At this point, lignin breakdown accounts for around 10% of the mass loss. The structure of waste tyres is not as complex as that of castor seed oil cake. The TGA of waste tyres has also been reported in the literature [45, 46] with three main steps: a first step of the process is related to

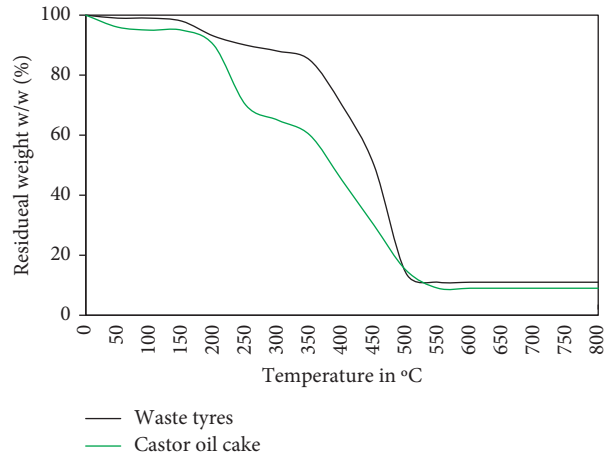


Figure 1: Thermogravimetric analysis of the feedstocks.

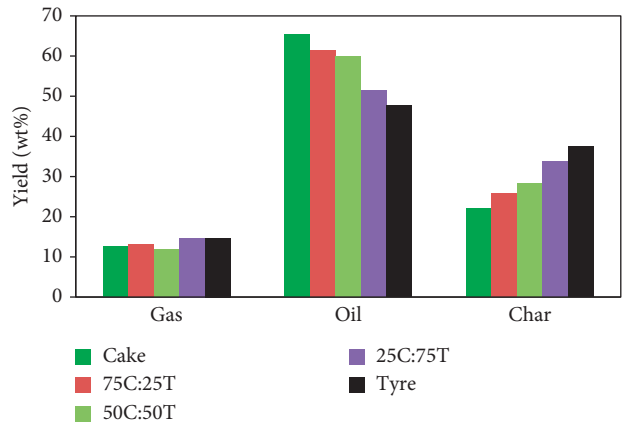


Figure 2: Experimental product yields performed at 500°C.

the pyrolysis of rubber additives, natural rubber, and synthetic rubber decomposition. From this analysis, it can be found that both the materials decomposed completely between 250°C and 500°C. At this temperature, the pyrolysis of castor seed oil cake and that of waste tyres overlap. As a result, radicals produced during the pyrolysis process may coexist at this temperature. So, for further experimental works, the temperature was fixed at 500°C. Figure 1 shows the TGA curve of the feedstock materials.

*3.3. Pyrolysis Product Yield.* Figure 2 shows the product yields obtained from individual and copyrolysis processes. The maximum oil products were acquired from castor seed oil cake. Overall, the oil production from both materials is high when compared to char and gas. The higher oil yield from biomass is attributed to the presence of higher volatile matters than waste tyres [47]. Compared to biomass, waste tyres produced more char. This is due to the existence of more ash in the tyres and carbon clack used for the formation of the tyre. During experimentation, the oil and char yield follows a linear tendency with the addition of increased tyre particles. The production of oil is decreased with increased char yield by increasing tyre materials. The fraction

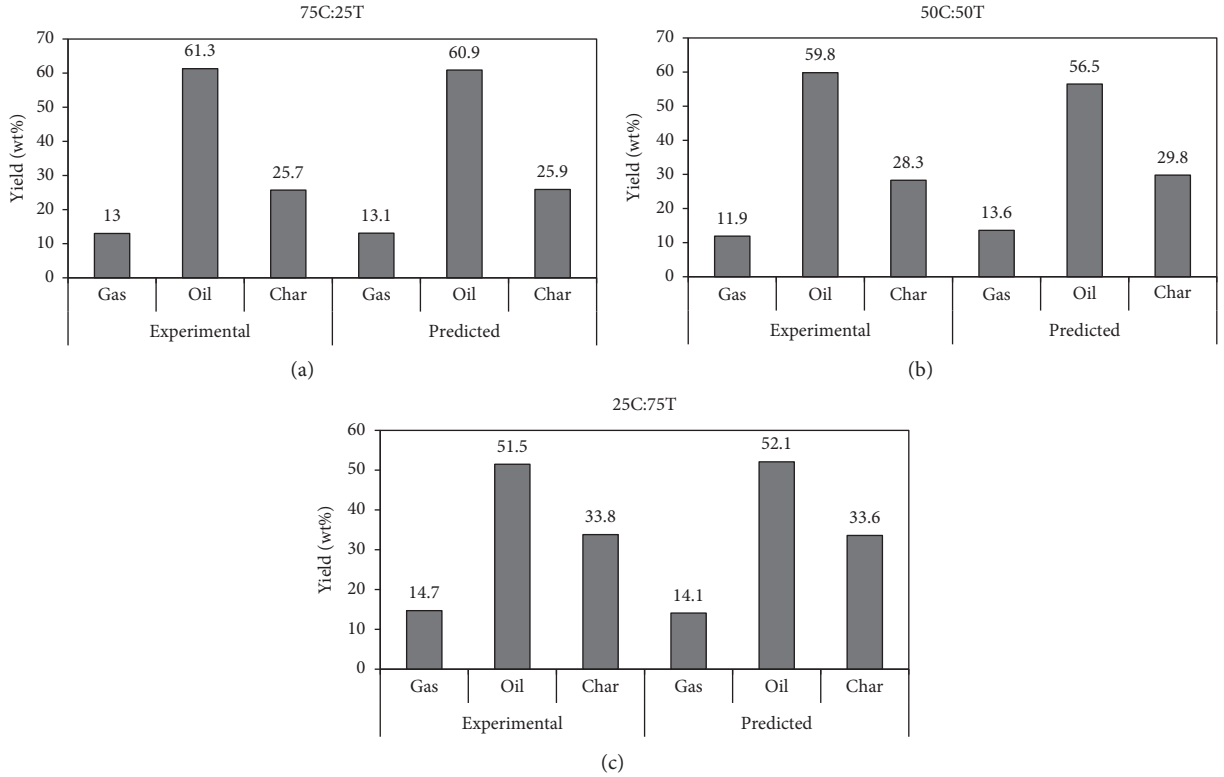


Figure 3: Experimental and theoretical product yields during copyrolysis performed at 500°C.

Table 2: Properties of copyrolysis oil.

| Elements | Unit | Copyrolysis oil[$] | Diesel [53] |
|---|---|---|---|
| Density | $kg/m^3$ | 925 | 850 |
| Viscosity | cSt | 3.82 | 3.9 |
| Flash point | °C | 35 | 57 |
| pH | — | 3.62 | — |
| Carbon | wt% | 78.35 | 86.5 |
| Hydrogen | wt% | 9.56 | 13.2 |
| Nitrogen | wt% | 0.50 | 0.02 |
| Sulphur | wt% | 0.92 | 0.24 |
| Oxygen[a] | wt% | 10.67 | — |
| Heating value | MJ/kg | 38.72 | 43.6 |
| Empirical formula | — | $CH_{1.453}N_{0.0005}O_{0.102}$ | — |

of oil varied from 65.3 wt% to 47.8 wt% and the char yield varied from 22.1 wt% to 37.5 wt%. The yield of gas fractions is similar for all of the feedstocks studied, ranging from 11.9 wt% to 14.7 wt%.

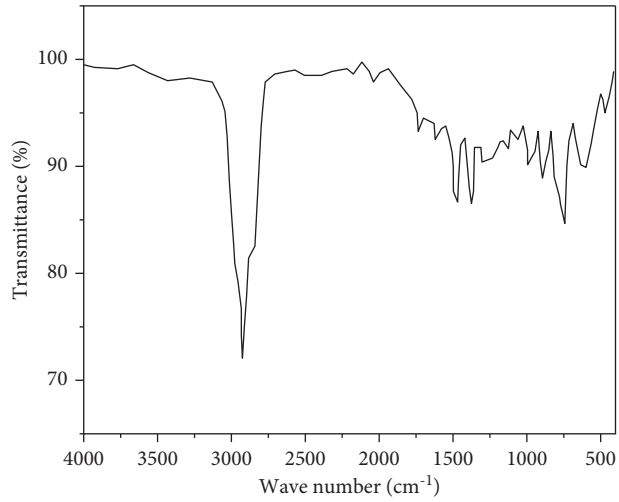


Figure 4: FT-IR analysis of the oil.

*3.4. Synergistic Analysis.* Figures 3(a)–3(c) show the comparison of theoretical and experimental yields during the copyrolysis process under different blends of biomass and tyres. The copyrolysis process at the proportions of 75 : 25 and 50 : 50 results in a slight decrease in gas and char yield, while the oil fractions increased significantly, which indicates a positive synergistic effect. At 75 C : 25T, the yield of oil increased by 0.66% compared to the predicted value. Likewise, the value was increased to 5.84% for the 50C : 50 T blend. This can be explicated by the exchange of hydrogen atoms and the creation of free radicals [48]. This creates a cross-reaction between biomass and waste tyres [49]. At 25 C : 75T blended samples, the positive synergy was observed for char and gas fractions, whereas the yield of char and gas was improved by 0.6% and 4.26%, respectively, with respect to the predicted value. Based on the results provided in Figure 3, it can be inferred that when the blend of oil cake and tyres surpasses 50 : 50, there is no evident synergetic effect on oil fractions. The experimental work conducted by Cao et al. [40], Uçar and Karagöz [42], Farooq et al. [50], and

Table 3: GC-MS analysis of oil.

| RT/min | Compound name | Molecular name | % area |
|---|---|---|---|
| 4.26 | 2-Furanmethanol | $C_5H_6O_2$ | 0.18 |
| 4.94 | Acetic acid | $C_2H_4O_2$ | 4.04 |
| 5.60 | Methanol | $CH_4O$ | 2.14 |
| 7.11 | 2-Butanone | $C_4H_8O$ | 0.59 |
| 7.56 | 2-Methoxy-phenol | $C_7H_8O_2$ | 2.87 |
| 8.21 | Octanal | $C_8H_{16}O$ | 2.46 |
| 10.25 | Phenol | $C_6H_6O$ | 0.81 |
| 11.12 | 2-Methoxy-4-(2-propenyl)-phenol acetate | $C_{12}H_{14}O_3$ | 3.04 |
| 11.98 | 1-Hydroxy-2-pentanone | $C_5H_{10}O_2$ | 2.93 |
| 12.09 | Butanedial | $C_4H_6O_2$ | 3.77 |
| 12.94 | 2-Methoxy-4-methyl-phenol | $C_8H_{10}O_2$ | 0.98 |
| 13.52 | Levoglucosan | $C_6H_{10}O_5$ | 2.94 |
| 16.75 | 2,4-Dimethylstyrene | $C_{10}H_{12}$ | 0.74 |
| 17.01 | 2-Methyl-Naphthalene | $C_{11}H_{10}$ | 0.83 |
| 18.25 | D-Limonene | $C_{10}H_{16}$ | 8.11 |
| 18.67 | 2,6-Dimethoxyphenol | $C_8H_{10}O_3$ | 1.59 |
| 19.41 | 2,6-Dimethyl-Naphthalene | $C_{12}H_{12}$ | 0.66 |
| 20.08 | Methylbenzene | C7H8 | 3.37 |
| 20.71 | Methylene-cyclohexane | $C_7H_{12}$ | 0.94 |
| 21.21 | 1,2-Dihydro-6-methyl-naphthalene | $C_{11}H_{12}$ | 3.98 |
| 21.84 | o-Xylene | $C_8H_{10}$ | 1.45 |
| 21.99 | Benzothiazole | $C_7H_5NS$ | 0.40 |
| 22.44 | 3,7,7-Trimethyl-1,3,5-cycloheptatriene | $C_{10}H_{14}$ | 1.91 |
| 23.04 | 4-Ethenyl-cyclohexene | $C_8H_{12}$ | 2.56 |
| 23.74 | 1,2,3-Trimethyl-benzene | $C_9H_{12}$ | 7.50 |
| 24.89 | 1,4-Dimethylbenzene | $C_8H_{10}$ | 7.31 |
| 25.22 | 2-Pyrrolidinone | $C_4H_7NO$ | 2.40 |
| 25.80 | 2-Methoxy-6-methyl-4H-pyran-4-one | $C_7H_8O_3$ | 0.80 |
| 26.10 | 3-Methylene-4-(1,2-propadienyl)-cyclohexene | $C_{10}H_{12}$ | 1.72 |
| 26.71 | 2-Methyl-2-cyclopenten-1-one | $C_6H_8O$ | 0.88 |
| 27.14 | Acetamide | $C_2H_5NO$ | 3.51 |
| 27.77 | 1-Acetylpyrrolidine | $C_7H_{11}NO_3$ | 1.18 |
| 28.00 | 5,6-Dihydro-6-methyluracil | $C_5H_8N_2O_2$ | 2.12 |
| 28.95 | Picolinamide | $C_6H_6N_2O$ | 1.37 |
| 29.11 | 1-Ethynyl-1-cyclohexene | $C_8H_{10}$ | 2.22 |
| 29.38 | Cyclohexene | $C_6H_{10}$ | 1.14 |
| 30.10 | Hexahydropyrrolo [1,2- a] pyrazine-1,4-dione | $C_7H_{10}N_2O_2$ | 1.73 |
| 30.25 | Methylstyrene | $C_9H_{10}$ | 0.68 |
| 31.22 | 1-Ethynyl-1-cyclohexene | C8H10 | 2.11 |
| 31.94 | 1-Isopropenyl-4-methyl-1,3-cyclohexadiene | $C_{10}H_{14}$ | 4.77 |
| 32.47 | Tetramethylbenzenes | $C_{10}H_{14}$ | 0.23 |
| 33.14 | 1-Methylnaphthalene | $C_{11}H_{10}$ | 3.16 |

Abnisa and Daud [51] showed a maximum oil yield of 47.2, 47, 44, and 48.1 wt% during the copyrolysis of wood, pine nut shells, wheat straw, and palm shells combined with waste tyres. In all the above experiments, the yield of oil has increased with the addition of tyres. However, the trend found in this investigation is the contrary, which gives lower oil output with the addition of tyres with biomass. This is due to the higher yield of maximum initial oil production from castor seed oil cake compared to other biomasses.

### 3.5. Oil Characterization

*3.5.1. Physical Analysis.* Table 2 displays the various properties of the copyrolysis oil. The table shows that the oil has a higher amount of carbon and hydrogen with reduced nitrogen and sulphur. The presence of oxygen is the fundamental factor that distinguishes biooils from hydrocarbon fuels. The oxygen content of the oil is 10.67 wt%, which is very low compared to other biomass pyrolysis oil [52]. The higher oxygen content in the biooil reduces the heating value of the oil, and it may corrode the engine parts while it is used as fuel for heating applications. The density of the derived oil is greater than the conventional diesel, and the viscosity is found to be nearly equal to the diesel fuel [53]. The heating value was estimated at 38.72 MJ/kg. From this, it can be implicit that the oil can be used as a fuel for furnaces and boilers.[$]Obtained at 50C : 50 T. [a]By difference.

*3.5.2. FT-IR Analysis.* The FT-IR analysis of the oil showed numerous peaks at various wavenumbers pertaining to

various functional groups (Figure 4). The various functional groups in the oil are ascribed to the different structures of the biomass and tyre material. During reaction, the waste tyres play a significant role as a hydrogen donor [54]. Alkanes, aliphatic, and aromatic compounds are the major elements present in the oil. The O-H stretching vibration at 2925.38 $cm^{-1}$ represents the existence of alcohols in the oil. The presence of alkanes is represented by the C-H stretching vibration at 2925.38 $cm^{-1}$. The $C = C$ stretching vibration at 1627.94 $cm^{-1}$, 1497.68 $cm^{-1}$, and 1389.95 $cm^{-1}$ represents the availability of an alkane group in the oil. The C-O stretching and O-H bending at 995.24 $cm^{-1}$ represents the presence of alcohols and phenols. The C-H bending at 771.75 $cm^{-1}$ shows the occurrence of aromatic compounds in the oil.

*3.5.3. GC-MS Analysis.* This analysis also showed that the copyrolysis oil contained a variety of aliphatic and aromatic compounds with considerable phenolic compounds. The existence of phenolic and its derivatives was identified due to the decomposition of lignin in the samples. Benzene and its derivatives were also present more in the oil. Previously, pyrolysis of scrap tyres has revealed similar chemical compounds, which have been ascribed to the breakdown of rubber [55]. The chemical elements in the oil samples are traced using the NIST library and are listed in Table 3 with increased retention time. The oil's stability is improved by the reduced oxygenated components in tyre pyrolysis oil. D-Limonene, 1,2,3-trimethyl-benzene, 1,4-dimethylbenzene, 1-isopropenyl-4-methyl-1,3-cyclohexadiene, and acetic acid are available majority in the sample.

## 4. Conclusion

Copyrolysis of castor seed oil cake and waste tyres under different mass ratios was performed to understand the synergistic effect for maximum oil production. During the pyrolysis process, the biomass interacted with waste tyres and impacted the oil yield and quality. The product distribution is different at different feedstock ratios. The copyrolysis experiment showed maximum synergy on oil yield. Compared to the prediction, the copyrolysis process at a 50 : 50 blend ratio yielded 5.84% more oil products. The physiochemical characteristics of the oil obtained at the maximum synergistic effect were done to understand its basic compositions. The oil showed a maximum heating value of 38.72 MJ/kg, which is better to be used as a heating fuel for a furnace. The chromatographic study showed that oil is a combination of different aliphatic and aromatic compounds with considerable phenolic compounds. The identified chemical compounds are used as feedstock for various chemical industries.

## Data Availability

The data used to support the findings of this study are included within the article.

## Conflicts of Interest

The authors declare that there are no conflicts of interest.

## References

[1] C. Sowmya Dhanalakshmi and P. Madhu, "Utilization possibilities of Albiziaamara as a source of biomass energy for bio-oil in pyrolysis process," *Energy Sources, Part A: Recovery, Utilization, and Environmental Effects*, vol. 41, no. 15, pp. 1908–1919, 2019.

[2] H. Hassan, J. K. Lim, and B. H. Hameed, "Recent progress on biomass co-pyrolysis conversion into high-quality bio-oil," *Bioresource Technology*, vol. 221, pp. 645–655, 2016.

[3] V. Anand, V. Sunjeev, and R. Vinu, "Catalytic fast pyrolysis of Arthrospiraplatensis (spirulina) algae using zeolites," *Journal of Analytical and Applied Pyrolysis*, vol. 118, pp. 298–307, 2016.

[4] A. Singh, S. Nanda, and F. Berruti, "A review of thermochemical and biochemical conversion of Miscanthus to biofuels," *Biorefinery of Alternative Resources: Targeting Green Fuels and Platform Chemicals*, pp. 195–220, Springer, Berlin, Germany, 2020.

[5] S. Pourkarimi, A. Hallajisani, A. Alizadehdakhel, and A. Nouralishahi, "Biofuel production through micro-and macroalgae pyrolysis–A review of pyrolysis methods and process parameters," *Journal of Analytical and Applied Pyrolysis*, vol. 142, Article ID 104599, 2019.

[6] K. Drugkar, W. Rathod, T. Sharma et al., "Advanced separation strategies for up-gradation of bio-oil into value-added chemicals: a comprehensive review," *Separation and Purification Technology*, vol. 283, Article ID 120149, 2022.

[7] Q. Lu, W. Z. Li, and X. F. Zhu, "Overview of fuel properties of biomass fast pyrolysis oils," *Energy Conversion and Management*, vol. 50, no. 5, pp. 1376–1383, 2009.

[8] A. Imran, E. A. Bramer, K. Seshan, and G. Brem, "High quality bio-oil from catalytic flash pyrolysis of lignocellulosic biomass over alumina-supported sodium carbonate," *Fuel Processing Technology*, vol. 127, pp. 72–79, 2014.

[9] D. S. Ogunniyi, "Castor oil: a vital industrial raw material," *Bioresource Technology*, vol. 97, no. 9, pp. 1086–1091, 2006.

[10] S. Sun, G. Wang, and P. Wang, "A cleaner approach for biodegradable lubricants production by enzymatic glycerolysis of castor oil and kinetic analysis," *Journal of Cleaner Production*, vol. 188, pp. 530–535, 2018.

[11] H. Mutlu and M. A. R. Meier, "Castor oil as a renewable resource for the chemical industry," *European Journal of Lipid Science and Technology*, vol. 112, no. 1, pp. 10–30, 2010.

[12] R. Kaur and T. Bhaskar, "Potential of castor plant (Ricinuscommunis) for production of biofuels, chemicals, and value-added products," in *Waste Biorefinery*, pp. 269–310, Elsevier, Amsterdam, Netherlands, 2020.

[13] H. F. Gercel, "The production and evaluation of bio-oils from the pyrolysis of sunflower-oil cake," *Biomass and Bioenergy*, vol. 23, no. 4, pp. 307–314, 2002.

[14] E. David and J. Kopac, "Pyrolysis of rapeseed oil cake in a fixed bed reactor to produce bio-oil," *Journal of Analytical and Applied Pyrolysis*, vol. 134, pp. 495–502, 2018.

[15] G. Duman, M. Pala, S. Ucar, and J. Yanik, "Two-step pyrolysis of safflower oil cake," *Journal of Analytical and Applied Pyrolysis*, vol. 103, pp. 352–361, 2013.

[16] A. E. Pütün, E. Apaydin, and E. Pütün, "Bio-oil production from pyrolysis and steam pyrolysis of soybean-cake: product

yields and composition," *Energy*, vol. 27, no. 7, pp. 703–713, 2002.

[17] P. Madhu, L. Vidhya, S. Vinodha et al., "Co-Pyrolysis of hardwood combined with industrial pressed oil cake and agricultural residues for enhanced bio-oil production," *Journal of Chemistry*, vol. 2022, Article ID 9884766, 12 pages, 2022.

[18] C. Sowmya Dhanalakshmi and P. Madhu, "Biofuel production of neem wood bark (Azadirachta indica) through flash pyrolysis in a fluidized bed reactor and its chromatographic characterization," *Energy Sources, Part A: Recovery, Utilization, and Environmental Effects*, vol. 43, no. 4, pp. 428–443, 2021.

[19] E. David and J. Kopač, "Upgrading the characteristics of the bio-oil obtained from rapeseed oil cake pyrolysis through the catalytic treatment of its vapors," *Journal of Analytical and Applied Pyrolysis*, vol. 141, Article ID 104638, 2019.

[20] I. A. Aldobouni, A. B. Fadhil, and I. K. Saied, "Conversion of de-oiled castor seed cake into bio-oil and carbon adsorbents," *Energy Sources, Part A: Recovery, Utilization, and Environmental Effects*, vol. 37, no. 24, pp. 2617–2624, 2015.

[21] C. Kalinke, A. S. Mangrich, L. H. Marcolino-Junior, and M. F. Bergamini, "Biochar prepared from castor oil cake at different temperatures: a voltammetric study applied for Pb2+, Cd2+ and Cu2+ ions preconcentration," *Journal of Hazardous Materials*, vol. 318, pp. 526–532, 2016.

[22] K. G. Kalogiannis, S. D. Stefanidis, C. M. Michailof, and A. A. Lappas, "Castor bean cake residues upgrading towards high added value products via fast catalytic pyrolysis," *Biomass and Bioenergy*, vol. 95, pp. 405–415, 2016.

[23] E. B. Mubofu, "Castor oil as a potential renewable resource for the production of functional materials," *Sustainable Chemical Processes*, vol. 4, no. 1, pp. 11-12, 2016.

[24] R. V. Silva, A. D. Goncalves, J. O. Vinhal et al., "Bioproducts from the pyrolysis of castor seed cake: basic dye adsorption capacity of biochar and antifungal activity of the aqueous phase," *Journal of Environmental Chemical Engineering*, vol. 9, no. 1, Article ID 104825, 2021.

[25] R. V. Silva, A. Casilli, A. L. Sampaio et al., "The analytical characterization of castor seed cake pyrolysis bio-oils by using comprehensive GC coupled to time of flight mass spectrometry," *Journal of Analytical and Applied Pyrolysis*, vol. 106, pp. 152–159, 2014.

[26] K. Formela, "Sustainable development of waste tires recycling technologies–recent advances, challenges and future trends," *Advanced Industrial and Engineering Polymer Research*, vol. 4, no. 3, pp. 209–222, 2021.

[27] E. B. Machin, D. T. Pedroso, and J. A. de Carvalho, "Energetic valorization of waste tires," *Renewable and Sustainable Energy Reviews*, vol. 68, pp. 306–315, 2017.

[28] W. M. Lewandowski, K. Januszewicz, and W. Kosakowski, "Efficiency and proportions of waste tyre pyrolysis products depending on the reactor type—a review," *Journal of Analytical and Applied Pyrolysis*, vol. 140, pp. 25–53, 2019.

[29] I. Hita, M. Arabiourrutia, M. Olazar, J. Bilbao, J. M. Arandes, and P. Castaño, "Opportunities and barriers for producing high quality fuels from the pyrolysis of scrap tires," *Renewable and Sustainable Energy Reviews*, vol. 56, pp. 745–759, 2016.

[30] D. Czajczyńska, K. Czajka, R. Krzyżyńska, and H. Jouhara, "Waste tyre pyrolysis–Impact of the process and its products on the environment," *Thermal Science and Engineering Progress*, vol. 20, Article ID 100690, 2020.

[31] E. Yazdani, S. H. Hashemabadi, and A. Taghizadeh, "Study of waste tire pyrolysis in a rotary kiln reactor in a wide range of pyrolysis temperature," *Waste Management*, vol. 85, pp. 195–201, 2019.

[32] R. Abdallah, A. Juaidi, M. Assad, T. Salameh, and F. Manzano-Agugliaro, "Energy recovery from waste tires using pyrolysis: Palestine as case of study," *Energies*, vol. 13, no. 7, p. 1817, 2020.

[33] J. D. Martínez, F. Campuzano, N. Cardona-Uribe, C. N. Arenas, and D. Muñoz-Lopera, "Waste tire valorization by intermediate pyrolysis using a continuous twin-auger reactor: operational features," *Waste Management*, vol. 113, pp. 404–412, 2020.

[34] G. Lopez, J. Alvarez, M. Amutio et al., "Waste truck-tyre processing by flash pyrolysis in a conical spouted bed reactor," *Energy Conversion and Management*, vol. 142, pp. 523–532, 2017.

[35] P. T. Williams, "Pyrolysis of waste tyres: a review," *Waste Management*, vol. 33, no. 8, pp. 1714–1728, 2013.

[36] S. Xiong, J. Zhuo, H. Zhou, R. Pang, and Q. Yao, "Study on the co-pyrolysis of high density polyethylene and potato blends using thermogravimetric analyzer and tubular furnace," *Journal of Analytical and Applied Pyrolysis*, vol. 112, pp. 66–73, 2015.

[37] S. R. Khan, M. Zeeshan, and A. Masood, "Enhancement of hydrocarbons production through co-pyrolysis of acid-treated biomass and waste tire in a fixed bed reactor," *Waste Management*, vol. 106, pp. 21–31, 2020.

[38] Z. Wang, K. G. Burra, M. Zhang et al., "Co-pyrolysis of waste tire and pine bark for syngas and char production," *Fuel*, vol. 274, Article ID 117878, 2020.

[39] O. Sanahuja-Parejo, A. Veses, M. V. Navarro et al., "Catalytic co-pyrolysis of grape seeds and waste tyres for the production of drop-in biofuels," *Energy Conversion and Management*, vol. 171, pp. 1202–1212, 2018.

[40] Q. Cao, L. Jin, W. Bao, and Y. Lv, "Investigations into the characteristics of oils produced from co-pyrolysis of biomass and tire," *Fuel Processing Technology*, vol. 90, no. 3, pp. 337–342, 2009.

[41] J. D. Martínez, A. Veses, A. M. Mastral et al., "Co-pyrolysis of biomass with waste tyres: upgrading of liquid bio-fuel," *Fuel Processing Technology*, vol. 119, pp. 263–271, 2014.

[42] S. Uçar and S. Karagöz, "Co-pyrolysis of pine nut shells with scrap tires," *Fuel*, vol. 137, pp. 85–93, 2014.

[43] I. N. Manickam, P. Madhu, and H. Kanagasabapathy, "Conversion of cotton residues to bio-oil and chemicals through flash pyrolysis in a fluidised bed reactor," *International Journal of Energy Technology and Policy*, vol. 14, no. 1, pp. 20–33, 2018.

[44] P. Madhu, M. Sasireka, R. Samikannu et al., "Production and characterization of maximum liquid oil products through individual and copyrolysis of pressed neem oil cake and waste thermocol mixture," *Advances in Polymer Technology*, vol. 2022, Article ID 5258130, 11 pages, 2022.

[45] R. Murillo, E. Aylón, M. V. Navarro, M. S. Callén, A. Aranda, and A. M. Mastral, "The application of thermal processes to valorise waste tyre," *Fuel Processing Technology*, vol. 87, no. 2, pp. 143–147, 2006.

[46] K. Januszewicz, M. Klein, E. Klugmann-Radziemska, and D. Kardas, "Thermogravimetric analysis/pyrolysis of used tyres and waste rubber," *Physicochemical Problems of Mineral Processing*, vol. 53, 2017.

[47] J. Alvarez, M. Amutio, G. Lopez, L. Santamaria, J. Bilbao, and M. Olazar, "Improving bio-oil properties through the fast co-pyrolysis of lignocellulosic biomass and waste tyres," *Waste Management*, vol. 85, pp. 385–395, 2019.

[48] V. S. Kaushik, C. S. Dhanalakshmi, P. Madhu, and P. Tamilselvam, "Co-pyrolysis of neem wood bark and low-density polyethylene: influence of plastic on pyrolysis product distribution and bio-oil characterization," *Environmental Science and Pollution Research*, Springer, Berlin, Germany, 2022.

[49] W. Chen, S. Shi, J. Zhang, M. Chen, and X. Zhou, "Co-pyrolysis of waste newspaper with high-density polyethylene: synergistic effect and oil characterization," *Energy Conversion and Management*, vol. 112, pp. 41–48, 2016.

[50] M. Z. Farooq, M. Zeeshan, S. Iqbal, N. Ahmed, and S. A. Y. Shah, "Influence of waste tire addition on wheat straw pyrolysis yield and oil quality," *Energy*, vol. 144, pp. 200–206, 2018.

[51] F. Abnisa and W. M. A. Wan Daud, "Optimization of fuel recovery through the stepwise co-pyrolysis of palm shell and scrap tire," *Energy Conversion and Management*, vol. 99, pp. 334–345, 2015.

[52] E. Önal, B. B. Uzun, and A. E. Pütün, "Bio-oil production via co-pyrolysis of almond shell as biomass and high density polyethylene," *Energy Conversion and Management*, vol. 78, pp. 704–710, 2014.

[53] D. Raguraman, A. Kumar, S. Prasanna Raj Yadav et al., "Performance and emission characteristics of pyrolysis oil obtained from neem de Oiled cake and waste polystyrene in a compression ignition engine," *Advances in Materials Science and Engineering*, vol. 2021, Article ID 3728852, 10 pages, 2021.

[54] S. Ucar, S. Karagoz, A. R. Ozkan, and J. Yanik, "Evaluation of two different scrap tires as hydrocarbon source by pyrolysis," *Fuel*, vol. 84, no. 14-15, pp. 1884–1892, 2005.

[55] H. Pakdel, D. M. Pantea, and C. Roy, "Production of dl-limonene by vacuum pyrolysis of used tires," *Journal of Analytical and Applied Pyrolysis*, vol. 57, no. 1, pp. 91–107, 2001.